Hydrogen Fuel Technologies for Vehicular Transportation

By

Darrell C. Dean

A thesis submitted to the Graduate Program in Chemistry

in conformity with the requirements of the

Degree of Doctor of Philosophy

Queen's University

Kingston, Ontario, Canada

Final Submission May 2012

Abstract

With continually increasing concern over anthropogenic carbon dioxide emissions and their effect on global climate, the search for alternative fuels, especially for mobile applications such as in vehicles, is of immediate concern. Herein, research towards hydrogen as an alternative energy carrier is discussed; first, with the investigation of "hybrid" hydrogen storage systems that are meant to provide hydrogen for a fully fuel cell powered vehicle via a chemical reaction; and second, that of a thermally regenerative fuel cell system (TRFC) to partially supplant the energy needs of transport trucks by harnessing engine waste heat.

Hybrid storage systems are comprised of a heterocyclic carrier that undergoes endothermic hydrogen release (indoline) and an organic hydride that undergoes exothermic release (amine boranes). Different embodiments are considered, varying in the mechanism of exothermic release (thermolysis vs. hydrolysis) and the mode of combination (physical vs. chemical). A thorough investigation into the effect of catalyst, sterics and temperature on the heterogeneously catalyzed dehydrogenation rate of N-heterocycles was executed. A number of trends with respect to the catalyst identity and the level of steric protection around the nitrogen atom were observed.

The study towards a TRFC involved an investigation of the heterogeneous hydrogenation of benzylic ketones. Screening of a myriad of different catalysts was performed, including those with various supports, metals and modifications, and the examination of how both the sterics and electronics of the ketone affect the hydrogenation rate. A rapid hydrogenation at relatively low metal loadings and hydrogen pressures with extreme selectivity (>99.9%) is required. To date, however,

such a combination has been elusive. The best selectivity was obtained with commercial Pd/SiO_2 (99.99%), yet at a low conversion of 6%, after 1 h under 1 atm of H_2 at 100 ˚C. In addition to the poor conversion, SiO_2 is not electronically conductive and is therefore not fit for this application. The best viable catalyst, then, was a Pd/Vulcan XC-72 (carbon) catalyst made by the author with an observed 14% conversion and 98% selectivity under the same conditions. However, trends in activity and selectivity with respect to the catalyst and ketone have been characterized herein.

Acknowledgements

First and foremost, I'd like to thank Professor Philip Jessop for his support and supervision over the past five years. Your interest and excitement about the chemistry we do is truly inspiring. I'd also like to thank Professor Boyd Davis and Professor Brant Peppley for their advice on the more engineering aspects of the projects presented herein. I'd also like to mention Françoise Sauriol for her training and expertise with NMR spectroscopy and Dzmitry Malevich from the Fuel Cell Research Centre for his help with the cyclic voltammetry work.

I'd also like to thank all of the members of the Jessop group who have had a hand in my research during my time here. There are simply too many names to list everyone, however I will specifically mention those who have been a part of team hydrogen and have coauthored manuscripts with me in this time including Dr. Dominik Wechsler, Vanessa Renee Little and Andrew Carrier. Dr. Keith Huynh also deserves thanks for his impact on this work.

To my family and to the new friends I've met at Queen's and in Kingston, and those from before, thank you for being there for me. On top of completing an advanced degree in a particularly challenging subject, the last five years have been truly transformative for me personally, and none of that would have been possible without you. Whether it was a laugh on a regular day, a hug on a bad day, or a drink on a worse day, your love will stay with me long after we move on.

Statement of Originality

I hereby certify that all of the work described within this thesis is the original work of the author. Any published (or unpublished) ideas and/or techniques from the work of others are fully acknowledged in accordance with the standard referencing practices.

All contributions from collaborators are clearly noted in the text, and in particular the data and characterization presented Chapter 4.1 was done in heavy collaboration with Dr. Dominik Wechsler.

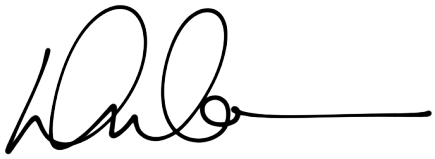

Darrell C. Dean

May, 2012

Copyright Information

Portions of this thesis have been published previously:

i) **Chapter 4.1** • Reproduced in part with permission from Wechsler, D.; Cui, Y.; Dean, D.; Davis, B.; Jessop, P.G.; "Production of H_2 from combined endothermic and exothermic carriers" *J. Am. Chem. Soc.* **2008**, *130*, 17195-19203. Copyright 2008 American Chemical Society.

ii) **Chapter 4.2** • Dean, D.; Davis, B.; Jessop, P.G.; "The effect of temperature, catalyst and sterics on the rate of N-heterocycle dehydrogenation for hydrogen storage" *New J. Chem.* **2011**, *35*, 417-422 - Reproduced by permission of The Royal Society of Chemistry (RSC) on behalf of the Centre National de la Recherche Scientifique (CNRS) and the RSC.

iii) **Chapter 5** • Carrier, A.C.; Dean, D.; Little, V.R.; Vandersleen, J.; Davis, B.; Jessop, P.G.; "Towards a thermally regenerative fuel cell for truck engines" *Energy Environ. Sci.*, **2012**, *5*, 7111-7123 - Reproduced by permission of The Royal Society of Chemistry (RSC).

Table of Contents

List of Tables

List of Figures

List of Abbreviations

AEO	Aluminum triethoxide
AFC	Alkaline fuel cell
BCC	Body-centered cubic (crystal unit cell)
BET	Brunauer, Emmett and Teller (adsorption mechanism)
BHS	Bound hybrid system
COSY	Correlation (NMR) Spectroscopy
DD	Double dehydrogenation (hybrid H_2 storage system)
DH	Dehydrogenation/hydrolysis (hybrid H_2 storage system)
DOE	(United States) Department of Energy
EI	Electron impact (ionization in mass spectroscopy)
EIA	(United States) Energy Information Administration
EW	Equivalent weight
FCC	Face-centered cubic (crystal unit cell)
GC	Gas chromatography
GHG	Greenhouse gas
ICE	Internal combustion engine
IPCC	Intergovernmental Panel on Climate Change
IR	Infrared (spectroscopy)
IUPAC	International Union of Pure and Applied Chemistry
MCFC	Molten carbonate fuel cell
MHS	Mixed hybrid system
MOF	Metal organic framework

MS	Mass spectroscopy
NASA	National Aeronautics and Space Administration
NMR	Nuclear magnetic resonance (spectroscopy)
NOESY	Nuclear Overhauser effect (NMR) spectroscopy
p.a.	*Per annum*
PAFC	Phosphoric acid fuel cell
PEMFC	Polymer electrolyte membrane fuel cell
PTFE	Polymerized tetrafluoroethylene
RDS	Rate determining step
RT	Room temperature
SOFC	Solid oxide fuel cell
TEOS	Tetraethyl orthosilicate
TOF	Turnover frequency
TRFC	Thermally regenerative fuel cell

List of Symbols

*	vacant active catalytic site
α	Kamlet-Taft hydrogen-bond donating ability parameter
A	pre-exponential factor
β	Kamlet-Taft hydrogen-bond accepting ability parameter
C	conversion
c	fitting constant (B.E.T. isotherm)
ΔG	change in Gibbs free energy
$\Delta G^{\ddagger}$	Gibbs free energy of activation
ΔH	change in enthalpy
$\Delta H^{\ddagger}$	change in enthalpy of activation
ΔH_c	change in enthalpy of chemisorption
ΔH_f	change in enthalpy of formation
ΔH_p	change in enthalpy of physisorption
ΔS	change in entropy
$\Delta S^{\ddagger}$	change in entropy of activation
e^-	electron
$E^{\ddagger}$	adsorption to chemisorption energy barrier
E_a	activation energy
E_{pa}	anodic peak potential (cyclic voltammetry)
E_{pc}	cathodic peak potential (cyclic voltammetry)
E^0	standard half-cell potential
E^0_{cell}	standard cell potential

E_{cell}	non-standard cell potential
θ	fractional surface coverage
F	Faraday constant (9.6485 C mol^{-1})
f	flux of incoming molecules
h	heat transfer coefficient
h	Planck's constant (6.626 x 10^{-34} J s)
I_{pa}	anodic peak current (cyclic voltammetry)
I_{pc}	cathodic peak current (cyclic voltammetry)
J	coupling constant (NMR spectroscopy)
K	equilibrium constant
k	rate constant
k_B	Boltzmann's constant (1.381 x 10^{-23} J K^{-1})
M	Metal
n	number of moles
n_0	original number of moles
π^*	Kamlet-Taft polarity ability parameter
P	pressure
p	para (1,4- aromatic substitution pattern)
R	ideal gas constant (8.314 J K^{-1} mol^{-1})
S	selectivity
s	number of active surface sites (heterogeneous catalysis)
σ_p	*para*-Hammett parameter
S_0	gas sticking probability
A	surface area
T	temperature

T_{d}	temperature of decomposition
$t_{1/2}$	half-life
Q	reaction quotient (non-equilibrium)
V	volume
χ	mole fraction

List of Numbered Compounds

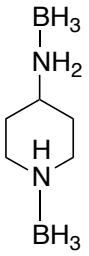

[1]

4-aminopiperidine N,N′-diborane

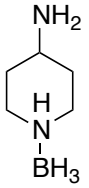

[2]

4-aminopiperidine-1-borane

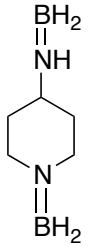

[3]

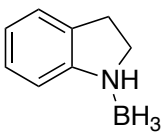

[4]

indoline N-borane

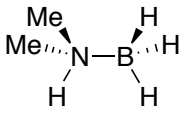

[5]

dimethylamine borane

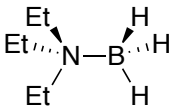

[6]

triethylamine borane

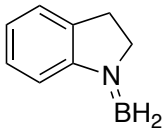

[7]

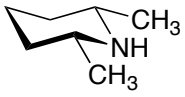

[8]

*2,6-*cis*-dimethylpiperidine*

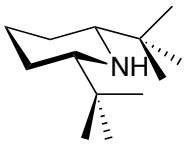

[9]

*2,6-*cis*-di-*tert*-butylpiperidine*

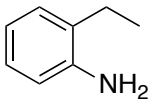

[10]

2-ethylaniline

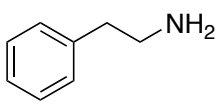

[11]

2-phenylethanamine

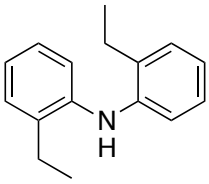

[12]

bis(2-ethylphenyl)amine

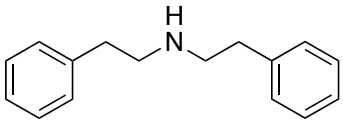

[13]

diphenethylamine

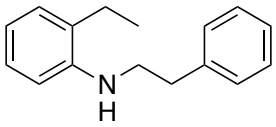

[14]

2-ethyl-N-phenethylaniline

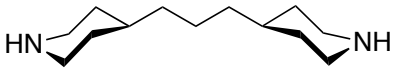

[15]

1,3-di(piperidin-4-yl)propane

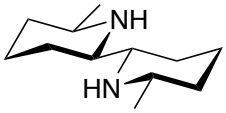

[16a]

6,6′-dimethyl-2,2′-bipiperidine

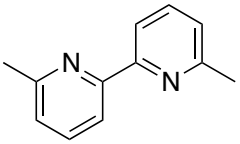

[16b]

6,6′-dimethyl-2,2′-bipyridine

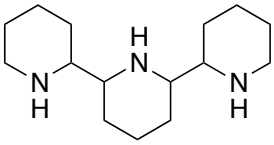

[17a]

2,2′:6′,2′′-terpiperidine

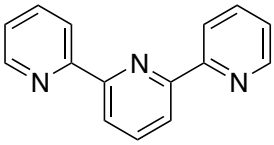

[17b]

2,2′:6′,2′′-terpyridine

Chapter 1 • Introduction

The worldwide energy demand has increased almost 50% since 1980 and steady increases are expected to continue (Figure 1-1).[1] These increases are not surprising if you consider that the planet has an ever-increasing population with continued reliance on technologies powered by electricity in developed countries and rapid technological growth in many developing countries.

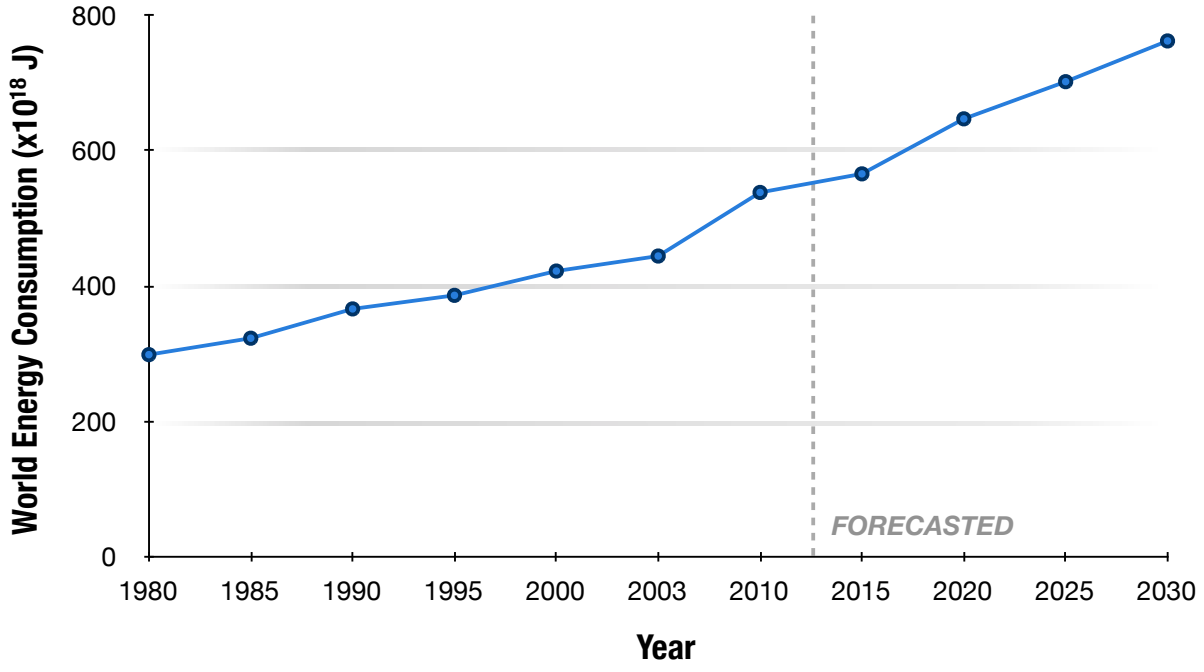

Figure 1-1 • World energy consumption, 1980-2030, adapted from [1].

The increase in energy demand itself is not necessarily a bad thing. The problem arises when the current *sources* of this energy are considered. If one considers that the burning of fossil fuels generates the majority of this energy, the problem becomes more

apparent: such practices will not be sustainable forever. The U.S. Energy Information Administration (EIA) estimated that 69% of the total power generated (not necessarily consumed) in the United States in 2010 was from the burning of coal, petroleum and natural gas. Only 10% comes from renewable resources, with the remaining 21% being supplied by nuclear power.[2] There are numerous problems with the burning of fossil fuels, predominantly depletion of natural resources and generation of air pollutants. The former is troubling in the sense that if all available fossil fuel reserves are depleted before an alternative energy source becomes available, we simply will have no way to produce energy on the scale it is required (currently greater than 5×10^{20} J p.a.). The generation of air pollutants, such as carbon dioxide, is also very disconcerting, especially with growing acceptance of the fact that our activities have started to take a toll on the environment, resulting in ozone depletion, global warming and climate change.[3]

Carbon dioxide, CO_2, has been identified as a greenhouse gas (GHG). GHGs allow the sun's ultraviolet radiation through to the earth's surface yet prevent infrared heat radiated from the surface of the planet from escaping. Large quantities of CO_2 and other greenhouse gases can therefore contribute to a gradual increase in the Earth's temperature. Imagine a car on a summer day with the windows rolled up. The windows are transparent to the incoming visible and ultraviolet radiation from the sun, but as the plastic and leather inside the vehicle start to heat up and release infrared radiation, it is trapped, warming up the car's internal air temperature drastically. Anthropogenic CO_2 production only accounts for a small percentage of the total CO_2 emissions worldwide each year (where the rest comes from animal life and plant decomposition). However, it is enough to make a difference over time. Since the burning of coal and oil as fuels started over 100 years ago, these cumulative effects are

starting to show. It has also been suggested that the situation might only get worse considering CO_2 solubility in water decreases with increasing temperatures: approximately 98% of terrestrial CO_2 is dissolved in oceans.[4] Increasing temperatures due to global warming would cause CO_2 to partition from the oceans into the atmosphere as temperatures rise, further compounding the problem. The time for action is now, then, as the global ecosystem is reaching a point where it can no longer mitigate our use of inefficient energy technology.

Although community energy generation is a large source of CO_2 emissions, transportation of goods and services around the planet is also a huge contributor. Half of all the crude oil burned for energy is done so for transportation, with an even higher percentage in the United States: upwards of two-thirds of the total used.[5] Millions of vehicles are manufactured annually, adding to the millions that are already on the roads, virtually all of them being powered by fossil fuel burning internal combustion engines. In Canada alone, in 2009, it was estimated that there were just over 20.5 million vehicles on public roads, driving over 333 billion kilometers, and burning just under 40 billion liters of gasoline and just over 16 billion liters of diesel.[6,7] It is generally accepted that per liter of gasoline burned, 2.3 kg of CO_2 is released, where for diesel, the number is approximately 2.7 kg L^{-1}.[8] From this, the total CO_2 from all vehicles in Canada in 2009 was approximately 100 billion kg! On a global scale, in 2008, 96 million terajoules (or 9.6×10^{19} J) of energy was consumed by the transportation sector.[9] If one assumes that is all from gasoline, it is equivalent to 2.8×10^{18} L of gasoline (34.66 MJ/L gasoline)[10] contributing 6400 quadrillion (6.4×10^{18}) kg of CO_2, and that's in just one year! With such staggering numbers, it is inevitable that such activity on earth will affect our ecosystem. An alternative is needed, and the implementation of that alternative needs to begin immediately as continued use on this scale will only continue

to aggravate an already bleak situation. While the implementation of any alternative energy to fossil fuels will undoubtedly be a slow and arduous process, the importance is, now, greater than ever.

1.1 • The Hydrogen Economy

Hydrogen, from the Greek *hydro* (water) and *genes* (forming), is the most abundant atom in the universe, making up approximately 90% of all atoms and 75% of the total mass of the universe.[11] On earth, molecular dihydrogen (H_2), a non-toxic gas as standard temperature and pressure, exists in very small amounts, only about 1 ppm by volume in the atmosphere. Most terrestrial hydrogen exists bonded to oxygen in the form of water, while the rest is constituted in organic matter and hydroxide minerals in the earth's crust. Hydrogen gas has many uses (with production in the US reaching over 80 billion L per year), including the Haber process for fixating nitrogen from the atmosphere, and the hydrogenation of animal fats and oils in food production. Hydrogen has, more recently, been suggested as a key component to the future of energy storage and use.

Hydrogen can be used to generate heat (and therefore electricity) by simple combustion (Eq. 1-1).[11] It can also be converted directly to electricity with the use of a fuel cell (see Chapter 1.3). In both cases, the only byproduct of the reaction is water; no CO_2 is produced.

$$H_2 + ½\ O_2 \longrightarrow H_2O \quad \Delta H = 286\ \text{kJ} \qquad \text{Eq. 1-1}$$

Because of this, a significant amount of research has been invested in the development of a hydrogen economy, especially with applications in the transportation industry. Vehicles are one of few technologies that are still powered by the direct, on-board burning of fossil fuels. To date, many prototype vehicles powered by hydrogen have been produced, from bicycles, scooters and golf carts to passenger cars and buses to airplanes, locomotives, boats and submarines.[12] The importance of such research is demonstrated by the significant amount of public funding that has been invested in trying to realize the hydrogen economy. The major contributing governments are those from the European Union, Japan and the United States, spending upwards of $5 billion over the last ten years, about two-thirds of the total global government expenditures for hydrogen funding.[1]

The implementation of the hydrogen economy involves replacing the current energy system, dominated by the burning of fossil fuels to generate heat and electricity, to one dominated by the use of hydrogen gas. The major difference between fossil fuels and hydrogen gas is that the former is a primary energy source, where the latter is a secondary energy source, or energy carrier. A primary source, such as natural gas, coal or oil, is available in its natural state and can be burned directly to produce energy. A secondary energy source, such as electricity or hydrogen, is generated from primary energy sources to be consumed later.

Hydrogen must, therefore, first be generated. It would not be sufficient to simply produce hydrogen from a process powered by the burning of fossil fuels. This would result in the CO_2 produced by burning fossil fuels on board a vehicle being, instead, generated by the burning of fossil fuels at an H_2 production facility. Such point-source

generation of CO_2 may be easier to mitigate using CO_2 sequestration than end-use generation (on board a vehicle); however, this would not be addressing the real problem. The epitome of the hydrogen economy would be the generation of H_2 using renewable primary energy sources such as wind and solar. This would result in a complete elimination of CO_2 production and fossil fuel combustion from the generation, storage and use of energy (save for any that is generated by the construction and maintenance of required infrastructure).

1.2 • Hydrogen Production

As mentioned above, hydrogen gas is a synthetic energy carrier as opposed to a primary energy source. Therefore, it must first be synthesized by using energy obtained from a primary energy source. Preferably these sources would be renewable, such as wind or solar, in order to truly sever the dependence on fossil fuels for energy generation. There are a number of different methods that have been developed for the production of hydrogen gas, including: steam reforming, coal gasification, biomass conversion and water electrolysis.

1.2.1 • Steam Reforming

Steam reforming is, by far, the cheapest and most widely used large-scale method of producing hydrogen gas today. Steam reforming produces approximately 95% of all hydrogen gas used in the US,[13] and can be produced at a cost of $5.60 per GJ of H_2

energy.[14] Natural gas (methane, CH_4) is exposed to steam at high temperatures (700-1000 ˚C) to produce carbon monoxide (CO) and three equivalents of H_2. The CO is then further exposed to steam over a nickel catalyst in the water-gas shift reaction to produce a further equivalent of hydrogen and carbon dioxide (Scheme 1-1).

$$\begin{array}{rcrcrcl} CH_4 & + & H_2O & \longrightarrow & CO & + & 3\,H_2 \\ CO & + & H_2O & \longrightarrow & CO_2 & + & H_2 \\ \hline CH_4 & + & 2\,H_2O & \longrightarrow & CO_2 & + & 4\,H_2 \end{array}$$

Scheme 1-1 • Steam reforming of methane

Despite the fact that natural gas is the cheapest CH_4 feedstock, its use is still two to three times more expensive than refining crude oil to gasoline.[1] Another issue is the fact that this conversion of CH_4 to H_2 is only about 90% energy efficient, meaning that burning the natural gas directly could produce relatively less CO_2 for the same amount of energy (although, burning natural gas is also not 100% efficient).[15]

1.2.2 • Coal Gasification

Coal gasification is one of the oldest methods of producing H_2. It was originally used in Europe and Australia to produce "town gas" before the availability of natural gas was widespread. Coal is heated until it changes to "coal gas," a mixture of CO, H_2, CO_2 and H_2O, and is then mixed with steam over a catalyst to produce synthesis gas (mixture of H_2 and CO). Steam reformation, as described above, can then be used to produce purer H_2. Another alternative is simply to burn the initial synthesis gas product directly to produce heat energy.[1]

1.2.3 • Biomass

Biomass, including agriculture and animal tissues, can also be used to generate H_2 by similar thermochemical processes to those mentioned above. The benefit of using biomass as a feedstock is that it results in almost zero *net* CO_2 emissions because the carbon released was originally taken up from the environment by photosynthesis (although, emissions may be generated during harvesting, transporting, drying and processing of the biomass). The major downside is the immense cost due to limited feedstock availability. Other processes such as fermentation, anaerobic digestion, metabolic processing, etc., are able to produce H_2 from biomass feedstocks; however, they are not nearly as efficient as other methods listed herein.

1.2.4 • Water Electrolysis

Water electrolysis is the simple conversion of electricity into chemical energy (contained in hydrogen) by splitting water. This process produces scrupulously pure H_2, yet its cost is prohibitive due to the immense amount of electricity needed to operate electrolysis on a large scale. The greenness of this process is therefore dictated by the greenness of the process used to generate the electricity in the first place. Using sources such as wind, solar, geothermal, hydroelectric or nuclear results in zero emission production of H_2. Regardless of the source of electricity, the reaction is the reverse of the oxidation of H_2, which has a standard potential of 1.23 V.[16] The process, however, is subject to losses such as polarization and ohmic losses, and therefore an even higher potential (overpotential) must be supplied in order to drive the reaction. For large-scale production, the energy requirement problem is exacerbated because these electrical

losses increase with the current density and therefore the H_2 production rate. Many different catalysts have been developed for water electrolysis, more recently some that mirror the processes of photosynthesis to use sunlight directly. The Nocera group has developed a self-assembled, Co-Ni catalyst that operates in pure water at atmospheric pressure and room temperature to split any water source into H_2 and O_2 using sunlight.[17] Peters and Gray have reported a new cobalt bis(imidopyridine) catalyst for neutral water reduction that is stable to degradation. However, the process requires a significant overpotential.[18] Kohl *et al.* described a different approach for the generation of hydrogen and oxygen gas from water. It, however, required heating to 100 ˚C for the initial thermal decomposition to give hydrogen catalyzed by a homogeneous ruthenium catalyst. The catalyst, now a cis dihydroxo complex, when irradiated between 320–420 nm, liberated oxygen and regenerated the initial ruthenium catalyst.[19]

1.3 • Fuel Cells

> *A fuel cell is an electrochemical "device" that continuously converts chemical energy into electrical energy (and some heat) for as long as fuel and oxidant are supplied.*[22]

The basic idea of a fuel cell was employed as early as 1839 when William Grove used an electrochemical device to reverse the electrolysis of water to produce electricity from hydrogen and oxygen.[20,21] Since then, a significant amount of research has gone into the development of a number of different kinds of fuel cells, all based around the

same basic principles. Major advances came from the National Aeronautics and Space Administration's (NASA) Gemini and Apollo programs where fuel cell technology was developed with the idea of generating electricity and drinking water on-board space shuttles. Many of these advances are still very applicable, and are evident in current fuel cells.[22]

Different types of fuel cells are applicable to different sectors of electricity generation because of their individual characteristics. Phosphoric acid fuel cells (PAFCs), molten carbonate fuel cells (MCFCs) and solid oxide fuel cells (SOFCs) are all technologies that are suitable for large-scale generation of distributed utility electricity. This is due to both their high system output (50 kW – 3 MW) and their high operating temperatures (150-200 ˚C, 600-700 ˚C and 650-1000 ˚C respectively).[23] Alkaline fuel cells (AFCs) work at relatively low operating temperatures of 90-100 ˚C and have high electrical efficiency (60%). These fuel cells are highly sensitive to degradation by CO_2, which is why their usefulness is restricted to specialized military and space applications. While none of these fuel cell technologies are appropriate for vehicular transportation, polymer electrolyte membrane fuel cells (PEMFCs) are an excellent fit for this type of power generation.

PEMFCs have electrical efficiencies of 53-58% (152 – 166 kJ mol^{-1}) for transportation applications.[23] They use a solid organic polymer as the electrolyte, the most common of which is a perfluorinated polymer invented by DuPont™ in the late 1960s and sold under the trade name Nafion® (Figure 1-2). It consists of a polymerized tetrafluoroethylene (PTFE) backbone, which makes it virtually chemically inert, with perfluorinated vinyl polyether side chains terminated by sulfuric acid groups. The sulfuric acid groups give the polymer its proton exchange abilities. The membrane must also act as an electrical insulator to prevent electrons from passing through and

thus allowing for electrical power generation. The molecular weight of the polymer is difficult to determine because of its insolubility, and therefore, its incompatibility with the usual techniques for determining molecular weight (light scattering and gel permeation chromatography). Instead, the polymer is described commercially by its equivalent weight (EW) and membrane thickness. The EW of Nafion is the number of grams of dry Nafion per mole of sulfonic acid groups, and can be determined by a simple acid-base titration.[24] Different versions of Nafion have been synthesized with varying values of x, y, and z (Figure 1-2). The most common, however, is Nafion 117 (EW = 1100, 172 μm thick).

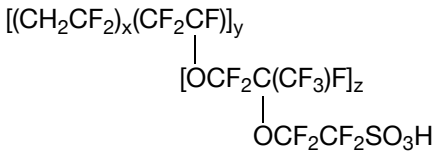

Figure 1-2 • Structure of Nafion® by DuPont™.

In a PEMFC, not unlike other types, hydrogen is used to produce electricity, which can be used, for example, to power a vehicle directly or charge a battery for that purpose. Pure hydrogen is supplied to the anode of the fuel cell where, catalytically, hydrogen atoms and electrons are separated in the hydrogen oxidation reaction (Eq. 1-2).

$$H_2\,(g) \longrightarrow 2\,H^+\,(aq) + 2\,e^- \quad E^0 = 0\ V\ (\text{by definition}) \qquad \text{Eq. 1-2}$$

The protons produced are able to selectively transfer through the membrane (such as Nafion) by the *Grotthuss mechanism*[25] where protons "hop" through the acidic channels of the membrane. In reality, it is not a single proton that is moving through the system, but rather a reorganization of the oxygen-hydrogen bonding networks of

the sulfonic acid end groups and water molecules so that an "excess" proton can be transported through the membrane (Figure 1-3). For this reason, Nafion must be hydrated by water to operate. The electrons produced are forced through an external circuit, because the membrane is an electrical insulator. This allows the generation of electricity.

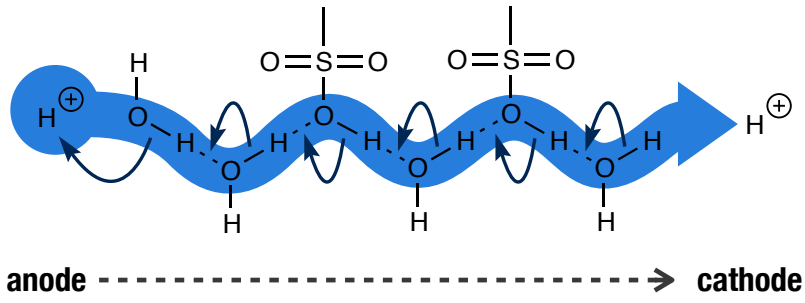

Figure 1-3 • Grotthus, or "proton-hopping," mechanism.

Once the protons reach the cathode, they are recombined with the electrons as they are oxidized by oxygen being delivered, usually in the form of air (Eq. 1-3). The products of this reaction are water and heat, which are simply expelled from the system.

$$O_2\,(g) + 4\,H^+\,(aq) + 4\,e^- \longrightarrow 2\,H_2O \quad E^0 = +1.229\ V \qquad \text{Eq. 1-3}$$

The cathode and anode reactions are both mediated by heterogeneous, precious metal catalysts (Pd, Pt, Ru), usually immobilized on carbon paper or cloth. This allows for rapid reactions and efficient power generation by the fuel cell. The metal nanoparticles must be able to receive protons from the membrane and electrons from the external cell. This is usually accomplished by using an electronically conductive catalyst support (such as carbon), and ensuring that the support is partially embedded in a proton-conductive polymer, which may be the same as or different from that used for the PEM itself. Fuel cells also include electrically conductive flow plates to collect

and deliver electrons. These flow plates have channels etched in them to allow reactive gases to be distributed over the entire electrode. A schematic of a fuel cell is shown in Figure 1-4.

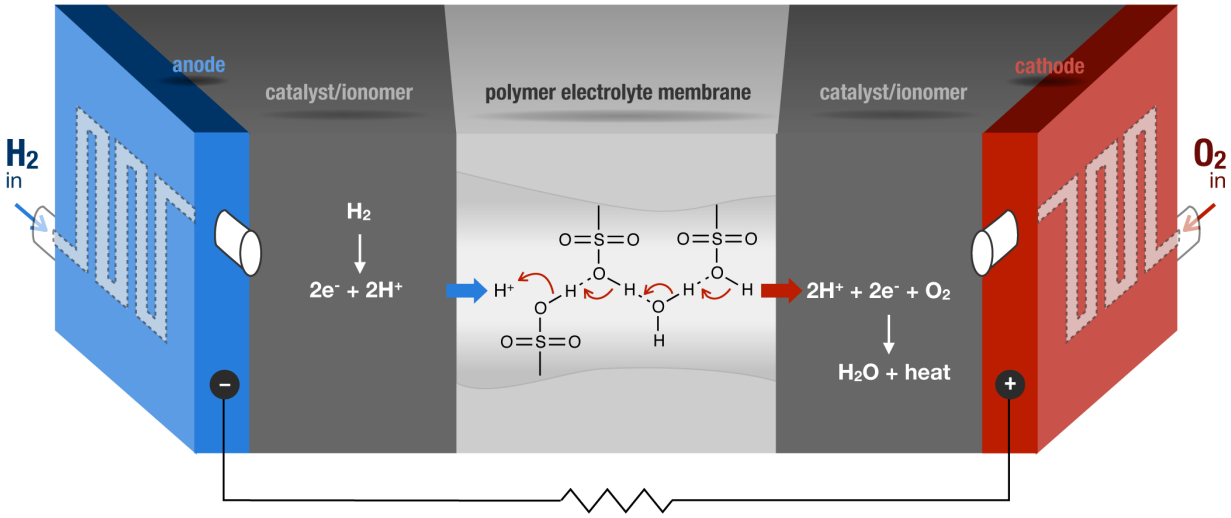

Figure 1-4 • Schematic of a polymer electrolyte membrane fuel cell.

1.4 • Hydrogen Storage Technology

Despite the significant amount of research devoted to the development and optimization of fuel cells for a wide range of energy generation applications,[26] there has been a significantly less amount of research done toward the development of portable hydrogen sources appropriate for vehicular transportation until recently. In 2005, the US Department of Energy issued a set of guidelines that potential hydrogen fuel systems should meet after 2010 and 2015. In 2011, after significant research in the field showed that these benchmarks were unreasonable, they were adjusted. The original

guidelines for 2010 were pushed to 2017. These new guidelines for 2017 include a net system gravimetric capacity of 5.5 wt% hydrogen and volumetric capacity of 40 (kg H_2) L^{-1}. These values must be calculated using the maximum system mass or volume, including the tank, material, valves, regulators, piping, mounting brackets, insulation, added cooling capacity, and/or other balance-of-plant components. Additionally, a cost ceiling of $2-4 per gas gallon equivalent for power produced is imposed.[27] While these gravimetric and volumetric capacities include all system components, values reported in the literature (and those reported herein) usually neglect the weights of these components and speak only of the material itself. This is mostly because the weight of the final system would be mostly unknown until implementation, and could vary greatly depending on the system's engineering. Other parameters such as flow rate and fueling time are also important, but at a later stage of fuel development. Ideally, any hydrogen storage medium developed could be implemented without extensive reconstruction of the current fuel distribution infrastructure while meeting all of the requirements delineated above. There are five main categories of hydrogen storage materials being considered for vehicular transportation: compressed and liquefied hydrogen, physically adsorbed hydrogen, metallic hydrides, complex hydrides and organic hydrides.

1.4.1 • Compressed and Liquefied Hydrogen

Compressed and liquefied hydrogen are the simplest methods of storing hydrogen, but both strategies have significant drawbacks. Compressed hydrogen at 298 K and an operating pressure between 350 and 750 atm[28] has a density between 23.6 and 41.5 kg m^{-3} (Figure 1-5).[29] These values do not include the added volume of the tank and

other components, and with these considerations, it is unlikely either case would result in a system that meets the 2017 DOE benchmarks. One should note that there is little room for improvement in the maximum storage densities of compressed or liquefied hydrogen; the only headway to be made is with the design of lightweight, low-volume storage tanks. Incorporating adequately sized and shaped tanks is also a major challenge. Another drawback is the cost associated with compressing or liquefying the hydrogen. Despite these challenges, compressed hydrogen still offers the best overall performance and is the most mature of all the technologies discussed. This is evident from the fact that it is already being employed for larger vehicles such as public city buses.[30] Also, Honda has recently unveiled a hydrogen-powered vehicle using compressed hydrogen; however, an estimated driving range of 386 km[31] is somewhat limiting.

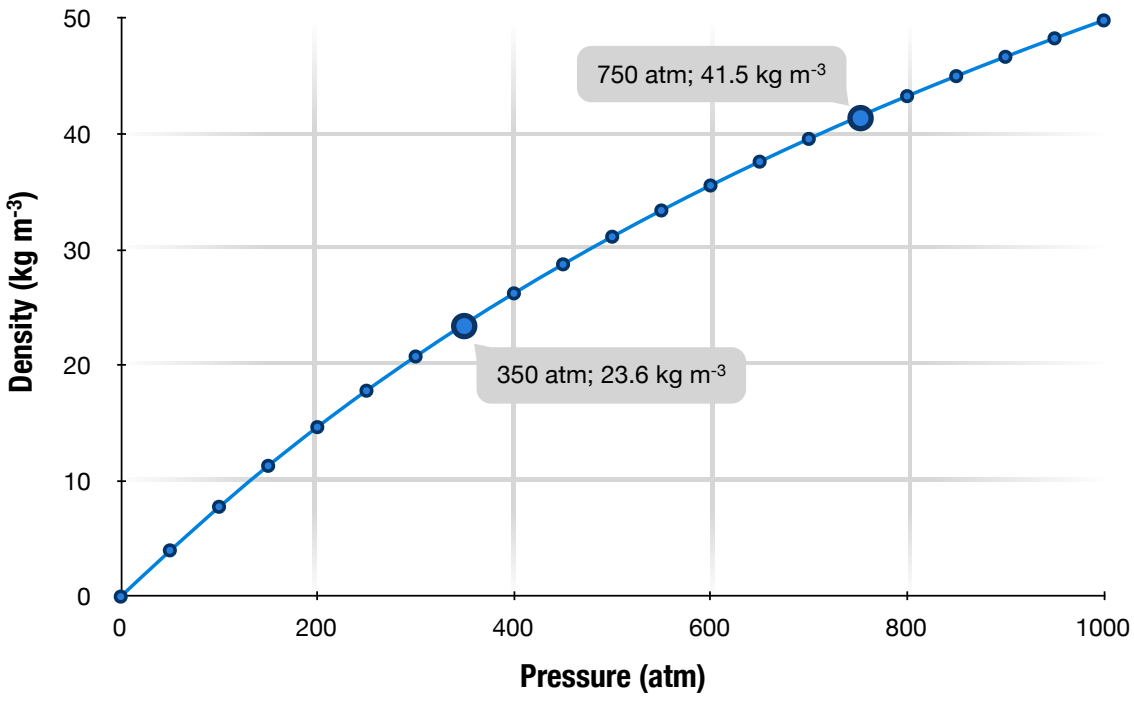

Figure 1-5 • Density of molecular hydrogen under various pressures.[29]

Liquid hydrogen is no longer seen as a viable strategy for vehicular transportation; there are simply too many technological challenges of housing the cryogenic liquid, mostly with regard to temperature management.[28] The liquid must be kept at between 20-30 K, significantly lower than the average surroundings temperature (~300 K). This results in a significant amount of thermal conduction through pipes, cables and mountings to the storage vessel, as well as thermal radiation from the surroundings. Even with significant insulation efforts involving multi-level vacuum layers and metal foil wrapping, it is estimated there is still a constant, unavoidable heat input of 2-3 W. This results in significant hydrogen off-gassing to maintain acceptable pressures within the tank as liquid hydrogen evaporates. Another drawback to the use of both compressed or liquefied hydrogen is the need to completely overhaul the current fueling infrastructure to distribute the new fuel to the public.[32]

1.4.2 • Physically Adsorbed Hydrogen

It is possible to physically adsorb hydrogen molecules onto the surface and into the pores of various materials such as zeolites, porous carbons and metal-organic frameworks (MOFs). The biggest drawback to this kind of storage is the need for cryogenic temperatures. The adsorption of hydrogen onto such surfaces involves very weak van der Waals interactions with enthalpies of adsorption on the order of 2-5 kJ mol^{-1}.[33] Because of this, very low temperatures (-196 ˚C) and/or high pressures must be reached and maintained for any significant hydrogen uptake by the material. This, by itself, is one of the largest technical barriers to this technology's use. The hydrogen adsorption capacity of these materials is proportional to their specific surface area and the structure and size of the pores. There is general agreement in the literature

of a linear relationship between the surface area and the hydrogen storage capacity. At -196 ˚C and several MPa H_2 the relationship is approximately 1.9×10^{-3} wt% H_2 g m^{-2}. At atmospheric pressure (0.1 MPa H_2), the value is reduced to 1.3×10^{-3} wt% H_2 g m^{-2}.[34]

Zeolites, crystalline materials with an open, three-dimensional structure, have also been proposed for physical adsorption of hydrogen. However, even the zeolite with the highest known pore volume (ITQ-33)[35] would only be able to theoretically store 2.5 wt% H_2. This makes their use for vehicular storage of limited utility. Carbon materials also suffer from poor storage capacities.

A graphene sheet, with adsorption on both sides, has an estimated surface area of 2630 m^2 g^{-1} (thought to be the maximum able to be achieved with carbon materials),[36] and would have a gravimetric storage density of only about 3.4 wt%.

MOFs are comprised of cubic networks of molecules with metal atoms at the vertices connected by organic molecules. They have very high surface areas, and very small pores. It has been estimated that their capacity is also proportional to the surface area at around 1.1×10^{-3} wt% g m^{-2},[37] but this value has been shown to be extremely temperature dependent. Some MOFs have been shown to have an uptake of 7.5 wt% H_2 at -196 ˚C and high pressure. At atmospheric pressure, the capacity drops to 1.6 wt%.[38] The idea of using MOFs for physical adsorption is still in its infancy and it is unknown whether a suitable system may be available in the future, yet none with all of the technical requirements has yet been discovered.

1.4.3 • Metallic Hydrides

Most metals can form hydrides when exposed to hydrogen at appropriate temperature and pressures.[39] Transition metals tend to form non-stoichiometric

hydrides where multiple metal atoms share each hydrogen molecule (such as $PdH_{0.6}$). Lighter metals, those in Groups 1 and 2, tend to form stoichiometric hydrides that have ionic character.[40] The biggest issues with metal hydrides for hydrogen storage applications are reversibility, fast hydrogen update and release kinetics and favorable thermodynamics (H_2 release temperature). Hydrides of light metals are advantageous, as they tend to give better gravimetric hydrogen capacity due to the low weight of the metals involved. Usually, however, they also have high enthalpies of formation (ΔH_f), an endothermic process for stable hydrides. Presuming that the uptake of hydrogen is reversible, the enthalpy of release is the negative of the enthalpy of uptake (formation), and this value is directly proportional to the decomposition temperature (T_d). From simple thermodynamics, when the $\Delta G = 0$, and the release reaction becomes spontaneous:

$$\Delta G = 0 = \Delta H - T_d \Delta S \qquad \text{Eq. 1-4}$$

$$T_d = \Delta H / \Delta S \qquad \text{Eq. 1-5}$$

Assuming there is little entropy change in the solid phase, the ΔS of the reaction is proportional to the entropy of the hydrogen released into the gas phase, which is similar for all hydrides (relative to the number of hydrogen molecules released per mole of the hydride); on average, for simple metal hydrides, this is about 130 J K^{-1} per mole of hydrogen. Also, theoretical calculations indicate that the change in entropy for complex metal hydrides is between 100 and 130 J K^{-1} per mole of hydrogen.[41] Therefore, the higher the value of T_d for the hydride, the larger the $-T_d \Delta S$ term becomes, the more favoured the reaction will be (as ΔG decreases and becomes negative). This, however, must be balanced with the fact that the higher the T_d, the more energy input is required to induce hydrogen release.

The enthalpy of the dehydrogenation reaction can be made more negative by stabilizing the dehydrogenated state, or by destabilizing the hydrogenated state, of the hydride. This has been accomplished by introducing other hydrides as additives. For example, the release of H_2 from $LiBH_4$ (wt% H_2 = 13.6) has a ΔH of 67 kJ (mol H_2)$^{-1}$. The addition of half an equivalent of $MgBH_4$ lowers the ΔH to 42 kJ (mol H_2)$^{-1}$, the combined system having a gravimetric capacity of 11.4 wt% H_2.[42] There are many other studies that also show effective enthalpy lowering by the addition of destabilizing additives.[43-45] A recent computational study by Alapati *et al.* looked a wide range of destabilizations by Group 2 and 3 hydrides. Whether these are physically practical is yet to be seen; however, a number of hydride combinations gave calculated enthalpies of formation of 25-30 kJ mol^{-1}, the target range for good thermodynamic and kinetic properties.[46] Continued development of these systems is still needed, as a metal hydride that can be easily regenerated, with fast H_2 update and release kinetics that also meets other DOE targets, has yet to be found.

1.4.4 • Organic Hydrides

Organic hydrides, including non-metal hydrides (amine boranes) and organic liquids (cycloalkanes and heterocycles), have shown potential for vehicular hydrogen storage applications.[32,47,48] They both store and release hydrogen chemically. Their use for vehicular fueling would involve an on-board chemical reaction to release hydrogen from the carrier, followed by an off-board recycling by re-hydrogenation (Figure 1-6).

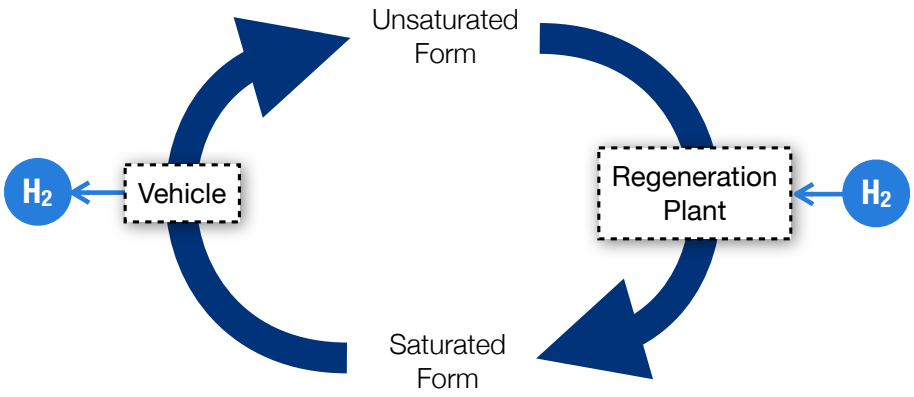

Figure 1-6 • Proposed hydrogenation cycle for organic hydrides.

For organic liquids, there are a number of studies in the literature where both homogeneous[49-53] and heterogeneous[54-55] catalysis are used to allow these reactions to occur with lower heat demands. Cyclohexane can be catalytically dehydrogenated to benzene, as can methylcyclohexane to toluene. Although aromatization occurs in both of these dehydrogenation reactions, further stabilizing the products relative to the reactants, the heat requirements are still too high.[56] It is known that the enthalpy of dehydrogenation of piperidine is much lower than that of cyclohexane: The replacement of one CH_2/CH fragment in cyclohexane/benzene with a NH/N fragment (to give piperidine/pyridine) results in a reduction of the heat of dehydrogenation by 24.2 kJ mol^{-1}. Crabtree and coworkers have performed computational studies using the 6-31++G** basis set to show the effect of further incorporation of nitrogen atoms and the dependence on their relative position.[48] Incorporation at the 2-position proved unfavourable, while incorporation at the 3- and 4-positions led to decreases in the reaction enthalpy of 22.1 and 15.7 kJ mol^{-1}, respectively, as shown in Figure 1-7. In the same publication, Crabtree *et al.* also discussed experiments where the dehydrogenation reactions of a number of fused ring compounds were examined experimentally. These

compounds included those where the saturated N-containing heterocycle was fused with an aromatic ring. The fused aromatic ring offers a further reduction in the reaction enthalpy because of conjugation with the forming double bond.

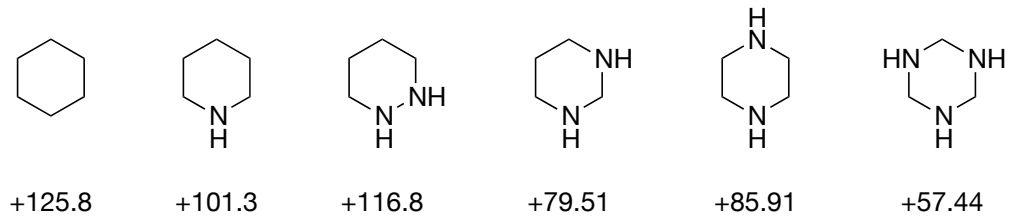

Figure 1-7 • Dehydrogenation enthaplies of various N-heterocycles (kJ mol^{-1})[48]

It has also been reported that the addition of electron donating and conjugating groups outside a piperidine ring will accelerate the rate of dehydrogenation and offer more favourable thermodynamics.[57] For non-conjugated substituents, a linear relationship was found between the Hammett parameter (σ) and the dehydrogenation enthalpy (calculated from experimental data). This was also verified by a number of experiments. The addition of conjugated groups outside the ring also resulted in a more rapid dehydrogenation and a lower dehydrogenation enthalpy compared to piperidine itself. This was demonstrated by the fact that piperidine-4-carboxamide underwent complete dehydrogenation much faster than would have been expected based simply on its σ-value.

Non-metal hydrides ($LiBH_4$, $NaBH_4$, etc) can be dehydrogenated via two exothermic processes that are both usually mediated by heterogeneous catalysis.[47] The first of these dehydrogenation processes is hydrolysis. This process involves the reaction of a chemical hydride with water to produce hydrogen (and heat) as in Scheme 1-2.[47] There are, however, some disadvantages to using an aqueous environment in hydrogen fuel systems. First, there would be a significant decrease in the maximum

possible gravimetric density of the system because the addition of further system components (i.e. water and related delivery apparatus) would increase the total system mass without increasing the mass of available hydrogen. This could be partially mediated, however, if the water for the dehydrogenation reaction was recycled from that generated by operation of the fuel cell. It has also been demonstrated that overcoming the energy barrier associated with the regeneration of the original chemical hydrides from the hydrolysis products is, thus far, prohibitive.[58] One major advantage of the exothermic hydrolysis of chemical hydrides is that the reaction takes place (and generates hydrogen) at room temperature.

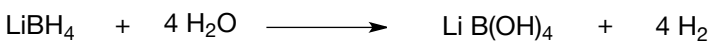

Scheme 1-2 • Hydrolysis of $LiBH_4$

The second dehydrogenation scheme is pyrolysis, where hydrogen is evolved upon decomposition at elevated temperatures. After the decomposition temperature is reached, the reaction then proceeds exothermically. Each equivalent of H_2 is evolved at successively higher temperatures. For example, $LiBH_4$ undergoes pyrolysis to produce hydrogen as shown in Scheme 1-3.[47] A temperature of 108 °C is required to produce only one mole of H_2 for every mole of $LiBH_4$, where much higher temperatures are required to evolve the second and third equivalents. These high temperature requirements are the most significant disadvantage of pyrolysis (over hydrolysis) as reaching these high temperatures would require the input of a significant amount of energy, and would decrease the overall energy efficiency of the system.

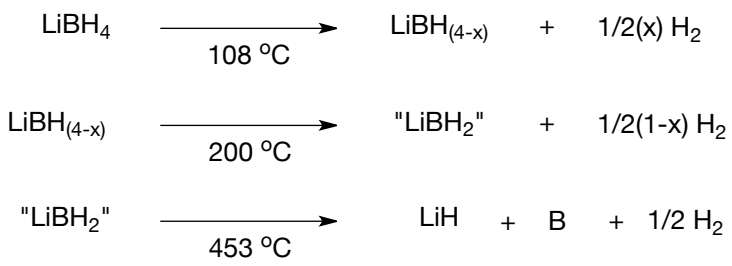

Scheme 1-3 • Pyrolysis of $LiBH_4$

Alternatively, ammonia borane ($H_3N{:}BH_3$) and substituted amine boranes ($R_3N{:}BH_3$) have shown promise for hydrogen storage applications, as they do not require such high temperatures for thermal decomposition. These boranes contain two different types of hydrogen atoms; the N—H hydrogen atoms are protic ($H^{\delta+}$) and the B—H hydrogen atoms are hydridic ($H^{\delta-}$). Hydrogen is evolved by the combination of one of each of these hydrogen atoms to form H_2, which allows dehydrogenation to occur at lower temperatures. Additionally, the B—N bond is strong enough that loss of H_2 is energetically favoured compared to the dissociation of the ammonia and borane fragments.[32] Also, these boranes have relatively high hydrogen storage densities because nitrogen and boron are relatively light elements compared to those found in other hydrides. A problem, however, is that ammonia borane produces borazine and higher order polymeric structures (polyborazylene) as part of a complex product mixture (Scheme 1-4). Not only can borazine poison the fuel cell, it has proven difficult to convert back to the ammonia borane.[59] More recently, some strategies for regenerating ammonia borane have been suggested in the literature. One example is the conversion of a mixture of borazine and polyborazylene, almost quantitatively, back to ammonia borane after exposure to high-pressure hydrazine (N_2H_4) and liquid ammonia (NH_3) at 40 ˚C in a sealed pressure-vessel.[60] While this strategy may be energetically demanding and experimentally cumbersome, it is a step in the right

direction for the future of ammonia borane as a possible hydrogen storage material. With improvements in catalysis also come improvements in the selectivity of the reaction for only one product, which can seriously aid in achieving efficient regeneration.

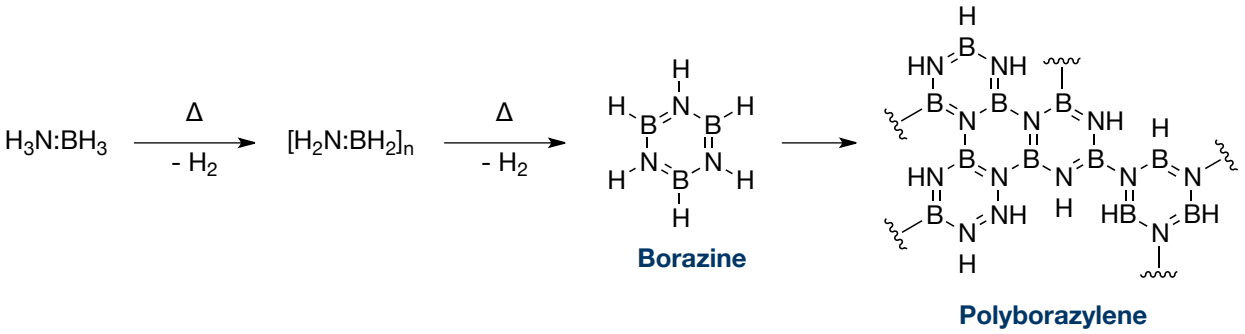

Scheme 1-4 • Formation of borazine and polyborazylene from ammonia borane.

Secondary amine boranes such as dimethylamine borane ($HNMe_2$:BH_3), produce dimers, instead of oligomers and polymers, via the dehydrocoupling reaction shown in Scheme 1-5. These adducts can be more easily regenerated.[61] It has been shown that $HNMe_2$:BH_3 can undergo catalyzed dehydrocoupling at room temperature when using a solvent (usually toluene) or neat at 45 °C ($HNMe_2$:BH_3 has a melting point of 35 °C), using a number of carbon supported metal catalysts (Rh, Ir, Ru and Pd).[61]

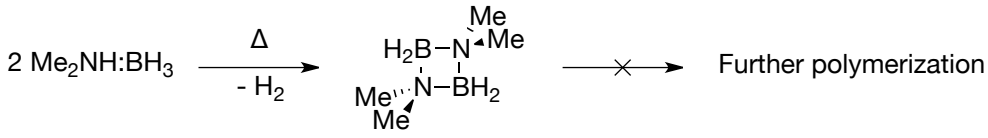

Scheme 1-5 • Dehydrocoupling of $HNMe_2$:BH_3 to give a cyclic dimer.

Despite significant research and development thus far, no examples of organic hydrides have proven adequate for vehicular hydrogen storage.

1.4.5 • Hybrid Hydrogen Storage

The Jessop and Davis groups proposed the idea of a "hybrid hydrogen storage" system in 2008, [62] in which two classical carriers, one that dehydrogenates exothermically and one endothermically, are combined. In this system, a heterogeneous catalyst would promote the dehydrogenation of both carriers where heat from the exothermic dehydrogenation reaction would drive the endothermic reaction.

The combination of an endothermic and an exothermic carrier into one system where both store hydrogen should offer a substantial improvement over the use of either of these systems independently. Primarily, the combination would establish a heat balance, allowing for greater overall efficiency, as the heat required for the endothermic reaction would be generated *in situ* by the exothermic reaction. The overall system should, however, be slightly net endothermic to prevent run-away reactions. Presuming both reactions are reversible, a heat balance for the off-board regeneration would also exist. A hybrid hydrogen storage system would require an endothermic and an exothermic carrier that are 1) miscible in both saturated and unsaturated forms, 2) mutually inert and 3) offer sufficient gravimetric and volumetric hydrogen storage capacities when combined. They must also both be able to be dehydrogenated under reasonable conditions by the same catalyst, while mixed with each other, without adverse effects.

Previously, there were limited examples of similar systems reported. In 2006, Gelsey published a patent describing a similar idea with the hydrolysis of $NaBH_4$ as the exothermic system and a metal hydride as the endothermic system. In this example, however, the carriers were physically separated from one another so that the advantage of a liquid mixture was not obtained.[63] In 2007, Thorn *et al.* demonstrated the use of a

mixed ammonia borane and perhydronaphthalene system at 250-280 ˚C, although they observed significant degradation, and did not identify any boron- or nitrogen-containing products.[64] In the same patent, they also discussed the use of non-hydrogen releasing reactions to supply heat for the release of H_2 from an endothermic carrier.

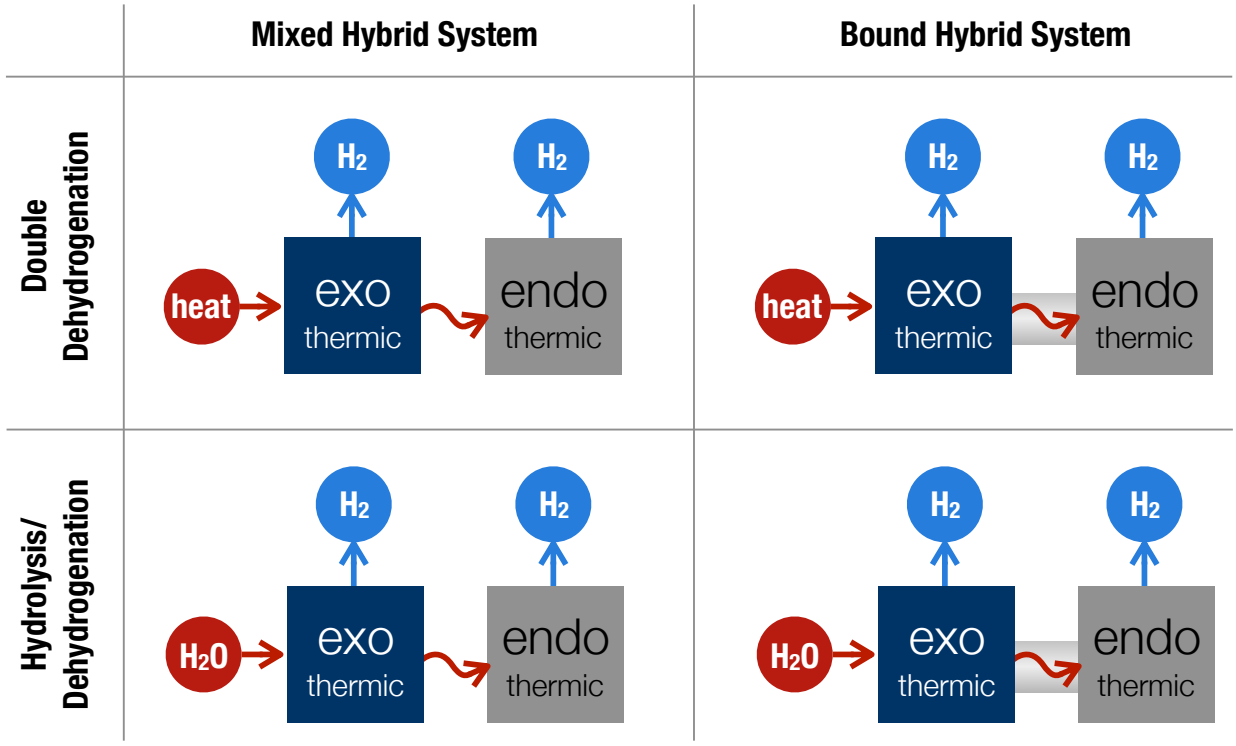

Figure 1-8 • Summary of different proposed hybrid system categories.

Four different categories of hybrid hydrogen storage systems have been proposed by our group, depending both on the type of dehydrogenation reaction being employed (hydrolysis or pyrolysis) and whether the two components are physically mixed or chemically bonded (Figure 1-8). The endothermic moiety can undergo thermal dehydrogenation while the exothermic moiety can undergo either hydrolysis or pyrolysis. When the two compounds are physically mixed, the systems are denoted dehydrogenation/hydrolysis (DH) and double dehydrogenation (DD) mixed hybrid

systems (MHS) respectively. For a system where the moieties are physically bonded to each other, they are denoted by dehydrogenation/hydrolysis and double dehydrogenation bound hybrid systems (BHS) respectively. The development of these systems was part of the work that will be discussed herein. (Chapters 4.1 and 4.1.2).

1.5 • Heterogeneous Catalysis

> *This new force, which was unknown until now, is common to organic and inorganic nature. I do not believe that this is a force entirely independent of the electrochemical affinities of matter; I believe, on the contrary, that it is only a new manifestation, but since we cannot see their connection and mutual dependence, it will be easier to designate it by a separate name. I will call this force catalytic force. Similarly, I will call the decomposition of bodies by this force catalysis, as one designates the decomposition of bodies by chemical affinity analysis.*
>
> *- Jöns Jacob Berzelius*[65]

Our knowledge about catalysis has come a long way since J. J. Berzelius first coined the term back in 1836. Today, the International Union of Pure and Applied Chemistry (IUPAC) defines a catalyst as *a substance that increases the rate of a reaction without modifying the overall standard Gibbs energy change in the reaction*.[66] In other words, it is a substance that increases the rate of a reaction by lowering the activation energy ($\Delta G^{\ddagger}$) without being used or modified in the process. In actuality, however, it is

possible that the catalyst *does* change over the course of the reaction, but is reconstituted to its original form at the end of the *catalytic cycle*. In this case, it is easier to think of the catalyst as something that is both a reactant and a product in a chemical transformation.

Today, over 90% of all chemical manufacturing processes use catalysts in one form or another.[67] In homogeneous catalysis, the catalyst is in the same phase as the other reactants, while in heterogeneous catalysis the reaction occurs at, or near, an interface between phases, usually between a solid catalyst and a liquid or gaseous reaction mixture. Homogeneous catalysis is better understood than heterogeneous catalysis as it can be probed with standard spectroscopic techniques such as NMR and IR spectroscopies. Homogeneous catalysis allows for high selectivity through selective binding of the reacting molecule to the metal centre as influenced by the size and shape of other ligands. Alternatively, heterogeneous catalysis has many advantages, despite the mechanisms of associated surface reactions being less understood. It allows for relative ease of separation due to the different phases, usually by simple filtration or venting. Heterogeneous catalysis is also easy to implement in continuous processes as the catalyst is immobilized and a reaction mixture can easily be passed over the catalyst in a flow system. Also, heterogeneous catalysts are typically robust and tolerant of extreme conditions, especially compared to their homogeneous counterparts. Whereas heterogeneous catalysis is a major component of this work, a brief explanation of the field is presented here.

1.5.1 • Surfaces

Heterogeneous catalysts are composed of small clusters of metal atoms finely distributed over a surface of an inert material, known as the support (Figure 1-9A).

Common catalytic metals include iron, zinc, nickel, copper, gold, platinum, palladium and ruthenium. Common supports include silica (SiO_2), alumina (Al_2O_3) and carbon (C). Supports are usually specially synthesized to express the largest surface areas possible, with many pores to allow for more metal clusters. The metal atoms are separated into small clusters of atoms where the different morphologies and arrangements can make differences in the activity and selectivity for different reactions. The specifics of these effects are not well understood, and are usually discussed in the literature for a particular reaction, under a specific set of circumstances, in a comparative way. The arrangement of the atoms on the faces of the clusters can have huge effects on reactivity. In Figure 1-9B, two different faces of rhodium are annotated: the (111) face and the (100) face.

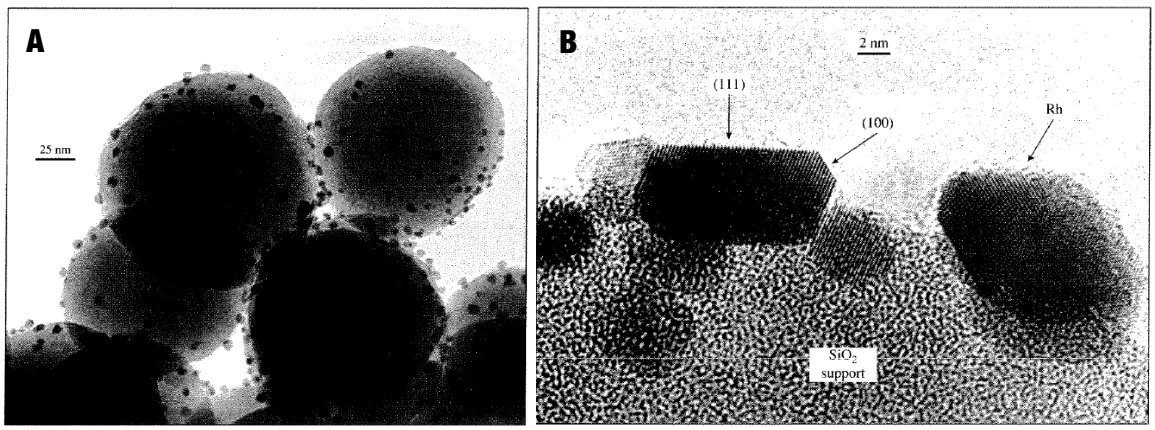

Figure 1-9 • A) Rhodium supported on silica particles, B) High resolution micrograph showing low-index faces. Reprinted, with permission, from [68].

The shorthand descriptions of the faces, (111) and (100), are known as Miller indices. They are determined by looking at where the plane of face intersects the unit cell of the cluster. The atoms and their arrangement on the surface of these faces, therefore, depend on what type of unit cell the metal atoms adopt. Two common types

of crystal packing are face-centered cubic (FCC, *e.g.* Rh, Pd, Pt) and body-centered cubic (BCC, *e.g.* Fe), as shown in Figure 1-10. This figure also shows the arrangement of atoms of three different possible faces of an FCC crystal: the (100), (110) and (111) face. These are by no means a representative sample of all of the available faces, many of which could be present on a single cluster of atoms; for example, a rounded cluster would have many faces contributing to the curvature (Figure 1-11).

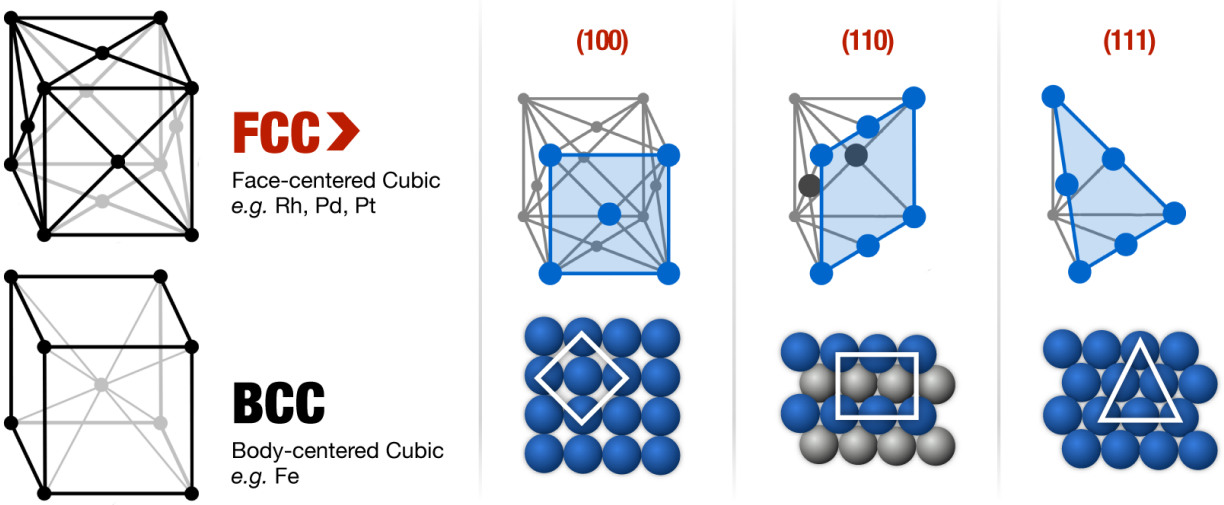

Figure 1-10 • Schematic of different cubic crystal unit cells and the (100), (110) and (111) face of a FCC crystal.

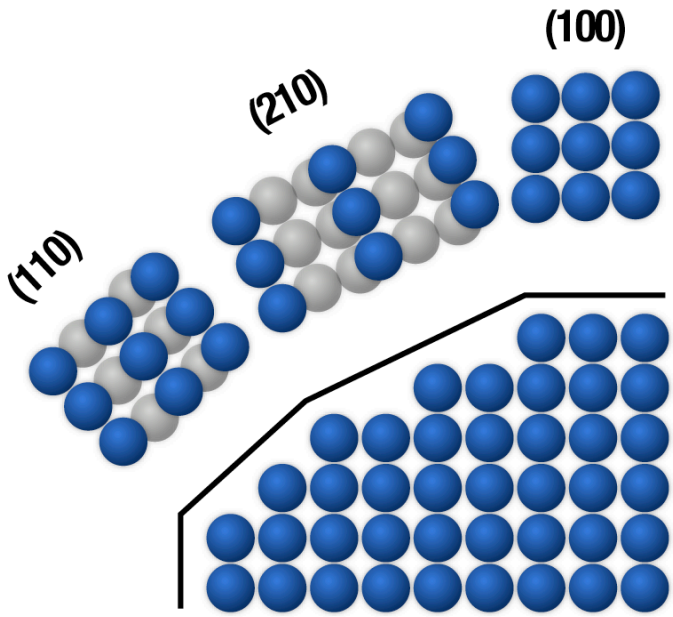

Figure 1-11 • Many different faces contribute to the curvature of a metal atom cluster.

Different faces promote binding with different molecules based on an arrangement of metal atoms that is complimentary with the orbitals of the molecule that participate in binding. There are other characteristics, however, that also contribute to differences in reactivity: surface defects. These occur on many faces, but are especially prevalent on faces where one index is much larger than another, giving a gradually sloping, stepped surface with many terraces (Figure 1-12). The types of defects include islands (small, single layer of more than two atoms on top of a terrace), holes (where a single atom is missing from the terrace), kinks (where steps are not continuous) and adatoms (single atoms sitting atop a terrace). All of these can affect the selectivity. Since it is often hard to know the exact composition of the surface of the particle, deconvoluting these effects is essentially impossible in real systems. Model systems have been developed where single layers of metal atoms are assembled to have a particular face identity, allowing one to study the performance of one face at a time as well as investigate support effects.[69,70] Some methods for synthesizing catalysts are

employed to generate surfaces with many defects, or few defects, depending on the desired reactivity, but this information is gained empirically and usually qualitatively.

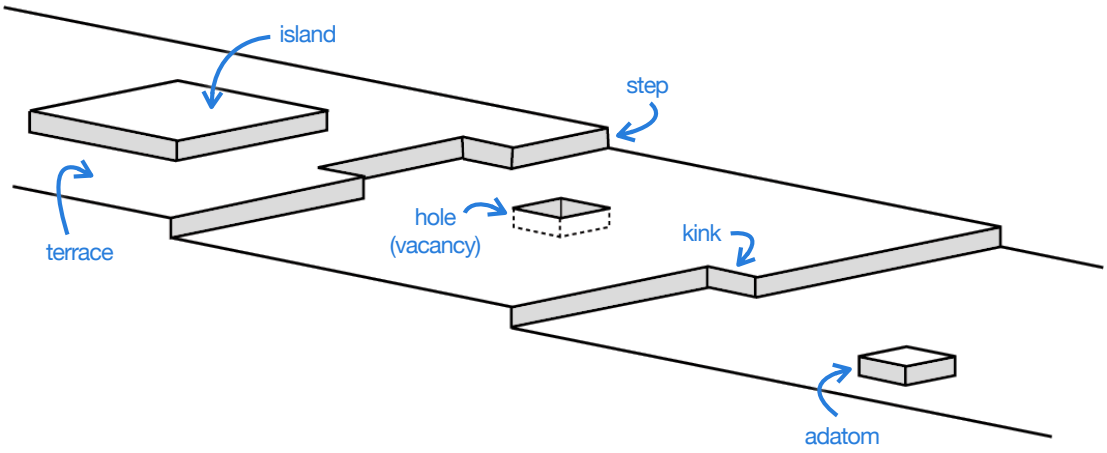

Figure 1-12 • Stepped surface showing different defects

1.5.2 • Adsorption

The first step in any heterogeneously catalyzed chemical reaction is the adsorption of the reacting molecule(s) on to the metal surface. The amount of a molecule that can be adsorbed onto the surface of a catalyst particle is proportional to its surface area (measured in m^2), often reported as the *specific* surface area, or the surface area per unit mass (measured in $m^2\ g^{-1}$). It is important to note the difference between *ad*sorption, which is involved in catalysis, and *ab*sorption. The latter happens within the bulk of the absorbing material (as opposed to at the surface) and the amount taken up is proportional to volume instead. As discussed in Chapter 1.4.2, there are two types of adsorption, chemical adsorption (chemisorption) and physical adsorption (physisorption). The former results in activation of the adsorbed molecules as chemical bonds are formed between the adsorbate and the metal surface. Chemisorption comes with some specificity, where only certain adsorbate-adsorbent combinations are

possible. This is reasonable considering the fact that new chemical bonds are being formed. Because there are bonds being formed between the surface and adsorbate, only a monolayer of the chemisorbed molecules is possible. Physisorption, alternatively, involves much weaker interactions that do not activate the molecules, and allow for more than one layer to adsorb to the surface.

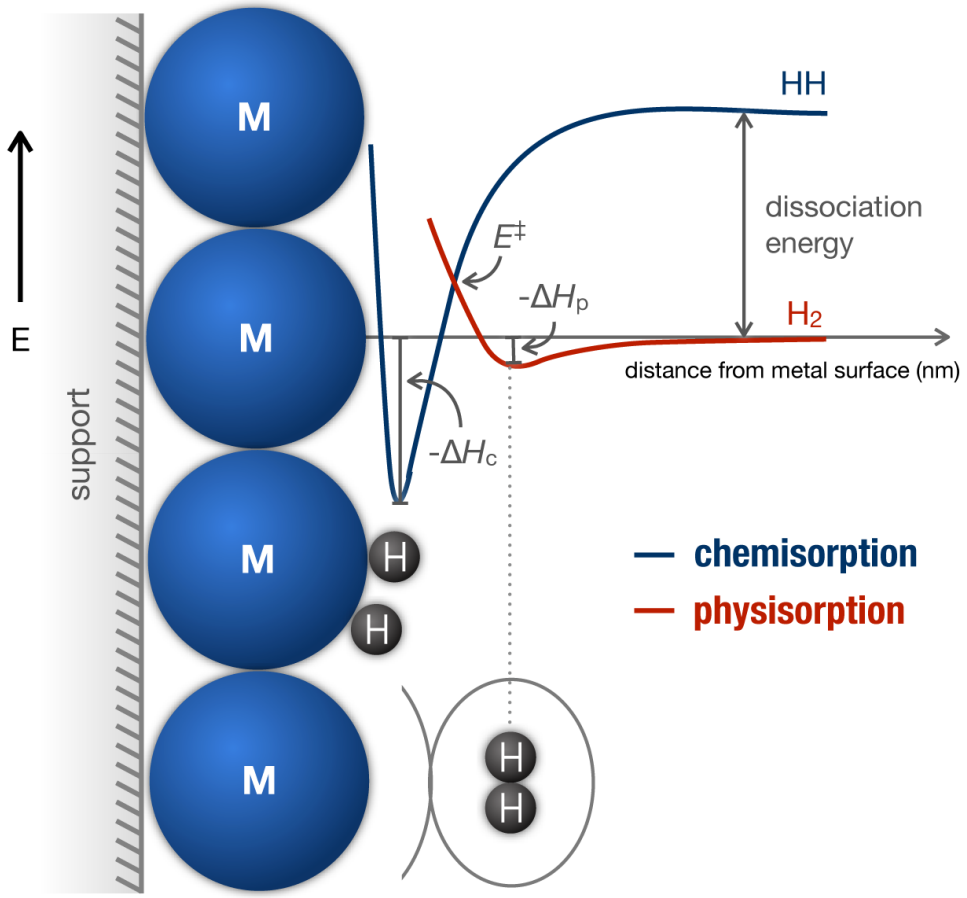

Figure 1-13 • Chemisorption vs. physisorption of H_2 on a metal surface

The difference between chemisorption and physisorption is demonstrated in Figure 1-13. As an adsorbate approaches a metal surface, there are two distinct energy minimums that can be achieved. The first, at a greater distance from the surface, is physisorption, associated with an enthalpy of physisorption, ΔH_p. At this stage, the

adsorbate (H_2 in this case) is still intact and has formed no chemical bonds with the surface. The energy gain is due to weak interactions such as van der Waals forces. As the adsorbate approaches closer to the surface, it may overcome the activation barrier to chemisorption ($E^{\ddagger}$), resulting in the breaking of the H-H bond, and formation of two M-H bonds to reach the second minimum at the chemisorbed state associated with the enthalpy of chemisorption, ΔH_c. These, now hydrogen *atoms*, are ready to react with another chemisorbed molecule.

1.5.3 • Activity and Selectivity

In general, a heterogeneously catalyzed reaction can be described by the classical rate expression: the product of the apparent rate constant (k) and a pressure (P) or concentration dependent term:

$$\text{Rate} = k \cdot f(P) \qquad \text{Eq. 1-6}$$

The apparent rate constant includes the rate constants of all elementary reactions in the overall transformation that precede the rate-determining step (RDS). This constant is dependent, however, on experimental conditions such as temperature. The dependence of k on T is described by the Arrhenius equation:

$$k = A' \exp(-E_a / RT) \qquad \text{Eq. 1-7}$$

where A' is the temperature-dependent pre-exponential factor (related to the number of molecular collisions with appropriate orientations for reaction), E_a is the activation energy, R is the ideal gas constant and T is the temperature. The problem with this, when dealing with heterogeneous catalysis, is that the observed activation energy that appears in the Arrhenius equation does not equal the actual activation energy because,

not only are there changes to the catalyst surface over the course of a reaction, the concentration of species on the catalyst surface is also proportional to temperature.[67] While the rate law of a heterogeneously catalyzed reaction is still important to understanding the mechanism of a reaction (Chapter 1.5.4), the activity of a catalyst is usually described by turnover frequency (TOF). This concept is more convenient for these applications because it is not based on activation energy. Instead, it is simply the number of times the overall catalytic reaction takes place to produce the product, per catalytic site (s) per unit time (t) under a specific set of experimental conditions:

$$\mathrm{TOF} = \frac{number\ of\ molecules\ of\ a\ given\ product\ produced}{(number\ of\ active\ sites)(time)} = \frac{1}{(s)}\frac{\mathrm{d}n}{\mathrm{d}t} \qquad \text{Eq. 1-8}$$

In homogeneous systems, s is easy to define since there are a known number of active sites based on the stoichiometry and mass of the added catalyst. This is not so simple in most examples of heterogeneous catalysis, since it is very difficult to count the number of surface sites. Often for such situations, where the number of active sites is unavailable, s is replaced by the total surface area of the catalyst, SA. Since the number of active sites is undoubtedly less than the total surface area, the TOF equation becomes:

$$\mathrm{TOF} \geq \frac{1}{(SA)}\frac{\mathrm{d}n}{\mathrm{d}t} \qquad \text{Eq. 1-9}$$

Turnover frequency is an excellent way to compare catalytic activity of different catalysts for the same reaction under the same experimental conditions. Another useful metric for such comparative analysis is simply looking at the reaction conversion at a fixed temperature after a fixed time. For example, if the reaction conversion after a certain time using one catalyst is 10% higher than that using another catalyst in the same amount of time, keeping all other variables constant, the former catalyst can be said to be more active for that transformation. Conversion (C) is defined as the molar

percent of reactant molecules that are converted to product, whether the desired product or not. For a single batch reaction of A going to B and C, conversion is:

$$C = \frac{n_A^o - n_A}{n_A^o} \times 100\% \qquad \text{Eq. 1-10}$$

Where n^0_A is the number of moles of A at the beginning of the reaction and n_A is the number of moles of A at the end of a reaction. Conversion after a fixed time will be the standard metric used to assess catalytic activity herein.

While these, and others, describe the rate of a chemical reaction, the selectivity (S) of these catalyzed reactions is also of utmost importance. It is a measure of how selective a particular reaction (or a particular catalyst) is for one particular product over all other products that might be generated. For the reaction above, the selectivity for B (in the final reaction mixture) would be:

$$S = \frac{n_B}{n_B + n_C} \qquad \text{Eq. 1-11}$$

As mentioned above, the metal surfaces' morphologies are very important for selectivity, while the exact mechanisms of these effects is widely unknown. Most information about these effects has been garnered qualitatively for specific reactions under a certain set of conditions. Electronic and steric factors with regard to the substrates themselves can also have powerful effects on selectivity and conversion. Again, information detailing these effects is not widely applicable to all systems, but it will be discussed in detail herein where it applies to this research study.

1.5.4 • Kinetics

There are many general mechanisms that can be applied to reactions that take place on a metal surface, depending on how the reagents adsorb to the surface. The Langmuir-Hinshelwood and Eley-Rideal mechanisms hold true far more often than others, while the former is employed most frequently. These are general mechanisms, so sometimes the distinction between the two (or other) mechanisms is blurred, and often, subtleties with regard to a particular reaction will arise.

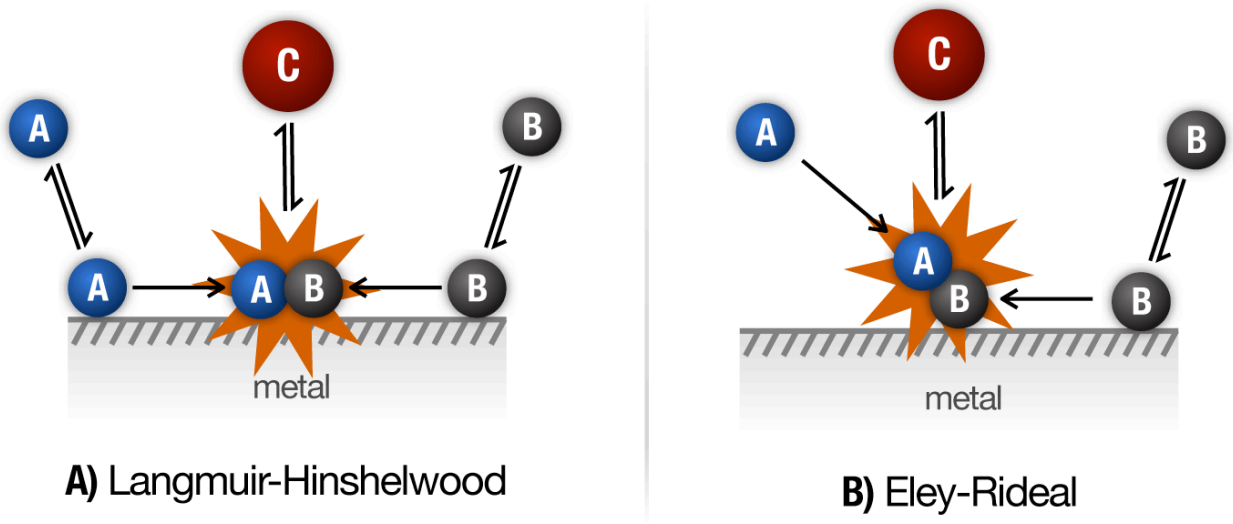

Figure 1-14 • a) Langmuir-Hinshelwood and b) Eley-Rideal general heterogeneous catalysis mechanisms for A + B ⟶ C

In the Langmuir-Hinshelwood mechanism (Figure 1-14A), both reagents, A and B, reversibly adsorb to the metal surface separately. They then migrate along the metal surface until they meet and react to form the product, C, still adsorbed to the surface. The product can then reversibly desorb from the surface to free up the active site for further reactions. In the Eley-Rideal mechanism (Figure 1-14B), one of the reagents reversibly adsorbs to the surface, and reacts with a second reagent as it approaches

from the bulk phase, without adsorbing. This forms the product on the surface, which can then reversibly desorb. The elementary steps in the rate law used to describe the reaction will vary depending on which mechanism is taking place.

The rate law for such a bimolecular reaction can then be developed from the elementary steps involved. For the reaction above, for the Langmuir-Hinshelwood mechanism, there are four elementary steps involved (Scheme 1-6), where subscript "*g*" represents a gaseous species, subscript "*a*" represents an adsorbed species, and an asterisk (*) is used to delineate a vacant active surface site. For this example, we assume that the rate-determining step (RDS) of the process is the surface reaction between A and B.

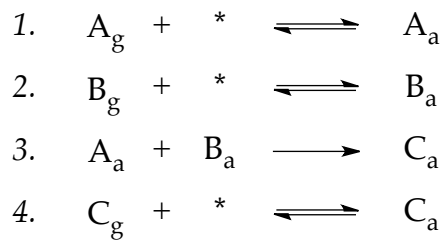

Scheme 1-6 • Elementary steps of heterogeneous bimolecular reaction

The rate of adsorption can be described by a number of constants, which eventually get combined to give the apparent rate constant of adsorption, k_a:

$$-\frac{\mathrm{d}\left[A_g\right]}{\mathrm{d}t} = S_0 \times f \times (1-\theta) \times P_A = k_a (1-\theta) P_A \qquad \text{Eq. 1-12}$$

where S_0 is the sticking probability of the gas on a perfectly clean surface, f is the flux of incoming molecules (proportional to temperature and the mass of incoming molecules), P_A is the pressure of A, and θ is the fraction of the surface covered. In heterogeneous catalysis rate laws, θ is used in place of concentration in classical rate law expressions.

In Eq. 1-12, (1–θ) describes the fractional blocking of the surface by adsorbate, representing the fraction of surface sites available for adsorption. The Langmuir adsorption isotherm describes the surface coverage as it is related to the gas pressure and the rates of adsorption and desorption at a specific temperature:

$$\theta_i = \frac{K_i P_i}{1 + K_i P_i} \qquad \text{Eq. 1-13}$$

where K_i is the adsorption equilibrium coefficient for the particular gas, a ratio of the rate of adsorption and desorption.

The rate law for the surface reaction can then be written as:

$$rate = \frac{d[C]}{dt} = k_3 \theta_A \theta_B \qquad \text{Eq. 1-14}$$

The steady state approximation can be used to determine the surface coverage of A and B since the rate of change of surface adsorbed species is unlikely to change during the reaction. As gaseous molecules are adsorbed on the surface, they either react or are desorbed. From this, the surface coverage of A is:

$$\theta_A = \frac{K_A P_A}{1 + K_A P_A + K_B P_B + K_C P_C} \qquad \text{Eq. 1-15}$$

where the surface coverage of B is expected to be similar:

$$\theta_B = \frac{K_B P_B}{1 + K_A P_A + K_B P_B + K_C P_C} \qquad \text{Eq. 1-16}$$

and from this, the rate of the reaction is (see Appendix A for full derivation):

$$rate = \frac{k_3 K_A P_A K_B P_B}{\left(1 + K_A P_A + K_B P_B + K_C P_C\right)^2} \qquad \text{Eq. 1-17}$$

This rate law assumes that both A and B adsorb to the surface with similar energies. If one reactant is more weakly adsorbed (has a much smaller adsorption equilibrium coefficient), then the terms involving that adsorbate are eliminated from the denominator, and the catalytic activity is retarded by high coverage of the strongly binding adsorbate.

1.5.5 • Catalyst Preparation

The earliest example of a material that could be considered a heterogeneous catalysis was created when Döbereiner simply mixed platinum black with clay in order to dilute the catalytic action of the metal.[71] Indeed, this is still a key goal of distributing metals on supports, especially with precious metals due to their relatively high cost and scarcity. Since then, the preparation of solid catalysts has grown exponentially with new reviews of the topic being authored frequently.[72-75] This is driven by the continual search for catalysts that have better chemical and mechanical stability, give higher activity and selectivity for a particular product, and have fewer and fewer unnecessary metal atoms to reduce cost. Also, with the greater understanding of the surface reactions that are taking place that has been gleaned in the recent past, and how metal dispersion and support affect these reactions, more specific optimizations can be made to the solid catalyst.

There are two different general classes that the preparation of supported catalysts can be broken down into: a) where the metal is deposited as the support is being formed and b) where the metal is deposited on a preformed support. Regardless of the method of preparation, it is always followed by the removal of solvent by filtering and/or heating and/or evacuation, followed by a high temperature calcination step

which reduces the metal precursor to its oxide and removes any counter ions left within the support. Further reduction to the bare metal can be done directly with hydrogen gas.

The former, generally less used, category includes the *sol-gel method*, which is used extensively in this study, and will therefore be explained in detail here. The term sol-gel comes from the two roots, sol and gel. A *sol* is a colloidal suspension of small (1 nm to 1 μm) solid particles in a liquid, while a *gel* is made up of continuous solid and liquid phases of colloidal dimensions. It is continuous in the sense that the whole could be traversed in both the liquid and solid phase without entering the other phase. Therefore, specifically the sol-gel method is one where a gel is formed from the particles of a sol. In general, however, the term has come to be used to describe the process by which a gel is formed from a homogeneous solution of soluble support and active metal precursors.

The sol-gel method can be theoretically used to generate almost all metal oxides, and is widely used for the formation of silica, alumina, titania and zirconia. The synthesis starts with the dissolution of the support precursor into an alcohol solvent. The precursor is most commonly the metal alkoxide, $M(OR)_x$ where M = the metal (Si, Al, Ti, Zr), R = an alkyl group (commonly CH_3, C_2H_5, C_3H_7 or C_4H_9) and x = the valency of the metal. These metal alkoxides are used because they are readily soluble in alcohol and can be readily hydrolyzed to the corresponding hydroxide, either thermally or with the addition of an acid or base catalyst.

$$M(OR)_x + H_2O \rightleftharpoons HO\text{-}M(OR)_{x-1} + ROH$$

While a catalyst is not always required, Brønsted acids and bases are both capable of catalyzing this reaction. With acid hydrolysis, the alkoxide groups are first

protonated, resulting in more electron deficient metal centers that undergo more facile attack from water. With base catalysis, hydroxide ions are formed in solution and then attack the alkoxide metal centre. If there is sufficient water present in the system, it is possible to drive the reaction to completion to give the fully hydrolyzed metal, $M(OH)_x$. The partially and fully hydrolyzed molecules can then undergo a condensation polymerization to produce larger and larger molecules, releasing a molecule of water or alcohol each time (Scheme 1-7). The final step of the catalyst synthesis is the drying and high temperature calcination of the dried catalyst. Either evaporative drying to yield a xerogel or supercritical drying to yield an aerogel is then usually performed followed by calcination at 400–500 ˚C. This high temperature step is required to volatilize the remaining organic and inorganic residues that are not part of the catalyst matrix. Temperatures cannot be taken too high, however, as to result in the sintering of support and/or metal particles.

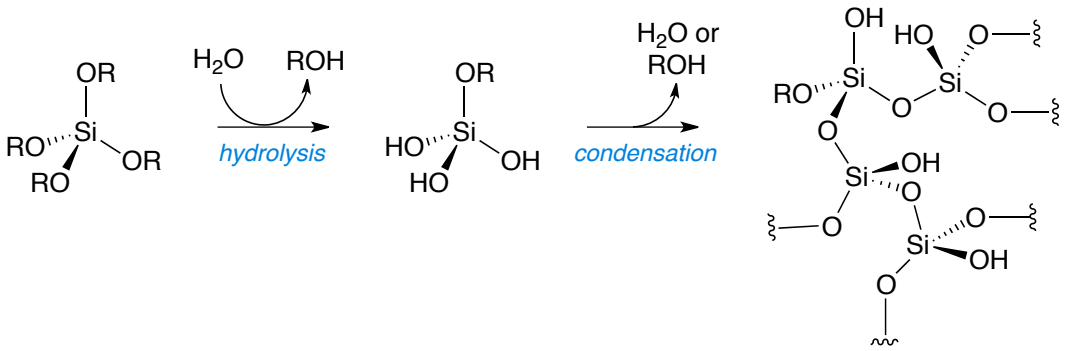

Scheme 1-7 • Sol-gel process involving hydrolysis and condensation of a silica alkoxide

There are a number of benefits to the use of the sol-gel method for preparing solid catalysts. The method is widely applicable to different metal oxides, including the generation of mixed oxides with various compositions due to the ability to simply alter the stoichiometry of the support precursors. The deposition of the metal happens

during the support formation, and is widely dispersed and strongly anchored throughout the material. This leads to unique structural characteristics that are not accessible from classical preparation methods where the metal is added to the pre-formed support.

The second class of catalyst preparation methods is much more widely used and has proliferated into a number of different procedures. *Impregnation* is a very popular method of catalyst preparation where an aqueous (or organic) solution of either a metal salt or complex is mixed with the pre-formed solid support. The metal ions are then drawn into the pores of the support by osmosis. *Ion exchange* involves the exchange of acidic protons for cationic precursors of the metal. Both of these methods are used herein. Another popular method is *deposition/precipitation*, where a metal precursor (usually the hydroxide) is precipitated onto the support, which serves as a nucleation site for its formation. All of these methods are rather straightforward and well studied in the literature.

1.5.6 Catalyst Characterization

As previously mentioned, there are limited ways to quantitatively probe the surface of a heterogeneous catalyst for details regarding the morphologies present. However, it is often useful to be able to compare the size of supported metal clusters, as well as the number of exposed metal atoms, between catalysts purchased from different suppliers or derived from various synthetic techniques. For the former information, transmission electron microscopy or X-ray diffraction are often used. Transmission electron microscopy can give an actual 'photograph' of the metal surface (such as above, in Figure 1-9) where X-ray diffraction gives information about the bulk sample. The

number density of exposed metal atoms can be determined by selective chemisorption or physisorption of a probe molecule, such as H_2, N_2, CO or O_2.

Surface area is a very important characterization of a particular catalyst. Surface area is correlated with catalyst activity since the higher the surface area, the more space available for active reaction sites (exposed atoms on metal clusters). The pore size and volume also play a role as they may determine the availability of these sites to certain substrates (*e.g.* larger molecules). A common method of measuring the surface area of a solid uses N_2 as a probe molecule and is known as the B.E.T. method after its creators, Brunauer, Emmett and Teller.[76] In the B.E.T. adsorption mechanism, molecules do not adsorb to the surface layer by layer, but in more of a random fashion. This mode of adsorption is described by the B.E.T. adsorption isotherm:

$$\frac{P}{V_{ads}\left(P_0 - P\right)} = \left(\frac{c-1}{cV_m}\right)\frac{P}{P_0} + \frac{1}{cV_m} \qquad \text{Eq. 1-18}$$

where P is the equilibrium pressure of the gas, P_0 is the saturation vapour pressure, V_{ads} is the volume of the adsorbed gas molecule, V_m is the volume of gas corresponding to a monolayer, and c is a fitting constant. A plot of $\{P/V_{ads}(P_0 - P)\}$ against $\{P/P_0\}$ should yield a straight line. The slope and intercept can then be used to calculate the value of V_m in ml g^{-1}. Once the volume of the monolayer is known, the specific surface area can be calculated from the molar volume of an ideal gas, Avogadro's number and the cross-sectional area of the adsorbing molecule (A):

$$SA\left[\frac{m^2}{g}\right] = V_m \text{ ml} \times \frac{\text{mol}}{0.0224 \text{ ml}} \times \frac{6.022 \times 10^{23} \text{ molecules}}{\text{mol}} \times \frac{A \text{ m}^2}{\text{molecule}} \qquad \text{Eq. 1-19}$$

1.5.7 • Support and Modifier Effects

It was suggested as early as the 1950s that the use of amorphous and acidic SiO_2 and Al_2O_3 as a support was beneficial for petroleum reforming reactions.[77] Schwab[78] and Solymosi[79] carried out the first deliberate studies on the effect of supports in the 60s and 70s. Metal-support interactions (MSIs) are complex and include many different caveats. Studying MSIs is complicated by the presence of particle size effects. Average particle size, particle size distribution and particle location within the catalyst support may often be influenced by the support itself during formation; these attributes affect the rate and selectivity of heterogeneously catalyzed reactions. There are a number of possible ways that a support can have a direct effect on the metal. The chemical makeup of the support itself can affect the electronic properties of the metal, by either donating or withdrawing electron density to the metal clusters. For example, it has been shown that adding MgO and CeO_2 to an Al_2O_3 support for the gold catalyzed oxidation of ethylene offered improved activity and selectivity.[80] Another type of support effect is "spillover." In this instance, the active substrate can initially bind to the metal and migrate to the support[81] or vice versa.[82] The active substrates can also be adsorbed on both the support and the metal, where the reaction takes place at the interface.[83] Despite a number of different mechanisms of support effects, it has been demonstrated that only weak metal-support interactions are present between metals and non-reducible oxide (SiO_2, Al_2O_3) and carbon supports.[84] Most effects observed with these supports are likely due to particle size and distribution, although differences in these characteristics are likely a result of the interactions between the metal and the support during catalyst synthesis.

Modifiers can also be incorporated into heterogeneous catalysts. Small amounts of additives, that are themselves inert, can have drastic effects on the catalytic activity and selectivity of a particular reaction.[85] They can be used to alter the support or the metal to either increase or maintain activity or increase selectivity by blocking unwanted reactivity or promoting desired activity. There are two broad classes of modifiers: those that are chiefly associated with the support, and those associated with the metal or the metal-support interface. The former class has, basically, two modes of action. Such modifiers can either stabilize the support against degradation over the course of a reaction, especially under extreme conditions, or they can neutralize acidic sites that might lead to the catalysis of unwanted reactions. Modifiers associated with the metal can exert electronic effects, where they can donate or withdraw electron density from nearby metal atoms, either promoting or selectively poisoning reactivity. It is also possible that these modifiers can be added to occupy certain sites or defects on the metal surface. These sites may lead to unwanted products, and blocking them would prevent such reactivity. These types of modifiers are known as selective poisons, and almost exclusively lead to a decrease in activity due to the blocking of active sites.[86-88] There are a number of known selectivity promoters for heterogeneous metal catalysts. Adding electron rich metals such as copper, silver, gold, mercury, tin, lead and germanium can lead to improved multiple bond hydrogenation selectivity, and suppression of hydrogenolysis. The same effects can be seen with other electron-rich species, including chlorine, sulfur ions, nitrogen bases, and CO. An overabundance of these species, however, can easily block more than the sites leading to unwanted reactions, resulting in a severe retardation or complete arrest of catalytic activity. An example of industrial modifier use in heterogeneous catalysts can be seen in the Fischer-Tropsch process to synthesize hydrocarbons. Oxides of electropositive elements (alkali

and alkaline-earth metals) are used to control chain growth, while mid-transition oxides (MoO_x, VO_x, TiO_x) are used to promote yields of oxygenates, by preventing carbon monoxide desorption,[89] and give higher alkene/alkane ratios.

1.6 • Thermally Regenerative Fuel Cells

A thermally regenerative fuel cell (TRFC) is a special application of a fuel cell that take advantage of a closed system and a directly reusable proton source whereby electricity can be generated solely from the input of heat. In this way, it is able to convert low-grade thermal energy into electrical energy without producing any byproducts. There was a significant amount of research dedicated to developing TRFC systems between the 1950s and 1970s for space applications.[90,91] These systems operated at very high temperatures and used inorganic metal hydrides as their hydrogen source. More recent examples, which use organic liquids as the hydrogen source and operate at much lower temperatures, will be discussed further below. Depending on the type of TRFC, heat could be supplied by a furnace for that purpose, by renewable sources, such as solar or geothermal, or from another process that releases heat as a byproduct (an internal combustion engine, for instance).

In the invention's simplest embodiment, heat is used to drive a dehydrogenation reaction of an organic or inorganic proton carrier, XH_2, at the surface of the fuel cell anode to produce protons, electrons and the dehydrogenated carrier, X:

$$\text{heat} + XH_2 \xrightarrow{\text{anode}} X + 2H^+ + 2e^- + \text{work} \qquad \text{Eq. 1-20}$$

As in a classical PEMFC, protons selectively transfer through the membrane, while electrons are forced through an external circuit, generating electrical energy (work in Eq. 1-20). The electrons and protons recombine with X at the cathode to reconstitute XH_2 to be reused at the beginning of the cycle:

$$X + 2H^+ + 2e^- \xrightarrow{\text{cathode}} XH_2 \qquad \text{Eq. 1-21}$$

It is also possible to envision a system where one or both of the above events could be separated into two separate events, with the dehydrogenation and/or hydrogenation reactions taking place in separate chambers, away from the fuel cell electrodes. If the first reaction were divided between a separate reactor and the fuel cell anode, Eq. 1-20 would become:

$$\text{heat} + XH_2 \xrightarrow{\text{reactor}} X + H_2 \qquad \text{Eq. 1-22}$$

$$H_2 \xrightarrow{\text{anode}} 2H^+ + 2e^- + \text{work} \qquad \text{Eq. 1-23}$$

Similarly, if the second reaction were split, Eq. 1-21 would become:

$$2H^+ + 2e^- \xrightarrow{\text{cathode}} H_2 \qquad \text{Eq. 1-24}$$

$$X + H_2 \xrightarrow{\text{reactor}} XH_2 \qquad \text{Eq. 1-25}$$

Regardless of which set of equations is used, however, the end result is the same. If you add together Eq. 1-20 and Eq. 1-21 (or another combination of the expanded sets of equations), the system of equations simplifies to one that is very desirable where, as mentioned above, heat (or thermal energy) is converted to work (electrical energy) by the TRFC with no byproducts:

$$\text{heat} \xrightarrow{\text{TRFC}} \text{work} \qquad \text{Eq. 1-26}$$

Ando *et al.* proposed the first example of an organic TRFC,[92] which is closely related to the work presented herein. Their system used a low-grade heat source (such as solar heat) to heat the anode of a fuel cell and drive the dehydrogenation of 2-propanol to acetone. A cooling system at the cathode provided conditions suitable for acetone rehydrogenation. In a second paper, Ando described a system with the same hydrogen carrier pair (2-propanol and acetone), but where the dehydrogenation took place in a reactor separate from the fuel cell itself.[93]

Another example of an organic TRFC is described in a patent from Akimoto that also used 2-propanol as the hydrogen carrier.[94] In this case, both the hydrogenation and dehydrogenation took place away from the fuel cell in separate reactors. Generation of electricity at the fuel cell, therefore, depended on a hydrogen pressure difference between the anode and the cathode. If the pressures were the same, no electricity would be generated because the reduction and oxidation potentials at both electrodes would be the same, resulting in a total cell voltage, $E^0_{cell} = 0$ V. The Nernst equation shows how the total voltage (electromotive force) of the fuel cell is affected by pressures of the reactive species at the anode and cathode, described by the reaction quotient, (Q):

$$E_{cell} = E^0_{cell} - \frac{RT}{nF} \ln Q \qquad \text{Eq. 1-27}$$

where E_{cell} is the voltage at the non-equilibrium conditions described by Q, E^0_{cell} is the cell voltage at standard conditions (1 atm or 1 M in reactive species and room temperature), R is the ideal gas constant ($R = 8.314$ J K^{-1} mol^{-1}), T is the temperature, n is the number of moles of electrons transferred per mole of reaction and F is the Faraday constant: the charge, in coulombs, of one mole of electrons ($F = 9.6485 \times 10^4$ C mol^{-1}).

The TRFC that has been proposed by the Jessop Group[95, 96] employs the dehydrogenation of XH_2 in a separate reactor and reduction of X back to XH_2 at the cathode surface. The designed use of this TRFC is to capture waste heat from the internal combustion engine (ICE) of a long-haul transport truck. In Canada, in 2009, transport trucks travelled over 28 billion km, burning over 8.7 billion L of diesel and gasoline and producing over 17.3 billion kg of CO_2.[6,8] Considering such large consumption and emission values, even small increases in overall efficiency could make a significant impact. A diesel burning ICE designed for use in a passenger vehicle uses about 20% of the chemical energy released from combustion to move the vehicle forward.[97] About 6% is lost to overcoming friction and almost 17% is lost when the vehicle is idling. Depending on the vehicle, the alternator, which supplies electrical energy to power things like climate control, lighting and power steering and breaking, uses 2-10% of the fuel energy.[98] One can imagine that some of these losses may be larger in a transport truck than in a passenger vehicle. With more wheels, and therefore more axels, it is only reasonable to assume greater losses due to friction in the drive train. Also, depending on the type of transport truck, the battery could be required to supply significantly more energy, to power a refrigerated trailer, for example. Regardless, the remainder of the energy generated, about 45-55%, is lost as waste heat to the surroundings, and this is the wasted energy that this system would attempt to harness. Assuming that the energy used for auxiliary components can be generated completely by the proposed TRFC system, huge savings could be made, up to 6–13% in the vehicle's mileage, by not having to use mechanical energy produced by the engine to directly charge the battery via the alternator. Specifically, if one considers the maximum fuel savings of 10%, and a 2000 survey of Canadian trucking companies

detailing fuel use, savings of 4,900-9,300 L fuel and $6,000-11,000 per truck per year could be expected.[99]

For the system discussed herein, the dehydrogenation reaction chamber would be positioned adjacent to the engine block as to obtain a desired dehydrogenation temperature of 200-240 ˚C, far greater than the 80 ˚C for Ando's systems discussed above. The operating temperature of the fuel cell, between 100 and 140 ˚C (depending on the membrane) would be the target temperature for efficient reduction of X back to XH_2. A schematic of the proposed system is shown in Figure 1-15.

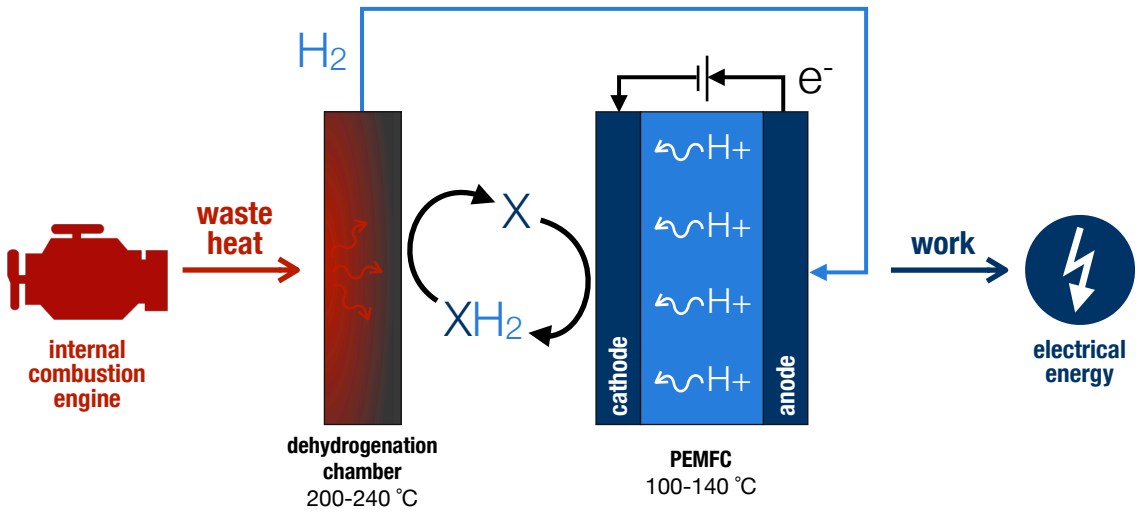

Figure 1-15 • Schematic of proposed waste heat driven TRFC.

There are a number of components of such a system that will need to work together for such an invention to come to fruition: identity of the fuel cell membrane and other membrane assembly components, the catalyst used at both the cathode of the fuel cell and in the dehydrogenation chamber, and the identity of the fluid couple (X/XH_2). The membrane and cathode ionomer (the polymer used to interface proton transfer from the PEM to the catalyst site) must be stable to degradation and

solubilization by the fluids at high temperatures. They must also offer good proton conductivity and electrical insulation, as any classical PEM would also require. The reaction that is taking place at the anode is similar to classical PEMFCs (Eq. 1-23), and therefore catalysts employed as such should be appropriate. However, this can only be established after a working prototype has been developed. All of the catalysts will need to be heterogeneous and stable to leaching into the chosen fluids so they can be isolated as needed within the system, preventing unwanted reactivity elsewhere. The fluids and catalysts must be chosen to allow for rapid, chemoselective dehydrogenation and electrochemical reduction under an atmosphere of H_2. The dehydrogenation must be done under an atmosphere of hydrogen because, in the final system, all areas will be under such an environment. The gravimetric and volumetric H_2 storage densities are not an issue with this type of system because of the constant recycling of the carrier. The liquids should remain stable in the condensed state over the temperature range of the system (as low as 100 ˚C, and preferably room temperature (RT) or lower to as high as 200-240 ˚C). A neat reaction mixture is also desirable since any dilution of the working liquids will result in slower kinetics for both reactions involved, lowering the maximum power available from the system.

The development of a suitable membrane and ionomer, as well as the investigation of dehydrogenation catalysts, are outside the scope of the project presented herein, and are currently under development within the Jessop Research Group. Herein, the optimization of the 'hydrogenation' or reduction of X to XH_2 will be discussed in detail. Previous work has shown that phenyl alkyl ketones and their corresponding benzyl alcohols show promise for the hydrogen carrier fluid system, specifically propiophenone and 1-phenyl-1-propanol.[96] Briefly, however, this liquid couple was chosen because both are liquid over the desired temperature range (RT –

218 °C), offer good conversion and selectivity over Pd/SiO_2 and have limited functionalities that can be easily transformed under these conditions. The latter point is important to try to mitigate the number of side reactions possible.

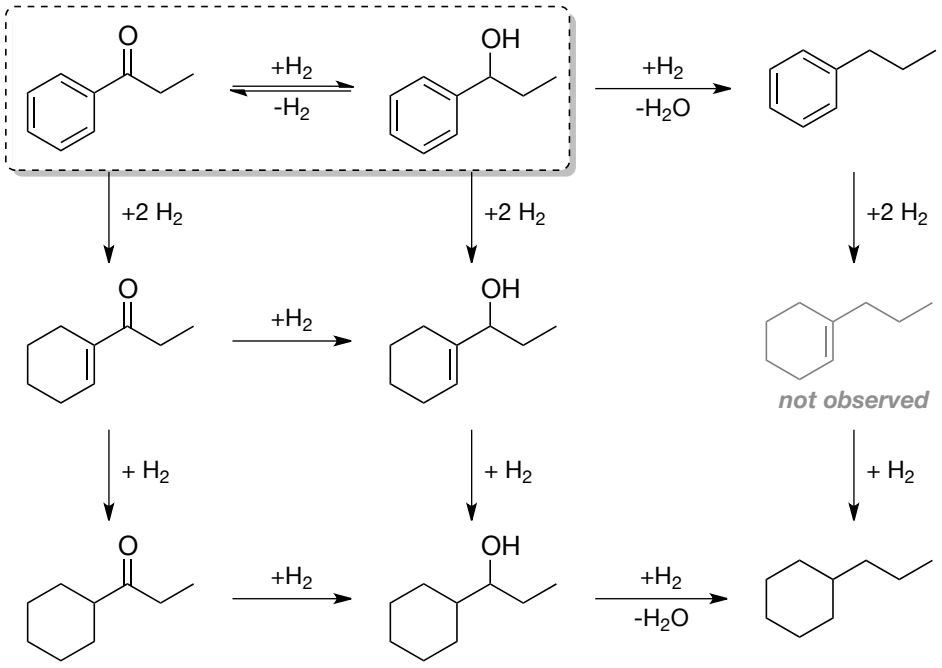

Scheme 1-8 • Possible byproducts from ketone/alcohol equilibrium under described conditions.

The reaction selectivities are very important for the proposed TRFC system because of the closed, cyclic nature of the hydrogen carrier fluids. The same mixture is cycled continuously, where each molecule would undergo many dehydrogenations and reductions over the course of the lifetime of the fluid. Any unreactive byproducts generated during either reaction would dilute the concentration of the active species, diminishing the total power output of the cell. For example, if both reactions were 99% selective for the desired product, there would be < 50% X/XH_2 remaining after only 70 cycles. At 99.9% selectivity for both reactions, the half-life increases to about 700 cycles, while 99.99% selectivity allows the liquid to last for 7000 cycles. These values assume

that for each time each molecule passes through the dehydrogenation chamber or the cathode it will react, which is, likely, an exaggeration. The frequency of the reactions will likely be much less than this and will ultimately depend on: the total volume of the system, the liquid flow rate past the catalysts, and the rates of the reactions themselves. Despite limiting the number of reactive functional groups to one, the alcohol/ketone equilibrium proposed is susceptible to the formation of a number of byproducts under H_2 and over a precious metal catalyst (Scheme 1-8). Ultimately the selectivity will dictate how often the liquid will have to be replaced within the vehicle, and the longer this is, the better.

For the hydrogenation reaction specifically, there has been relatively little work toward achieving such high selectivities for heterogeneously catalyzed reactions. There is often little reason for authors to report (or do the analytical analysis required to report) selectivity with such precision; it is, instead, sufficient to simply indicate that the chemoselectivity of the reaction is >99%, or even "100%". Classically, however, this transformation is done with stoichiometric inorganic hydride reducing agents ($LiAlH_4$, $NaBH_4$), which produce toxic residues.[100] There have indeed been some heterogeneous catalysts reported in the literature, but they usually require additives such as amines or NaOH, are performed in a solvent in order to achieve high selectivities, and operate under moderate to high H_2 pressures.[101] While the use of additives could be incorporated, their selection must be done very carefully to avoid unwanted interactions with the liquids, catalysts and membrane electrode assembly components. Such strategies were, therefore, avoided in this initial investigation. Zaccheria *et al.* report high selectivities (97-100%) with high conversions (>99%) after moderate reaction times at 90 ˚C under 1 atm H_2 for a selection of phenyl ketones with an 8 wt% Cu/Al_2O_3 catalyst.[102] Despite the fact that these conditions are close to those described for our

desired system, catalyst loadings were extremely high (almost stoichiometric amounts) and the reactions were carried out in a dilute mixture in *n*-heptane. Additionally, in the authors' hands, the catalyst prepared as described proved inactive under our conditions (*vide infra*). We have found no reports of any heterogeneous hydrogenations of phenyl ketones where no solvent is used. Because an appropriate catalyst system was not found in the literature, a large-scale screening and development project was undertaken to try to find an appropriate combination of hydrogenation catalyst and X/XH_2 couple (Chapter 5).

1.7 • Objectives

The objectives of the projects presented herein can be broken down into two main categories. First, work toward the development of hydrogen storage systems for use with classic PEM fuel cells will be described. These molecules would undergo a chemical reaction on board the vehicle to generate hydrogen as needed by the fuel cell, to generate all electricity needed to operate the vehicle. The initial proof of concept experiments and further development of the different classes of hybrid hydrogen storage are discussed, where these systems can offer more potential advantages over classic, single-component systems, including a low overall reaction enthalpy. This involved the testing of a number of different combinations of endothermic and exothermic hydrogen releasing molecules to determine their ability to undergo dehydrogenation without negatively affecting that of the other carrier.

From this, a need to enhance the rate of the endothermic system was realized. Therefore, the effect of changing the temperature or catalyst, and sterically protecting the heteroatom on the rate of N-heterocycle dehydrogenation (indoline mostly, also substituted piperidines) was investigated. As discussed, the effect of electron donating groups on the ring of piperidine has been demonstrated to affect favourably both the thermodynamics and kinetics their dehydrogenation. Furthering this discussion to other strategies of accelerating the rate was the main objective here, in order to help overcome the rate disparity and improve the viability of the system. This study completed the Jessop Group's foray into researching molecules or combinations thereof for onboard hydrogen storage systems as the main means of energy.

Secondly, the focus shifted to partially supplanting the energy needs of a vehicle with the implementation of an organic thermally regenerative fuel cell. Theoretically, this would allow the engine waste heat lost to the environment to be harnessed and converted to electricity using a fuel cell, with no other byproducts being generated directly. Where this is a large-scale project, herein the focus is on improving the rate and selectivity of the hydrogenation of the propiophenone and related ketones with implications for the reaction at the cathode of the TRFC. Where there is limited scope of such studies in the literature involving neat ketone without the use of additives, such experimentation with regards to temperature, catalyst and ketone variation was carried out. The main objective here was to find trends in the reactivity with regard to the catalyst metal and support as well as the electronic and steric factors contributed to the ketone.

Chapter 2 • Experimental

2.1 • General

Manipulations of air-sensitive compounds were conducted in the absence of oxygen and water under an atmosphere of N_2, by use of standard Schlenk methods, utilizing glassware that was oven-dried (130 ˚C) and evacuated while hot prior to use. Unless otherwise specified, all reagents were purchased from chemical suppliers (Sigma Aldrich, Pressure Chemicals, Alfa Aesar, Strem) and used without further purification. Most ^{1}H, ^{13}C, and ^{11}B NMR spectra were collected at 300 K on a Bruker AV-400 spectrometer operating at 400.3, 100.7, and 128.4 MHz (respectively) with chemical shifts reported in parts per million downfield of $SiMe_4$ (for ^{1}H and ^{13}C) or BF_3-Et_2O (for ^{11}B). Some were also collected at 300 K on a Bruker AV-500 spectrometer. Qualitative GC/MS analyses for degradation product analyses were performed on an Agilent Technologies 6850 GC coupled with an Agilent Technologies 5975C VL MSD with Triple-Axis Detector. MS spectra were analyzed by library comparison using NIST MS Search 2.0. Quantitative GC analyses were performed on a Shimadzu GC-17A equipped with a DB-5 column (0.25 mm i.d., 30 m, 0.25 mm film thickness) from Agilent Technologies (see Appendix B for calibration curves). Catalyst surface areas and pore sizes were determined using Micromeritics Accelerated Surface Area and Porosimetry System 2010 manufactured by Micromeritics Instrument Corporation. Electrochemical

measurements were made using an SP-150 potentiostat from BioLogic Science Instruments using a PC running EC-Lab Software (version 10.02). The gas chromatography limit of detection was needed in order to ensure that selectivity measurements to ≥ 99.99% were valid. This was verified by analyzing a control sample containing a byproduct (propyl benzene) at the concentration that would be present if its selectivity was 0.01% at 6% conversion. The peak was clearly visible on the GC trace while no such peaks were observed in the samples prepared from the reaction mixtures. This proves that the spectrometer is able to give selectivities of at least 99.99% accurately.

2.2 • Preparation of Compounds

2.2.1 • 4-Aminopiperidine N,N'-diborane [1]

A Schlenk flask was charged with a stir bar and 4-aminopiperidine (1.0 mL, 9.4 mmol) followed by the addition of ~2.6 equiv. of 1 M BH_3-THF in THF (25 mL, 25 mmol) and magnetically stirred for 16 h. The solvent was removed *in vacuo*, leaving behind a white solid. The solid was washed several times with distilled water and dried in vacuo, yielding **3a** as a white solid (1.04 g, 8.1 mmol, 86%). ^{1}H NMR (DMSO-d_6) δ 5.78 (br s, 1H, NH), 5.26 (br s, 2H, NH_2), 2.96 (d, $^3J_{HH}$ = 12.6 Hz, 2H, C2-H and C6-H), 2.44 (m, 1H, C4-H), 2.30 (q, $^3J_{HH}$ = 12.6 Hz, 2H, C2-H and C6-H), 1.95 (d, $^3J_{HH}$ = 12.6 Hz, 2H, C3-H and C5-H), 1.39 (qd, $^3J_{HH}$ = 12.6 Hz, J_{HH} = 3.5 Hz, 2H, C3-H and C5-H), 1.26 (br m, 6H,

BH_3s); $^{13}C\{^1H\}$ NMR (DMSO-d_6) δ 52.4 (C4), 51.0 (C2 and C6), 29.4 (C3 and C5); ^{11}B NMR (DMSO- d_6) δ -14.8 (br s, NH-BH_3), -21.4 (br s, NH_2-BH_3).

2.2.2 • 4-Aminopiperidine-1-borane [2]

To a round-bottom flask equipped with a condenser containing a magnetically stirred solution of **3a** (0.12 g, 0.94 mmol) in THF (3 mL) was added 4-aminopiperidine (0.10 mL, 0.94 mmol). The mixture was heated at 60 ˚C for 18 h. The solvent and other volatiles were removed *in vacuo*. Methanol (4 mL) was added, and the solution was filtered through diatomaceous earth. The filtrate was dried in vacuo, resulting in a white solid (0.16 g, 1.4 mmol, 72%). ^1H NMR (CD_3OD) δ 3.14 (dd, $^3J_{HH}$ = 13.6 Hz, J_{HH} = 1.9 Hz, 2H, C2-H and C6-H), 2.78 (m, 1H, C4-H), 2.47 (apparent t, $^3J_{HH}$ = 13.6 Hz, 2H, C2-H and C6-H), 1.88 (dd, $^3J_{HH}$ = 11.9 Hz, J_{HH} = 1.4 Hz, 2H, C3-H and C5-H), 1.39 (qd, $^3J_{HH}$ = 11.9 Hz, J_{HH} = 4.0 Hz, 2H, C3-H and C5-H); $^{13}C\{^1H\}$ NMR (CD_3OD) δ 53.2 (C2 and C6), 48.5 (C4), 35.3 (C3 and C5); ^{11}B NMR (CD_3OD) δ -15.6 (apparent d, J_{BH} = 96 Hz); ^{15}N NMR (CD_3OD) δ 35 (br s, NH), 38 (br s, NH_2).

2.2.3 • Indoline borane [4]

To a Schlenk flask charged with a stir bar were added indoline (0.80 mL, 7.1 mmol) and 1 M BH_3-THF solution in THF (14.3 mL, 14.3 mmol) and stirred overnight (16 h). Solvent was removed in vacuo, leaving behind a yellow solid to which hexanes was added (3 mL). The hexanes dissolved the yellow impurity, leaving behind a white precipitate. The hexanes were decanted, and the remaining solid was washed several times with fresh hexanes (3 × 5 mL) followed by drying in vacuo, leaving

behind a white solid (0.80 g, 6.0 mmol, 85%). Storage of compound **3** at low temperature is preferred to inhibit decomposition. It appears to be mildly pyrophoric in air. In solution under air, it degrades over hours. ^{1}H NMR (C_6D_6) δ 7.42 (d, $^{3}J_{HH}$ = 7.5 Hz, 1H, C7-H), 6.94 (t, $^{3}J_{HH}$ = 7.5 Hz, 1H, C6-H), 6.88 (t, $^{3}J_{HH}$ = 7.5 Hz, 1H, C5-H), 6.75 (d, $^{3}J_{HH}$ = 7.5 Hz, C4-H), 5.01 (br s, 1H, NH), 3.07 (m, 1H, C2-H2), 2.87 (m, 1H, C2-H), 2.50 (m, 1H, C3-H2), 2.16 (m, 1H, C3-H2), 2.49 (apparent q, $^{1}J_{HB}$ = ~90 Hz, 3H, BH_3; partially underneath CH_2 peaks); ^{13}C{^{1}H} NMR (C_6D_6) δ 146.5 (C3a), 134.9 (C7a), 128.0 (C6), 127.7 (C5), 125.2 (C4), 120.3 (C7), 55.3 (C2), 29.0 (C3); ^{11}B NMR (C_6D_6) δ -13.8 (q, $^{1}J_{BH}$ = 91 Hz, BH_3).

2.2.4 • 6,6'-dimethyl-2,2'-bipiperidine [15a]

A 31-ml steel pressure vessel was charged with a magnetic stir bar, 6,6'-dimethyl-2,2'-dipyridyl (250 mg, 2.71 mmol) and 1 mol% loading of 5 wt% Rh/C (55.9 mg catalyst, 0.0271 mmol Rh). The vessel was then sealed, flushed three times with H_2, heated to 130 ˚C with stirring, pressurized to 80-90 bar H_2, and stirred for 24 h. After cooling, the pressure was released from the vessel. The desired product was separated from the solid catalyst by filtration in a 31% isolated yield (0.162 g, 0.83 mmol). ^{1}H NMR ($CDCl_3$) δ 2.64-2.58 (m, 2H, C14–H, C11–H), 2.47-2.30 (m, 2H, C7–H, C6–H), 1.80 (dt, 2H, *J* = 2.7, 12.8 Hz, C9–H, C4–H), 1.63-1.56 (m, 6H, NHs, C10–H, C8–H, C5–H, C3–H), 1.32 (qt, 2H, J = 3.6, 12.8 Hz, C9–H, C4–H), 1.18 (m, 2H, C8–H, C5–H), 1.06 (d, 6H, J = 6.0 Hz), 1.01 (m, 2H, C10–H, C3-H); ^{13}C{^{1}H} NMR ($CDCl_3$) δ 62.0 (C7, C6), 52.7 (C14, C11), 34.4 (C10, C3), 27.9 (C8, C5), 24.8 (C9, C4), 23.1 (methyl groups), ES-MS 197.180 m/z $[M+H]^+$, calc. value 197.202 m/z.

2.2.5 • 2,2':6',2''-terpiperidine [16a]

A 31-ml steel pressure vessel was charged with a magnetic stir bar, 2,2':6',2''-terpyridine (251.4 mg, 1 mmol) and 1 mol% loading of 5 wt% Rh/C (20.6 mg catalyst, 0.01 mmol Rh). The vessel was then sealed, flushed three times with H_2, heated to 130 ˚C with stirring, pressurized to 80-90 bar H_2, and stirred for 24 h. After cooling, the pressure was released from the vessel. The solid catalyst was separated by filtration. ^{1}H and ^{13}C NMR spectroscopy indicated the product was not formed to any appreciable extent, while degradation appeared to have taken place.

2.2.6 • 2,6-*cis*-Dimethylpiperidine [8]

To a 31-ml steel pressure vessel, equipped with a magnetic stir bar, 2,6-dimethylpyridine was added with 1 mol% Pd/C under air. The vessel was then sealed, flushed three times with H_2, heated to 100 ˚C, pressurized to 80-90 bar with H_2, and stirred for 18 h. After cooling, the pressure was released from the vessel. The desired product was separated from the solid catalyst by filtration. Purity was determined by ^{1}H NMR spectroscopy. In all cases, a 98-99% conversion with > 99% selectivity was observed. The identity of the product was confirmed by comparing the ^{1}H NMR spectrum to published literature data.[103]

2.2.7 • 2,6-*cis*-Di-*tert*-butylpiperidine [9]

To a 31-ml steel pressure vessel, equipped with a magnetic stir bar, 2,6-di-tert-butylpyridine was added with 1-2 mol% Pd/C under air. The vessel was then sealed,

flushed three times with H_2, heated to 100 °C, pressurized to 80-90 bar with H_2, and stirred for 18 h. After cooling, the pressure was released from the vessel. The desired product was separated from the solid catalyst by filtration. Purity was determined by ^{1}H NMR spectroscopy. In all cases, a 98-99% conversion with > 99% selectivity was observed. The identity of the product was confirmed by comparing ^{1}H NMR spectrum to published literature data.[104]

2.3 • Catalyst Preparation Methodologies

2.3.1 • Sol-gel catalysts

Based on a procedure from the literature,[105] tetraethoxy orthosilicate (21.5 mmol, 4.8 ml), anhydrous ethanol (2.0 ml), palladium(II) chloride (0.6 mmol, 108.0 mg) and 30% aqueous ammonium hydroxide (0.3 ml) were combined in a 15 ml round bottom flask equipped with a magnetic stir bar and a water condenser under air. The mixture was stirred magnetically and heated at 80 °C for 10 min under argon flow *via* syringe needles at the top of the condenser. Water (2.0 ml) was then injected directly into the reaction mixture through the septum at the top of the condenser using a 30 cm needle and then stirred for an additional 4 h, during which time gel formation took place. The reaction mixture was filtered, dried under dynamic vacuum for 18 h, and then further dried in an oven at 400 °C for 4 h. The BET surface area of the synthesized Pd/SiO_2 was determined to be 13.3 $m^2 g^{-1}$ with an average pore size of 43 nm. Other catalysts were

prepared by replacing tetraethoxy orthosilicate and/or $PdCl_2$ with similar amounts of different support precursors as delineated in Table 2-1. For a more detailed look at the calculations, see Appendix C.

Table 2-1 • Amounts of reagents used for sol-gel catalyst syntheses

Catalyst[a]	Support precursor	Metal precursor	EtOH (ml)	H_2O (ml)	NH_4OH (ml)
Co/SiO_2	2.4ml tetraethyl orthosilicate	130.4 mg $CoCl_2 \bullet 6H_2O$	1.0	1.0	0.15
Cu/SiO_2	2.4 ml tetraethyl orthosilicate	50.3 mg CuCl	1.0	1.0	0.15
Fe/SiO_2	2.4 ml tetraethyl orthosilicate	93.8 mg $FeCl_3$	1.0	1.0	0.15
Ir/SiO_2	2.4 ml tetraethyl orthosilicate	50.2 mg $PdCl_3$	1.0	1.0	0.15
Ni/SiO_2	2.4 ml tetraethyl orthosilicate	71.3 mg $NiCl_2$	1.0	1.0	0.15
Pd/Al_2O_3	3.490 g aluminum triethoxide	91.3 mg $PdCl_2$	7.0	2.0	0.30
$Pd/SiO_2 \bullet Al_2O_3$	2.4 ml tetraethyl orthosilicate 1.745 g aluminum triethoxide	99.7 mg $PdCl_2$	2.0	2.0	0.30
Pd/TiO_2	6.4 ml titanium(IV) *iso*-propoxide	107.6 mg $PdCl_2$	2.0	2.0	0.30
Pd/ZrO_2[b]	5.836 g zirconium(IV) ethoxide	108.0 mg $PdCl_2$	2.0	2.0	0.30
$Pd \bullet Rh/SiO_2$[b]	4.8 ml tetraethyl orthosilicate	54.0 mg $PdCl_2$ 66.0 mg $RhCl_3$	2.0	2.0	0.30
$Pt \bullet Pd/SiO_2$[c]	4.8 ml tetraethyl orthosilicate	54.0 mg $PdCl_2$ 44.0 mg $PtCl_2$	2.0	2.0	0.30
Pt/SiO_2	4.8 ml tetraethyl orthosilicate	87.9 mg $PtCl_2$	2.0	2.0	0.30
Pt/Al_2O_3	3.490 g aluminum triethoxide	74.7 mg $PdCl_2$	7.0	2.0	0.30
Rh/SiO_2	4.8 ml tetraethyl orthosilicate	131.9 mg $RhCl_3$	2.0	2.0	0.30
Rh/Al_2O_3	3.49 g aluminum triethoxide	111.4 mg $RhCl_3$	7.0	2.0	0.30
Ru/SiO_2	2.4 ml tetraethyl orthosilicate	83.6 mg $RuCl_3 \bullet 3H_2O$	1.0	1.0	0.15

a | 5 wt% metal on support based on amount of metal precursor added during preparation
b | 2.5 wt% metal on support based on amount of metal precursor added during preparation
c | metal molar ratio of 1:1

2.3.2 • Selenium and potassium oxide containing sol-gel catalysts

For 5.1 wt% Pd/7.6 wt% Se/SiO_2, tetraethoxy orthosilicate (TEOS, support precursor, 21.5 mmol, 4.80 ml), anhydrous ethanol (solvent, 2.0 ml), palladium(II)

chloride (metal precursor, 0.7122 mmol, 126.3 mg), selenium tetrachloride (additive precursor, 1.418 mmol, 313.0 mg) and 30% (v/v) aqueous ammonium hydroxide (0.3 ml) were combined in a 15 ml round bottom flask equipped with a magnetic stir bar and a water condenser under air. The rest of the procedure follows that outlined above in Chapter 2.3.1. Other catalysts were prepared by varying the precursors added as delineated in Table 2-2; the amount of H_2O and NH_4OH are held constant; aluminum ethoxide (AEO) was used in place of TEOS for Al_2O_3 supported catalysts; potassium methoxide used in place of selenium tetrachloride for K_2O containing catalysts.

Table 2-2 • Amounts of reagents used for modified sol-gel catalyst syntheses

Catalyst	Additive precursor	TEOS (ml)	AEO (g)	Pd_2Cl (mg)	EtOH (ml)
4.8 wt% Pd/0.1 wt% Se/SiO_2	3.1 mg selenium tetrachloride	4.8	–	107.8	2.0
4.8 wt% Pd/0.2 wt% Se/SiO_2	6.3 mg selenium tetrachloride	4.8	–	108.0	2.0
4.8 wt% Pd/1.6 wt% Se/SiO_2	62.6 selenium tetrachloride	4.8	–	111.3	2.0
4.8 wt% Pd/1.6 wt% K_2O/SiO_2	16.7 mg potassium methoxide	4.8	–	111.3	2.0
5.1 wt% Pd/7.6 wt% K_2O/SiO_2	83.4 mg potassium methoxide	4.8	–	126.3	2.0
4.8 wt% Pd/0.8 wt% K_2O/Al_2O_3	13.0 mg potassium methoxide	–	3.490 g	218.1	7.0
4.9 wt% Pd/3.6 wt% K_2O/Al_2O_3	64.9 mg potassium methoxide	–	3.490 g	229.7	7.0

2.3.3 • Al_2O_3 xerogel

Aluminum ethoxide (43.0 mmol, 6.97 ml), anhydrous ethanol (16.0 ml), and 30% (v/v) aqueous ammonium hydroxide (0.6 ml) were combined in a 100 ml round bottom flask equipped with a magnetic stir bar and a water condenser under air. The mixture was stirred magnetically and heated at 80 ˚C for 10 min under argon flow *via* needles at the top of the condenser. Water (4.0 ml) was then injected directly into the reaction mixture through the septum at the top of the condenser using a 30 cm needle

and then stirred for an additional 4 h, during which time gel formation took place. The reaction mixture was then cooled, filtered, dried under dynamic vacuum for 18 h yielding a white powder (2.97 g). The measured BET surface area of the powder was 367 $m^2 g^{-1}$, while the pore volume and average pore diameter were measured at 0.242 $cm^3 g^{-1}$ and 25.0 Å, respectively.

2.3.4 • 10 wt% Cu/Al_2O_3

Based on a literature procedure,[102] copper(II) nitrate trihydrate (0.4 g, 1.7 mmol) was weighed into a 400 ml beaker, and distilled water (2.5 ml) was added. A 30% (v/v) aqueous ammonium hydroxide solution was added until the pH reached 9 by pH paper (approximately 20 drops). Crushed high surface area alumina pellets (1 g) were added followed by the slow addition of distilled water until the total volume reached about 300 ml, while being stirred. Stirring continued for 20 min at room temperature. The solid blue powder was separated using a Büchner funnel and washed with 50 ml distilled water and left to dry on the funnel for 30 min. The powder was then transferred to a ceramic crucible and dried at 120 ˚C for 24 h. Alternatively, an as-synthesized Al_2O_3 xerogel was used in place of the alumina pellets. The catalysts were reduced under flowing H_2 at 200 ˚C for 1 h immediately prior to screening runs.

2.3.5 • 5 wt% Pd/Vulcan XC-72

Vulcan XC-72 (1.0 g) was weighed into a 100 ml round bottom flask, to which 5.0 M HNO_3 (16 ml) was added. The mixture was heated to 50 ˚C in an oil bath and stirred magnetically for 2 h. The mixture was cooled, filtered, and the solid washed with

distilled water. It was then transferred to a clean 100 ml round bottom flask and 15% (w/w) NaOH (15 ml) was added and the mixture stirred for 60 min. The solid was again filtered and washed with distilled water before drying in a vacuum desiccator overnight. The prepared support was then mixed in a small round bottom with 15 ml dichloromethane and $Pd(OAc)_2$ (0.491 mmol, 110.3 mg), and stirred for 1 h. The solvent was removed by rotary evaporation to isolate the final catalyst. Before being used for a hydrogenation reaction, these catalysts were reduced under H_2 at 200 ˚C for 2 h.

2.3.6 *n*-Butyl tin modification of commercial catalysts

Based on a literature procedure,[106] commercial 5 wt% palladium on silica powder (1.0 g) was added to a three-neck, 250 ml round bottom flask along with a magnetic stir bar. The flask necks were fitted with a septum, a condenser with an H_2 (g) gas inlet (glass gas adapter with stopcock), and a vacuum line *via* a stopcock. The glassware was evacuated to remove air and then refilled with H_2 (g). Tetra-*n*-butyltin (93%, 29.8 μL, 0.084 mmol) was measured into a small vial *via* micropipette, and subsequently transferred to the reaction flask through the septum using a needle and syringe, rinsing the vial with 3 x 1.5 ml portions of *n*-heptane into the flask. A further 10 ml of *n*-heptane was then added through the septum. With H_2 (g) flowing through the system, the round bottom flask was partially submerged in a 90 ˚C oil bath, and stirred at 600 rpm for 4 h. The solid was separated via vacuum filtration through a Buchner funnel and washed with 4 x 20 ml aliquots of *n*-heptane. The solid was afterwards transferred to a 4 dram vial, which was capped with a septum and dried at 90 ˚C for 2 h under flowing argon (delivered via needle through the septum) to give the desired catalyst.

2.4 • Screening Methodologies

2.4.1 • Hydrolysis of N-heterocycle boranes

N-heterocycle boranes were exposed to 5 mol% loading of Pd supported on either carbon or silica. The mixtures were stirred and heated to 100 ˚C in a small round bottom flask under a cold-water condenser. After the desired reaction time, the flasks were cooled, and the solid catalyst filtered by passing the reaction mixture through a bed of diatomaceous earth. ^{1}H and ^{11}B NMR spectroscopy were used to characterize the product mixtures.

2.4.2 • Mixed dehydrogenation/hydrolysis screening

For indoline and $NaBH_4$, a round bottom flask was charged with a stir bar, indoline (0.56 ml, 5 mmol), sodium borohydride (37.8 mg, 1.0 mmol), distilled water (0.07 ml, 4 mmol) and 10% palladium on carbon (2 mol% loading, 106.4 mg catalyst, 0.1 mmol metal) and equipped with a condenser. The reaction mixture was immersed into a preheated oil bath (100 ˚C) and stirred magnetically for 2 h. After cooling, the suspension was extracted in $CDCl_3$ and filtered through a small plug of diatomaceous earth to remove the catalyst. The filtrate was analyzed by NMR spectroscopy. The relative amounts of reagents were altered over various experiments as described in the text (Chapter 4.1.2).

For indoline and $R_3N{:}BH_3$ where R = H or Et, a round-bottom flask was charged with a stir bar, indoline (0.18 mL, 1.6 mmol), triethylamine borane (0.24 mL, 1.6 mmol,

or 1.6 mmol ammonia borane), distilled water (0.087 mL, 4.8 mmol), and 10% palladium on carbon (0.085 g, 0.08 mmol) and equipped with a condenser. The reaction mixture was immersed into a preheated oil bath (100 ˚C) and stirred magnetically for 2 h under inert gas for the duration of the experiment. In order to get efficient borane hydrolysis, vigorous stirring is required, due to the insolubility of indoline and triethylamine borane in water, to produce consistent dispersion of the water throughout the reaction mixture. The reaction flask was then allowed to cool to room temperature, and the reaction mixture was extract with $CDCl_3$ followed by filtration through a small plug of diatomaceous earth to remove the remaining catalyst. The filtrate was analyzed by NMR spectroscopy, showing indole and hydrolyzed triethylamine-borane. The relative amounts of reagents were altered over various experiments as described in the text.

For indoline and $Me_2NH:BH_3$, a 25 mL Schlenk tube was charged with a stir bar, indoline (0.34 mL, 3.0 mmol), dimethylamine borane (0.059 g, 1.0 mmol), distilled water (0.054 mL, 3.0 mmol), and 10% palladium on carbon (0.064 g, 0.06 mmol). The tube was equipped with a condenser, immersed into a preheated oil bath, and stirred magnetically for 2 h at 100 ˚C under inert gas flow for the duration of the experiment. The reaction flask was then allowed to cool to room temperature, and the reaction mixture was extracted with $CDCl_3$ or CD_3OD and filtered through a small plug of Al_2O_3 powder or diatomaceous earth to remove any remaining catalyst. The filtrate was analyzed by use of NMR spectroscopy. The relative amounts of reagents were altered over various experiments as described in the text.

2.4.3 • Indoline dehydrogenation rate constant determination

Indoline (8.9 mmol, 1.0 ml) was injected via syringe into a 10 ml round bottom flask containing 10 wt% Pd/C (1 mol% loading, 0.089 mmol, 94.6 mg) and a magnetic stir bar, under air. The flask was equipped with a condenser, immersed in an oil bath pre-heated to 100 °C and stirred magnetically for 60 min with constant argon flow provided via a needle through a rubber septum at the top of the condenser to remove any H_2 formed *in situ.* A second needle leading to an oil- bubbler allowed gas to escape from the system. Small aliquots of the reaction mixture were obtained after 5, 10, 15, 30, 45 and 60 min, dissolved in $CDCl_3$, then filtered through diatomaceous earth. The conversion at each time was determined by comparing relative integrations in the ^1H NMR spectra. A plot of $\ln(n/n_0)$ of the starting material (indoline) versus time was linear for the duration of the experiment (one half life). The slope is equal to the negative of the rate constant.

2.4.4 • Hybrid hydrogen storage dehydrogenation catalyst

Indoline (3.0 mmol, 0.33 ml) was loaded into a 10 ml round bottom flask containing the catalyst to be screened (1 mol% loading of metal, 0.03 mmol) under air. The flask, which was equipped with a magnetic stir bar and a condenser, was immersed into an oil bath pre-heated to 100 °C under a constant argon flow and stirred magnetically. A needle leading to an oil bubbler allowed H_2 gas generated *in situ* to escape from the system. After 60 min the reaction was allowed to cool, and an aliquot was obtained, dissolved in $CDCl_3$, and filtered through diatomaceous earth. Yield was determined by ^1H NMR spectroscopy. A similar procedure was used with

2,6-di-*tert*-butylpiperidine (1.92 mmol, 378.4 mg) with Pd/SiO_2 (10 wt% palladium on support, 1 mol% loading of metal).

2.4.5 • Sterically protected N-heterocycle dehydrogenation rate screening

A small round bottom flask was charged with 2,6-di-*tert*-butylpiperidine (394.7 mg, 2.0 mmol) and 10% palladium on carbon (2 mol% loading, 42.6 mg catalyst, 0.04 mol Pd) and equipped with a condenser. Inert gas was constantly swept over the reaction headspace to remove H_2 generated for the duration of the experiment, through needles through the septum in the condenser opening. The round bottom was immersed in an oil bath at the screening temperature for the allotted time. The product mixture was then filtered through small bed of diatomaceous earth to remove the catalyst and characterized with ^1H NMR spectroscopy. A similar procedure was used with 2,6-dimethylpiperidine where the relative molar amounts were kept constant.

2.4.6 • Thermally regenerative fuel cell hydrogenation catalyst

Chapter 3 Propiophenone (1.0 ml, 7.5 mmol) was measured into a 16 x 100 mm disposable glass test tube containing 1.0 mol% (metal/ketone) of 5 wt% (metal/substrate) Pd/SiO_2 (159.6 mg catalyst, 0.075 mmol Pd) and a small magnetic stir-bar. The test tube was capped with a rubber septum and H_2 (g) was flushed through the test tube for 15 min using two needles: a gas inlet needle positioned just above the liquid level and a gas outlet needle leading to an oil bubbler. After this, the gas outlet needle was removed completely and the gas inlet needle was retracted to just below the septum. Atmospheric pressure of H_2 was maintained throughout the reaction as the gas

manifold was connected to an oil bubbler. The test tube was lowered into a 100 ˚C oil-bath so that the mixture was under the oil level, and the mixture stirred at 300 rpm at this temperature for 1 h. After this time, the test tube was transferred immediately to an ice bath to stop the reaction. The neat reaction mixture was then filtered through a plug of diatomaceous earth in a glass pipette to remove the catalyst. An aliquot of the filtrate was dissolved in $CDCl_3$ for analysis by ^1H NMR spectroscopy. The spectra of product mixtures were compared to those of the expected products and byproducts found in the literature, and conversions and selectivities were calculated by relative proton integrations. For screening of other phenyl ketones, the 1.0 ml scale was maintained (1.0 g was used for ketones that are solid at room temperature) and the amount of catalyst adjusted appropriately. For the very fine Vulcan XC-72 based catalysts, the reaction mixture was dissolved in Et_2O for easier handling during workup and passed through a thicker layer of diatomaceous earth. The Et_2O was removed by rotary evaporation before ^1H NMR spectroscopy of the residue.

3.1.1 • Thermally regenerative fuel cell dehydrogenation catalyst

The catalyst being tested (0.1 mol% Pd based on amount of 1-phenyl-1-propanol used, 0.073 mmol, 15.5 mg) was weighed and transferred into a 16 x 150 mm test tube. 1-phenyl-1-propanol (7.3 mmol, 1.0 ml) was added to the test tube *via* a needle and syringe. A small, magnetic stir bar was added and the test tube was capped with a rubber septum. The mixture was stirred magnetically at 300 rpm, and the headspace flushed with hydrogen gas delivered through a long needle injected through the septum, positioned just above the liquid level, for 15 min. Gas was allowed to escape through a second needle through the septum. At this time, the outlet needle was

removed, and the gas manifold line was opened to an external oil bubbler to maintain a hydrogen pressure in the vessel of approximately 1 atm. The test tube was then submerged in an oil bath held at 200 ˚C so that the liquid in the tube was just below the oil level and left while continuing to be stirred magnetically. After 1 h, the test tube was removed from the oil bath and placed directly into an ice bath to stop the reaction, while the line delivering hydrogen was also removed. A small aliquot of the reaction mixture was then removed into ~ 1 ml deuterated chloroform, and then this mixture passed through a 5″ glass pipette plugged with a lint-free tissue wipe under diatomaceous earth into an NMR tube for NMR spectroscopic analysis. Conversions and selectivities were then calculated using ^{1}H NMR spectroscopy

Chapter 4 • Hydrogen Storage

4.1 • Hybrid Hydrogen Storage Systems

A brief set of results related to early work with the bound hybrid hydrogen storage systems is presented below as I collaborated on this project briefly and the balance of the work done by other researchers in the Jessop group. A complete exploration of the hydrolysis/dehydrogenation hybrid systems, both bound and mixed, has been published.[62] Double dehydrogenation systems were not the main priority of the author, but have also been published.[107]

4.1.1 • Chemically Bound Systems

The investigation of possible hybrid hydrogen storage systems started with the testing of bound hybrid systems, where the organic (endothermic) moiety was chemically bound to the chemical hydride (exothermic) moiety. This type of system is advantageous as the two carriers are combined in one molecule, meaning accidental phase separation is not possible, the ratio of endothermic to exothermic carrier moieties is fixed, and the heat transfer between the two should be facile. Two new adducts involving an N-heterocycle bonded to a borane moiety were synthesized (Scheme 4-1). An excess of a borane-THF adduct (to ensure complete conversion) was stirred with 4-aminopiperidine at room temperature to form 4-aminopiperidine N,N'-diborane, **1**. An

additional equivalent of 4-aminopiperidine was also added to **1** to produce two equivalents of the monoborane adduct with borane complexation through the ring nitrogen **2**.

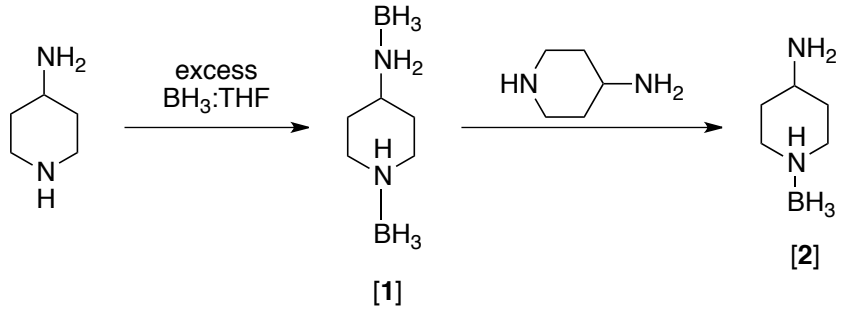

[**1**] [**2**]

Scheme 4-1 • Synthesis of 4-aminopiperidine-N,N'-diborane, **1** and 4-aminopiperidine-1-borane, **2**

The conversion to the desired borane adducts was indicated by the shrinking of the BH_3-THF ^{11}B NMR peak (q, δ ~1 ppm, from authentic sample) with the appearance of, in the case of **1**, peaks at δ -14.8 ppm and -21.4 ppm, assigned to borane moieties bound to the NR_2H and NRH_2 nitrogen atoms, respectively. Generally, ^{11}B NMR peaks for $R_2HN{:}BH_3$ are found between -10 and -20 ppm. Specifically, $Me_2HN{:}BH_3$ is known to have a ^{11}B NMR peak at -14.2 ppm in $CHCl_3$.[108] The connectivity was confirmed by comparing the ^1H spectrum of the products with the ^1H spectrum with ^{11}B decoupling ($^1H\{^{11}B\}$ NMR) at the known boron chemical shifts. In each case, the multiplet for the N-H proton collapses to a singlet, from a broad multiplet, with ^{11}B decoupling. Connectivity was further confirmed by ^1H–^1H Nuclear Overhauser effect spectroscopy (NOESY), which showed through space correlation between the established BH protons and appropriate ring hydrogen atoms. For **2**, the connectivity was further confirmed with X-ray crystallography (Figure 4-1). The measured B-N bond distance of 1.597(3) Å

agrees with normal B-N single bonds seen in the literature.[109-111] The melting points of these complexed species were all measured to be >220 ˚C.

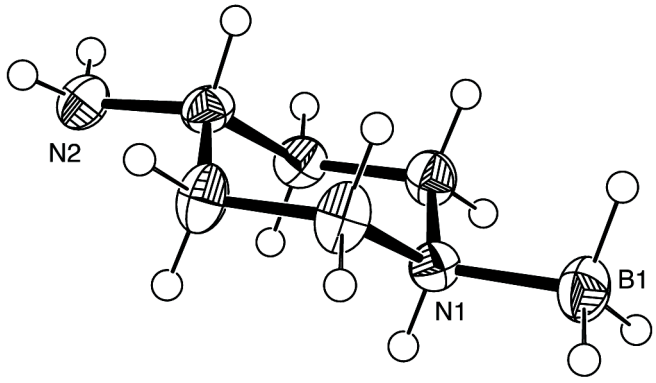

Figure 4-1 • Molecular structure of **2** from [62]

The dehydrogenation of these adducts was then attempted under flowing inert gas to remove any generated hydrogen, unless otherwise specified. With the addition of water in the presence of Pd/SiO_2, gas evolution was observed and hydrolysis of the B-H bonds in **1** and **2** was complete after 3 h at 100 ˚C (as shown for **1** in Scheme 4-2). It should be noted that the hydrolysis of such boranes can proceed in the absence of a catalyst as well, but it is present to see its effect, as it will be necessary in the final system for the endothermic dehydrogenation. This was indicated by a shift of the aforementioned BH_3 ^{11}B NMR peaks to a common, very broad singlet at δ 10–11 ppm, assigned to borate species such as $B(OH)_3$ and BO_2^-, which have been reported to be in equilibrium with each other.[112, 113] This borane hydrolysis was, however, not accompanied by any apparent ring dehydrogenation. In all instances, the ^1H NMR spectrum showed retention in CH splitting patterns, with only small changes in chemical shift. The hydrolysed product of **1** was then exposed to further, more extreme conditions, yet no dehydrogenation of the ring was observed. Even after 18 h at 200 ˚C

with 10 mol% loading of Pd/SiO_2 (in DMSO-d_6 because of the high melting points of the initial adducts), the ring could not be dehydrogenated. It should also be noted that the initial borane complexes were all insoluble in water; the borate complexes were all water-soluble.

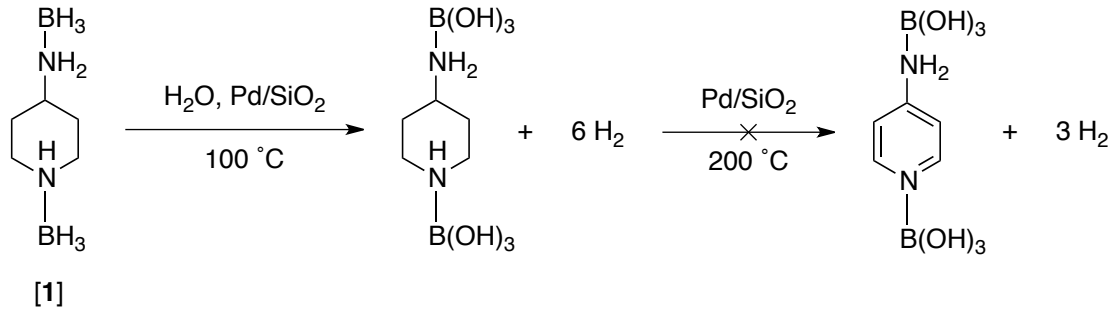

Scheme 4-2 • Hydrolysis of **1** with unsuccessful ring dehydrogenation. Only $B(OH)_3$ species are shown for clarity.

In comparison, the dehydrogenation of uncomplexed 4-aminopiperidine goes to competition over 0.5 h at 170 ˚C with Pd/SiO_2,[57] and in 15% conversion over 3 h at 100 ˚C.[62] The dehydrogenation of the ring in these adducts is, therefore, likely hindered by the boron moiety. The lone pair of electrons on the nitrogen atom is being donated to the borane moiety to form a dative bond, making the ring more electron-deficient, and therefore increasing the energy required to dehydrogenate the ring. This could be due to a lack of electron density available in the ring for binding the catalyst surface for reaction or in the carbon *p* orbitals for hybridization and reaction with the hydrogen atoms on the surface.

It was possible that the BH_3 adduct would dehydrogenate at the ring more easily than the $B(OH)_3$ adduct. To probe this, **1** was dissolved in triglyme or DMSO in the absence of water and mixed with Pd/SiO_2 for 3 h at 170 ˚C. From the ^1H NMR spectrum, it was clear that there had been no ring dehydrogenation, indicated by the

absence of any aromatic proton peaks. It was noted that the number of amine protons decreased from 3 to 1, based on relative peak integrations. This suggests the dehydrogenation of the B-N bonds to give **3** (Scheme 4-3). The product(s) of the reactions were neither isolated nor further characterized, but the experiment indicated that BH_3, like $B(OH)_3$, causes too much electron deficiency in the rest of the molecule to allow for ring dehydrogenation.

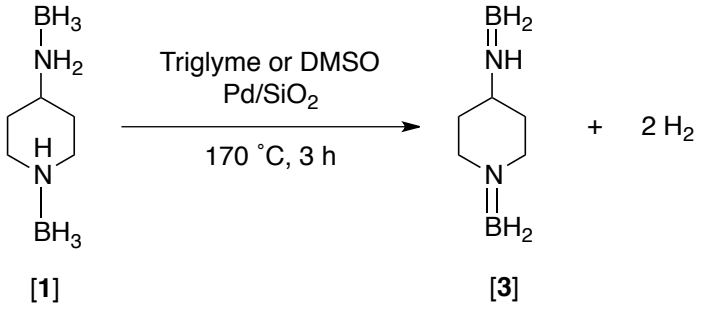

Scheme 4-3 • Suggested dehydrogenation of B-N bonds of **1**, without ring dehydrogenation

An indoline-borane adduct, **4**, was also prepared and tested for dehydrogenation reactivity (Figure 4-2). The dehydrogenation was thought to possibly be more thermodynamically favourable than for the aminopiperidine based adducts because the dehydrogenation of indoline itself is more favourable; indoline can be completely dehydrogenated over Pd/C in 0.5 h at 100 ˚C.[48] The formation of **4** was confirmed by NMR spectroscopy. A broad quartet at δ 2.48 ppm ($^1J_{HB}$ = ~90 Hz) in the ^{1}H NMR spectrum was reduced to a singlet in the ^{1}H{^{11}B} NMR spectrum. The proximity of the C7-H and amine protons to the borane protons was demonstrated with ^{1}H-^{1}H NOESY.

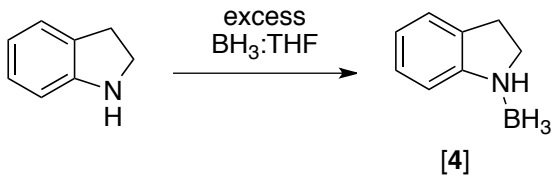

[**4**]

Figure 4-2 • Formation of indoline borane, **4**

To attempt tandem dehydrogenation, **4** was exposed to water over Pd/C for 2 h at 100 °C. The ^{1}H and ^{11}B NMR spectra of the product mixture showed complete borane hydrolysis with 71% indoline dehydrogenation (Scheme 4-4). A COSY (correlation spectroscopy) spectrum shows correlation between the NH proton peak at δ 11 ppm and olefinic indole protons, demonstrating retention of the NH bond, and therefore that there had been no B-N dehydrogenation. This was the first example of a hydrogen-storing molecule that releases hydrogen both endothermically and exothermically. It has a gravimetric hydrogen storage density of 6% not including the weight of water, which presumably could be recovered from the fuel cell waste stream. The hydrogen release is, however, still very exothermic. This is undesirable due to the wastage of energy and possibility of losing control of the reaction progress on board the vehicle. Adding together the enthalpy of borane hydrolysis (approximately -156 kJ mol^{-1}), [112,113] and that of indoline dehydrogenation (52 kJ mol^{-1})[114] gives an estimated overall enthalpy of -104 kJ mol^{-1} or -26 kJ (mol H_2)$^{-1}$. It would be desirable if this number were closer to zero. Lastly, despite the ease of complete unsubstituted indoline dehydrogenation under similar conditions, the fact that the dehydrogenation was not complete under these conditions suggests that, again, the electron-withdrawing nature of the borane fragment slows down the dehydrogenation of the organic portion.

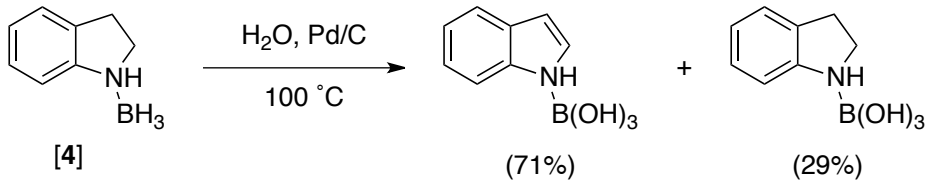

Scheme 4-4 • Tandem hydrolysis and dehydrogenation of **4**

In order to overcome these problems, the borane and amine fragments must be separated to give a mixture of two molecules instead. The focus therefore shifted to mixed hybrid systems.

4.1.2 • Physically Mixed Hydrolysis/Dehydrogenation Systems

Mixed hybrid systems are those that involve a mixture of two molecules, which are not chemically associated or bonded to each other, where one undergoes exothermic dehydrogenation while the other undergoes catalysed endothermic dehydrogenation. The lack of chemical bonding between the two species should prevent the inhibition of organic ring dehydrogenation unless there is an *in situ* borane transfer. It also allows for easier manipulation of the reaction stoichiometry toward achieving a heat balance. Another important caveat of such a system is solubility; a solventless system is advantageous because extra solvent weight and volume will only decrease the overall gravimetric and volumetric hydrogen capacities. If one of the carriers is a liquid, while the other is a solid, solubility of the latter in the former under all operating conditions is critical. Indoline was chosen as an ideal organic liquid (endothermic) to be paired with the exothermic carriers because of its rapid catalytic dehydrogenation at low temperatures. Also, indoline is the only endothermic system thus far studied that undergoes dehydrogenation when mixed with an exothermic carrier (*vide infra*).

Indoline is a liquid at room temperature, and has a boiling point of 220 ˚C, well above the operating temperature of a PEMFC (80-100 ˚C). This is important as we envision the heat required for the dehydrogenation being provided by the radiated heat of the fuel cell, and therefore this is the desired reaction temperature.

One drawback to the use of indoline is the relative difficulty that exists in regenerating indoline from indole, the dehydrogenation product. Generally, it would be envisioned that the organic ring could simply be re-hydrogenated catalytically, but the selectivity with which this must be done generates difficulties. The fact that the olefin that is to be hydrogenated is already highly stabilized by resonance with the aromatic ring also makes this transformation more difficult.[115] Transfer hydrogenation using reagents such as $NaBH_3CN$[116] have been shown successful for this transformation, but are required in at least stoichiometric amounts and therefore produce significant amounts of sometimes-toxic waste. The use of hydrogen gas as the hydrogen source for the hydrogenation would be ideal as there would be no such waste; however, there is a tendency for the molecule to be over hydrogenated to the octahydroindole species. More recently, however, some promising results have been published in the literature. Kulkarni *et al*. demonstrated the use of relatively low hydrogen pressures (30-50 bar) over Pd/C in water with the addition of one equivalent of a Brønsted acid such as trifluoroacetic acid or *p*-toluenesolfonic acid.[115] They were able to achieve the desired indoline products from a number of unprotected indoles (including indole itself) in 100% selectivity and 30% to quantitative conversion in 2–3 h. It should also be considered that it was chosen as an example heterocycle due to it is known ease of dehydrogenation, and should not be considered the only option for such hybrid systems. Indeed, it is gravimetric hydrogen storage density is low at only 1.7%. Nevertheless, it was chosen as a good model compound because of its rapid

dehydrogenation at relatively low temperatures and its high boiling point. Several different boranes were then examined for their appropriateness for dehydrogenation/hydrolysis mixed hybrid systems with indoline.

For the exothermic system, the focus was initially on those that released hydrogen via a hydrolysis reaction for the development of a dehydrogenation/hydrolysis mixed hybrid system. First, indoline was paired with $NaBH_4$ (Table 4-1), which is known to undergo exothermic hydrolysis under mild conditions (Scheme 4-5)[117] and a mixture of the two was shown to be stable to decomposition at room temperature; however, very low solubility of the salt in indoline was observed.

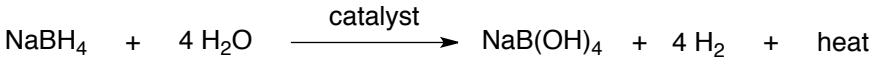

Scheme 4-5 • Exothermic hydrolysis of $NaBH_4$.

Initially, a 5:1 molar mixture of indoline and $NaBH_4$ was employed for dehydrogenation testing, establishing a nearly heat balanced system (for BH_4^- hydrolysis, ΔH = -250.5 kJ mol^{-1},[118] so the total enthalpy change for the mixed system is ΔH_{rxn} = -250.5 kJ mol^{-1} + 5 (52 kJ mol^{-1}) = +9.5 kJ mol^{-1}). When using 5 mol% loading of Pd/C and 4 molar equivalents of water (stoichiometrically balanced), neither dehydrogenation of indoline nor hydrolysis of $NaBH_4$ was observed after 2 h at 100 °C (entry 1). This was likely due to poor mass transfer because of the insolubility of $NaBH_4$ in the indoline/water mixture, and a significant amount of dry catalyst. Decreasing the amount of catalyst employed to 2 mol% (entry 2) also resulted in no product formation, by ^1H NMR spectroscopy. Increasing the amount of water in the system to 40 equivalents resulted in 80% dehydrogenation of the indoline with 100% hydrolysis of the $NaBH_4$ as determined by ^1H and ^{11}B NMR spectroscopy respectively (entry 3). It

was postulated that the presence of $NaBH_4$ could be hindering the dehydrogenation of indoline by forming a one to one complex as the 5:1 mixture resulted in 20% unreacted indoline. The indoline:$NaBH_4$ ratio was then changed to 2:1 (entry 4), if the hypothesis were true, only 50% dehydrogenation of the indoline would be expected, instead 91% dehydrogenation was observed with 100% hydrolysis of the $NaBH_4$. This was the first example of two separate hydrogen carriers dehydrogenating together in one system. As mentioned, however, $NaBH_4$ is not soluble in indoline, and is therefore not ideal for a mixed hybrid system.

Table 4-1 • Summary of mixed hybrid systems employing indoline and $NaBH_4$

Entry	Equivalents			Mol% catalyst loading	Results[a]	
	Indoline	$NaBH_4$	H_2O		% Indoline dehydrogenation	% $NaBH_4$ hydrolysis
1	5	1	4	5	0	0
2	5	1	4	2	0	0
3	5	1	40	2	80	100[b]
4	2	1	40	2	91	100[b]

a | reactions performed at 100 ˚C, 2 h over the delineated loading of 10 wt% Pd/C
b | no starting material or side products were evident in the ^{11}B spectrum.

Amine boranes were then investigated as possible exothermic hydrogen carriers; specifically, dimethylamine borane ($Me_2NH:BH_3$, **5**) and triethylamine borane ($Et_3N:BH_3$, **6**), as they were expected to be more soluble and their use widely precedented in the literature.[28,47,117,119-120] Dimethylamine borane (**5**) is a solid at room temperature, but it is completely soluble in indoline. No solvent should be needed as long as the hydrolysed product(s) are soluble in indoline as well. Baker and co-workers have previously described the standalone dehydrogenation behaviour of **5**.[32] Over a precious metal catalyst, complete dehydrocoupling of **5** occurs over several hours with gentle heating (26-45 ˚C) to give a dimer ($N_2B_2H_8$) and 2 eq. H_2 (Scheme 1-5); in the presence of water,

the products are $Me_2HN{:}B(OH)_3$ and 4 eq. H_2. We first looked at the standalone hydrolysis of **5** to allow for a direct comparison of our mixed system results. Without catalyst, after 2 h at 100 ˚C, a 1:3 mixture of **5**:H_2O results in partial borane hydrolysis, while at room temperature, no change in the ^{11}B NMR spectrum is observed (Table 4-2, entries 1 and 2). With 2 mol% loading of a commercial 10 wt% Pd/C catalyst, complete hydrolysis was observed after 2 h at 100 ˚C and at room temperature (entries 3 and 4). Complete hydrolysis means that only borate species are observed in the ^{11}B NMR spectrum, including the parent $B(OH)_3$ species at δ ~18 ppm and other borate species in equilibrium at δ 19, 8 and 2 ppm, as described by Xu and co-workers.[112-113]

Table 4-2 • The reactions of the mixed hybrid system employing indoline, $Me_2NH{:}BH_3$ and water

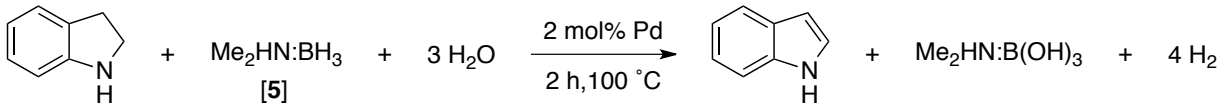

	Equivalents				Results[a]	
Entry	**Indoline**	**$Me_2NH{:}BH_3$**	**H_2O**	**Catalyst**	**% Indoline dehydrogenation**	**BH_3 hydrolysis**
1	0	1	3	None	—	Partial (~20%)
2[b]	0	1	3	None	—	None
3	0	1	3	Pd/C	—	Complete
4[b]	0	1	3	Pd/C	—	Complete
5	1	1	0	None	0	Shift to 6 ppm
6	1	1	0	Pd/C	0	Shift to 6 ppm
7	1	1	3	None	0	Partial (~20%)
8	1	1	3	Pd/C	91	Complete
9[c]	1	1	3	Pd/C	> 99	Complete
10	3	1	3	Pd/C	> 99	Complete
11[d]	3	1	3	Pd/C	72	Complete

a | reactions performed with 2 mol% loading of 10 wt% catalyst under flowing N_2 to remove any H_2 produced, determined by ^1H and ^{11}B NMR spectroscopy.
b | reactions performed at room temperature.
c | reaction performed with 6 mol% catalyst loading.
d | reaction perfomed without N_2 flow.

When indoline and **5** are mixed at room temperature, either with or without catalyst present, no changes in the indoline peaks of the ^{1}H NMR spectrum are observed, indicating that no indoline dehydrogenation has taken place (entries 5 and 6). This is expected for those reactions at room temperature, which were performed to verify no dehydrogenation would take place. In each case with no water present, however, the ^{11}B NMR spectrum showed that the BH_3 peak had shifted to δ ~6 ppm. This information, combined with the lack of indoline dehydrogenation, even with catalyst present, suggests that there may be borane transfer happening to produce a complex similar to **4**. Further characterization was not undertaken until later, and is fully described by another author elsewhere.[107] Briefly, crystals of the product were grown and X-ray crystallography indicated an N-B(H)-N complex where boron a BH moiety is bound to two indoline molecules (Scheme 4-6).

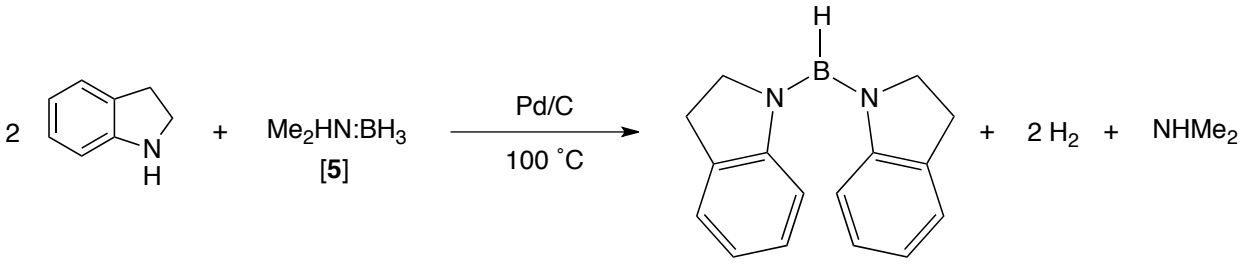

Scheme 4-6 • Formation of bis-indoline borane complex

When all three components are mixed in the absence of catalyst (Table 4-2, entry 7), no indoline dehydrogenation is observed, which is expected without catalyst. The presence of indoline did not seem to affect the hydrolysis of the borane as similar results were observed with and without it (entry 1). In the presence of 2 mol% loading of Pd/C (entry 8), complete hydrolysis is observed along with 91% indoline dehydrogenation. Increasing the metal loading to 6 mol% (entry 9), results in complete

indoline dehydrogenation. Finally, the mole ratio was then increased to 3:1 (indoline:**5**) in order to establish a heat balance based on the respective enthalpies of reaction (ΔH_{rxn} = -156 kJ mol^{-1} + 3(+52 kJ mol^{-1}) = 0 kJ mol^{-1}). This combination also allowed for complete borane hydrolysis and indoline dehydrogenation (entry 10). Finally, the reaction was carried out without flowing N_2 flushing the flask (entry 11) to determine the effect of a partial pressure of H_2 over the reaction mixture. This resulted in a modest drop in the extent of indoline dehydrogenation, which is to be expected based on Le Châtelier's principle. These results demonstrate that it is possible for two hydrogen-releasing reactions to take place in the same mixture without one adversely affecting the other. The gravimetric capacities, however, are low. For a 1:1 mixture, the gravimetric capacity is only 4.5 wt% (not including water, which would be supplied from the fuel cell waste stream), with a net exothermic enthalpy of -104 kJ mol^{-1}. While increasing the ratio to 3:1 (indoline:**5**) results in a net enthalpy of 0 kJ mol^{-1}, the gravimetric capacity decreases to 2.9 wt%.

The advantages of this system over those mentioned in Chapter 1.4.5 are that: both carriers operate independently in the same chamber without interfering with each other, the reaction temperature is moderate (100 ˚C) and within the operating temperature range of standard Nafion PEM fuel cells, and the endothermic carrier acts as a solvent for the exothermic carrier, producing a liquid mixture and thereby facilitating easier material handling. However, three major disadvantages of this system remain: the rate disparity between the two reactions, the low storage density, and the insolubility of the borate product in indoline. The exothermic reaction is very fast, resulting in immediate gas and heat evolution, while the endothermic system is much slower. This will be investigated further in Chapter 4.2.

With regard to the solubility problem, a sample of the dimethylamine borate product was prepared and tested for its solubility in a number of solvents. The Kamlet-Taft solvatochromic parameters of each solvent were plotted to help identify the type of solvent required to retain the borate in solution after reaction (Figure 4-3 and Figure 4-4).

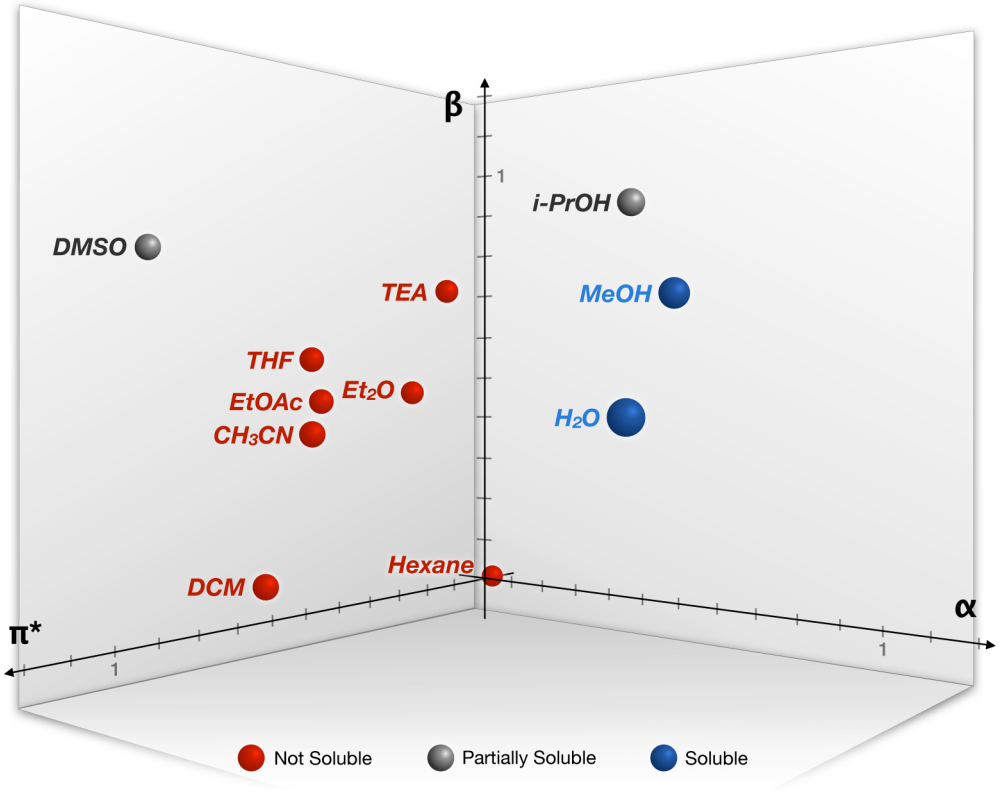

Figure 4-3 • Dimethylamine borate solubility in various solvents by Kamlet-Taft parameters

From the results, it is plain to see that the solubility of dimethylamine borate is poor in most solvents. No solubility was qualitatively observed in triethylamine, THF, ethyl acetate, ethanol, acetonitrile, dichloromethane or hexane after 24 h, all of which have zero or small α values, corresponding to poor hydrogen-bond donating ability. Isopropanol offered partial solubility after 24 h, but solid particulate was still quite

evident. DMSO eventually solubilized the borate after 1 h. Water and methanol both quickly solubilized the borate.

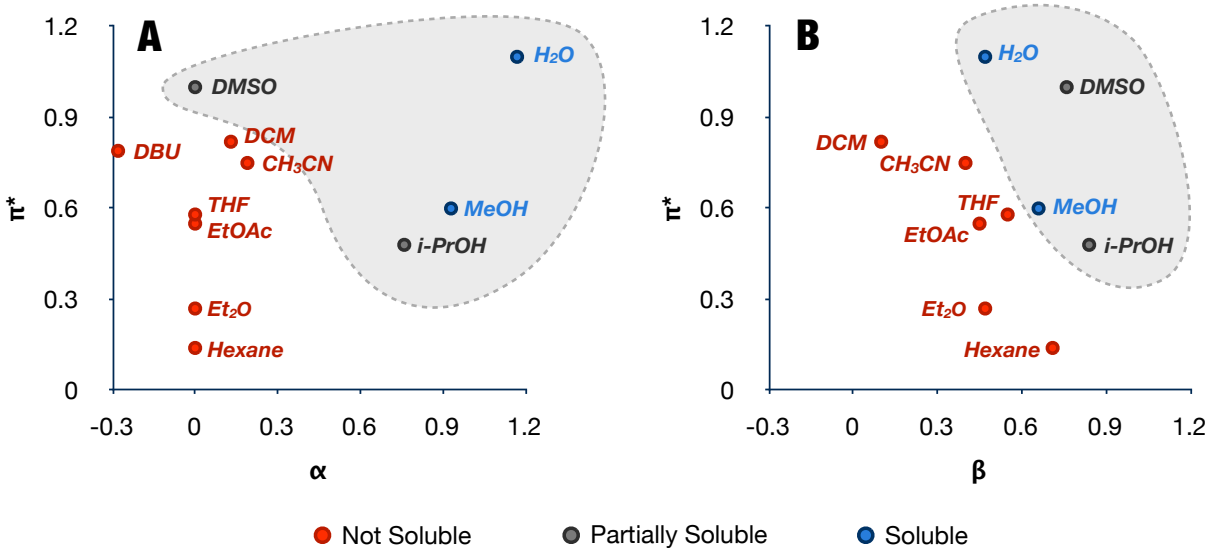

Figure 4-4 • Two-dimensional $Me_2HN:B(OH)_3$ solubility plots by Kamlet-Taft parameters where areas containing solvents that offer at least some solubility are highlighted

All solvents, except DMSO, that provide any solubility have high α values (Figure 4-4). It can also be noted from this plot that, regardless of the value of β or π^*, a solvent with a high α value will solubilize the borate. This is not surprising, as both the dimethylamine and borate moieties would interact favourably with hydrogen-bond-donating solvents. With a low α value, it appears that a high polarity can also induce solubilization (as with DMSO). A higher hydrogen-bond accepting ability (β) is also important, while not as important as α. The β value for 1,8-diazabicyclo[5.4.0]undec-7-ene (DBU) is unknown so it is only plotted below in the plot of π^* versus α (Figure 4-4A). While it is expected to have a high β value, and has a high measured value of π^*, the borate is still not soluble. This again indicates the importance of hydrogen-bond donating ability. Overall, it appears that highly polar, protic solvents should be able to

solubilize the borate products from the hydrolysis of dimethylamine borane. Unfortunately, the result of this study indicates that the only additives that may increase the solubility of the product are water and methanol, both of which will react rapidly with the borane at elevated temperatures. Since water is used for the hydrolysis of the borane anyway, and it is available from the waste stream of the fuel cell itself, it is possible that excess wastewater could be added to the spent fuel before removal to ensure that all components are removed.

Table 4-3 • Summary of mixed hybrid system employing indoline, $Et_3N{:}BH_3$ and water

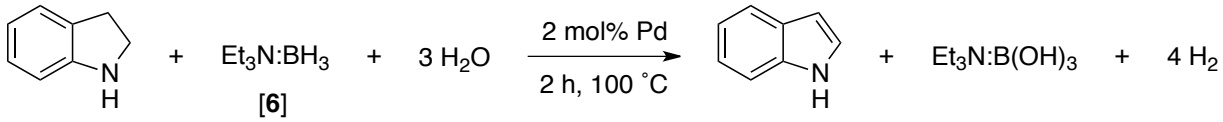

	Equivalents				Results[a]	
Entry	**Indoline**	**$Et_3N{:}BH_3$**	**H_2O**	**Catalyst**	**% Indoline dehydrogenation**	**BH_3 hydrolysis**
1	0	1	0	Pd/C	—	None
2	0	1	3	Pd/C	—	Complete
3[b]	0	1	3	Pd/C	—	Complete
4	0	1	3	None	—	Complete
5[b]	0	1	3	None	—	None
6	1	0	3	Pd/C	>99	—
7	1	1	0	None	0	None
8	1	1	0	Pd/C	>99	None
9	1	1	3	None	0	Complete
10	1	1	3	Pd/C	>99	Complete
11	3	1	3	Pd/C	>99	Complete

a | reactions performed at 100 ˚C, 2 h with 2 mol% loading of 10 wt% catalyst under flowing N_2 to remove any H_2 produced, determined by ^1H and ^{11}B NMR spectroscopy.
b | reactions performed at room temperature.

The second akylamine borane is triethylamine borane ($Et_3N{:}BH_3$, **6**), which is a liquid at room temperature and is completely miscible with indoline, was investigated (Table 4-3). First, **6** was held at 100 ˚C for 2 h in the presence of Pd/C without added

water for comparison to later experiments. The borane was stable as no change was observed in the ^{11}B NMR spectrum (Table 4-3, entry 1). With the addition of water, the hydrolysis of **6** is complete in 2 h at 100 ˚C or room temperature (entries 2 and 3). Even without catalyst, hydrolysis is complete at 100 ˚C (entry 4), but no change in the ^{11}B NMR spectrum is observed at room temperature (entry 5). As discussed before, indoline by itself is able to undergo complete dehydrogenation under these conditions and the addition of water does not affect this (Table 4-2, entry 6).

A mixture of indoline and $Et_3N{:}BH_3$ without catalyst leads, unsurprisingly, to no indoline dehydrogenation at 100 ˚C; also, no hydrolysis is observed (entry 7). With the addition of a catalyst, indoline dehydrogenation proceeds to completion, with no change observed in the ^{11}B NMR spectrum (entry 8). This is an interesting result when compared to a similar mixture with $Me_3N{:}BH_3$ (Table 4-2, entry 6), where a shift in the boron peak seen in the ^{11}B NMR spectrum suggested the formation of an indoline-borane adduct. No such formation is indicated here. Dimethylamine is a better Lewis base than of triethylamine,[121] which should result in a more easy transfer of the borane moiety from the amine to indoline. At elevated temperatures, however, the loss of borane to give gaseous dimethylamine would be more highly entropically favoured over the generation of triethylamine because the latter would remain in solution in the condensed phase.

Combining all three components in the absence of catalyst at 100 ˚C results in complete borane hydrolysis with (as expected) no indoline dehydrogenation (Table 4-3, entry 9). The addition of catalyst prompts complete indoline dehydrogenation and borane hydrolysis (entry 10). Finally, a similar result is also obtained when the ratio of indoline to $Et_3N{:}BH_3$ is increased to 3:1 in order to establish a heat balance (entry 11).

While the enthalpy of reaction should be similar to that of the dimethylamine borane system, the gravimetric storage capacity is lower because that of the specific amine borane is lower: For a 1:1 mixture of indoline and $Et_3N{:}BH_3$, the storage capacity is 3.4 wt% H_2, at 3:1, 2.5 wt% H_2.

The viability of using unsubstituted ammonia borane ($NH_3{:}BH_3$) hydrolysis as the exothermic system was also investigated due to its higher gravimetric storage density by another member of the group, and can be read about in detail elsewhere.[107] Briefly, however, it was demonstrated that a 3:1 (indoline:amine borane) mixture undergoes complete borane hydrolysis and indoline dehydrogenation when exposed to 3 equivalents of water, at 100 ˚C for 2 h over 2 mol% Pd/C. The increase in gravimetric capacity is modest (because the borane contains only a small amount of the non-hydrogen weight of the system) and reaches 5.3 wt% H_2 with a net $\Delta H = 0$ kJ mol^{-1}. Larger increases of the overall gravimetric capacity could be made with further exploration of different endothermic hydrogen release systems.

4.1.3 • Physically Mixed Double Dehydrogenation systems

A double dehydrogenation mixed hybrid system is one where two separate species in a single mixture undergo dehydrogenation, both without the addition of water. As there is precedent in the literature for the thermal dehydrogenation of dimethylamine borane, **5**, via a dehydrocoupling reaction (Chapter 1.4.4, Scheme 1-5), this was the first exothermic system paired with indoline. Alone, the dehydrogenation of **5** is catalysed by both Rh/C and Pd/C; mixing of **5** with the catalyst at room temperature results in immediate heat and gas release. As previously mentioned, indoline can be completely dehydrogenated over Pd/C after 0.5 h at 100 ˚C.

Initially, the question was: if these two components are mixed together over a precious metal catalyst at elevated temperature, will they independently dehydrogenate or will they interfere with one another? First, equimolar amounts of indoline and **5** were mixed together under an inert atmosphere with either Rh/C or Pd/C and heated to 100 ˚C for 2 h. In both experiments, changes in both the ^{1}H and ^{11}B NMR spectra were observed. The boron NMR signal for **5** (δ -12 ppm) disappeared with the appearance of a triplet at δ 26 ppm. In the proton spectrum, small shifts were observed in the aromatic indoline peaks, along with a change in the methylene peaks from four multiplets to two distinct triplets at δ 4.1 and 3.2 ppm. The methyl ^{1}H NMR peaks of **5** were not observed in the product mixture. It is likely that there is a boron transfer happening, from the dimethylamine fragment to indoline. Once dimethylamine is free of the borane moiety, it would easily evaporate under the reaction conditions (its boiling point is only 7 ˚C)[122] and be swept away by the nitrogen purge gas. However, the boron NMR peak did not match that expected for the simple indoline-BH_3 adduct, **4** [$\delta(^{11}B)$ -14 ppm]. This, along with the observed changes in the proton NMR spectrum, prompted the suggestion of a new compound, 1-borylindoline, **7**.[107] Connectivity was later confirmed by another researcher using $^{1}H\{^{11}B\}$ and 2D NMR spectroscopic techniques including NOESY, as before.

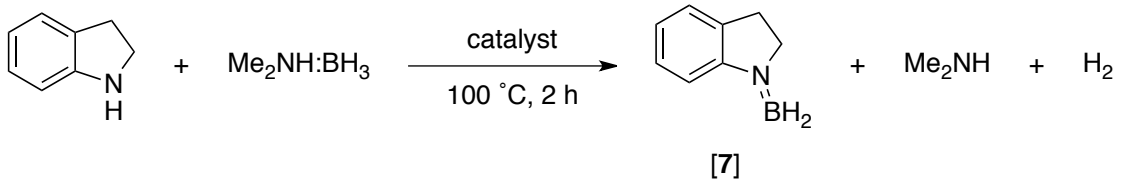

Scheme 4-7 • Formation of 1-borylindoline (**7**) from indoline and dimethylamine borane.

The formation of **7** demonstrates that these two hydrogen carriers cannot independently release hydrogen when mixed together due to a boron transfer. This again results in indoline being too electron deficient to undergo its usually facile dehydrogenation under these conditions. As is, this system releases only one equivalent of hydrogen (that's only about 1 wt% H_2), which would be far too low for any real-world application. With this, it is clear that one of the reagents has to be changed in order to prevent any *in situ* Lewis acid-base adduct formation.

It was first thought that an analogous heterocycle with a less basic heteroatom (2,3-dihydrobenzofuran) could be employed instead of indoline. Ideally, this would allow for the dehydrogenation of the two carriers without unwanted adduct formation. After 2,3-dihydrobenzofuran was exposed to 1 mol% metal loading of a 10 wt% Pd/C catalyst at 100 ˚C for 1 h, ^{1}H NMR spectroscopy indicated only 5% conversion mostly to product. At 180 ˚C, only 29% conversion was achieved after 1 h. These low conversions, even at extremely high temperatures for this application, indicate that the ring is too electron deficient to undergo rapid dehydrogenation, and was therefore abandoned.

The strategy employed was then to see if a sterically-protected amine could be dehydrogenated in the presence of dimethylamine borane. The commercial availability of substituted indoline analogues is limited, and therefore 2,6-disubstituted piperidines were investigated. Two protected cyclic amines, 2,6-*cis*-dimethylpiperidine, **8**, and 2,6-*cis*-di-*tert*-butylpiperidine, **9**, were synthesized by hydrogenating the analogous pyridines purchased from chemical suppliers. Both 2,6-dimethylpyridine and 2,6-di-*tert*-butylpyridine were completely hydrogenated in isopropanol after 18 h at 100 ˚C under 80 bar H_2 with 2 mol% Pd/C. Removal of the solvent *via* rotary evaporation gave

the products in quantitative yield. No further purification was required and the products' ^{1}H NMR spectra matched those found in the literature.[104,123]

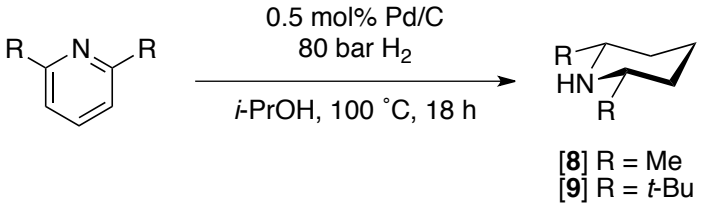

Scheme 4-8 • Hydrogenation of sterically encumbered pyridines to the analogous piperidines

The use of **9** was tested first because the two flanking *tert*-butyl groups have been shown previously to be sufficient to prevent formation of similar Lewis acid-base adducts. The steric bulk around the nitrogen in 2,6-di-*tert*-butylpyridine is enough to prevent complete adduct formation between the nitrogen lone pair and a BF_3 molecule, or even a fully solvated proton.[124,125] The dehydrogenation of **9**, by itself, proceeds to up to 83% conversion (rather irreproducibly) after 2 h at 100 ˚C over 2 mol% metal loading of 10 wt% Pd/C. In contrast, when **9** has been mixed with dimethylamine borane and heated to 150 ˚C for 4 h over a similar catalyst loading, various results have been obtained. When superfluous water is available to allow for borane hydrolysis instead of dehydrocoupling, the hydrolysis proceeds very quickly, and allows for good conversions of ring dehydrogenation (up to 85%). When extra care is taken to ensure no water is present, however, something very different happens. The product mixture shows no peaks in the ^{11}B NMR spectrum, and the piperidine peaks in the ^{1}H NMR spectrum are left unchanged. Since no boron containing species are found in the product mixture, there are two perceived possibilities as to the fate of dimethylamine borane. One possibility is that it, in its entirety, is being lost from the system. Because the system is mostly closed, other than the purging gas flow through the top of a

condenser 15 cm above the reaction mixture, and dimethylamine borane has a boiling point of >250 ˚C (49 ˚C, 0.01 Torr),[126] well above the reaction temperature of 150 ˚C, this situation is highly unlikely. Secondly, it is possible that the borane was not extracted from the catalyst before analysis. The separation of the borane and dimethylamine fragments with evaporative loss of the latter has been discussed previously, and is possible here as well. However, because there is no evidence in the NMR spectra of an adduct forming between the borane and the substituted piperidine, yet the dehydrogenation proceeds to a lesser degree than expected, it is proposed that the BH_3 poisons the catalyst surface through irreversible binding. Similar observations have been made by Manners and co-workers where, during the dehydrogenation of $Me_2NH{:}BH_3$, they noted that the heterogeneous catalysts were poisoned by "BH_3" generated *in situ*.[127] Because the hydrolysis product is incapable of such poisoning, the ring dehydrogenation is able to proceed when there is water present. Even though the concept of protecting the nitrogen sterically does prevent adduct formation, it does not allow both carriers to operate independently. If one were to employ this combination as a dehydrogenation/hydrolysis mixed system instead, it would have a gravimetric hydrogen density of only 2.4 wt% (not including the weight of water for reasons discussed previously).

In order to increase the maximum hydrogen storage density, it is important to decrease the weight of the piperidine itself. With this in mind, **8** was employed with $Me_2NH{:}BH_3$ for testing, which would have a combined theoretical 3.5 wt% H_2. The temperature of the reaction had to be lowered because the boiling point of **8** is only 127 ˚C.[128] At 100 ˚C, after 4 h over 2 mol% Pd/C, the piperidine, without the addition of **5**, only dehydrogenates, somewhat not reproducibly, to between < 1–5% conversion. With this, the idea of a mixed system with 2,6-dimethylpiperidine was abandoned.

In conclusion, our group was not able to show a double dehydrogenation mixed hybrid hydrogen storage system. However, a new observation in hydrogen storing organic liquids was discovered. It was noted that the dehydrogenation of 2,6-dimethylpiperidine was slightly faster than piperidine itself, and the rate enhancement with 2,6-di-*tert*-butylpiperidine was even more marked. Also, as previously mentioned, during the study of any of these hybrid systems, the rate disparity between the endothermic and exothermic hydrogen releasing components was extreme, and most of the time, prohibitive. Working to overcome this rate disparity became the focus of my research, including how this sterically promoted rate enhancement may be a possible means toward this end.

4.2 • Overcoming the rate disparity

With overall poor results from the double dehydrogenation systems, the investigation of how to improve the rate disparity between the rates of indoline dehydrogenation (endothermic release) and dimethylamine borane hydrolysis (exothermic release) was undertaken. Being unable to overcome this disparity would threaten the feasibility of the system. If the endothermic reaction were too slow to take up the heat released from the exothermic H_2 release before the heat dissipated into the surroundings, the heat balance of the system simply would not work. A simple calculation was therefore performed to predict a) how much of the heat would be lost to

the surroundings, and b) how much catalyst would be necessary to obtain the DOE-mandated rate of H_2 release.

Both reaction rates can be adjusted by modifying the conditions and method employed. Adding the necessary equivalents of water as needed would control the rate of dimethylamine borane hydrolysis; the reaction is essentially instantaneous at 100 ˚C in the presence of a precious metal catalyst. While the rate of indoline dehydrogenation is independent of the amount of indoline used (indoline is the solvent, so its concentration is independent of the amount used), the rate *is* dependent on the number of available catalyst sites. The rate should, therefore, increase with an increasing amount of catalyst.

4.2.1 • Changing catalyst loading

Increasing the rate of indoline dehydrogenation by increasing the catalyst loading should be possible. However, this will also increase the cost of the system. So the question of how much catalyst is needed to adequately increase the rate of the endothermic system to achieve a viable fuel comes to the forefront. The initial rate of hydrogen production from the system had to be determined at a number of catalyst loadings to confirm that the rate indeed increased linearly with moles of catalyst metal added. The conversion from indoline after 5 minutes was measured with 0.50, 1.0 and 2.0 mol% metal loading of a 10 wt% Pd/C (Table 4-4). The initial rate of indoline dehydrogenation (and hydrogen production) is the number of moles converted to product (i.e. indole and H_2) over 300 s. From the rightmost column, it is clear to see that the rate of the dehydrogenation scales with the amount of catalyst loading over, at least,

this range of loadings. The mean of the three calculated relative rates is 3.0×10^{-4} mol s^{-1} g-Pd^{-1}.

Table 4-4 • Initial H_2 production rates from indoline dehydrogenation with various catalyst loadings[a]

Catalyst loading (mol% metal)	Conversion at 5 min (%)	Initial rate ($x10^{-6}$ mol s^{-1})	Relative initial rate ($x10^{-4}$ mol s^{-1} g-Pd^{-1})
0.50	4.7	1.4	2.9
1.0	9.4	2.8	3.1
2.0	20	5.9	3.1

a | reactions performed at 100 ˚C under flowing N_2 to remove any H_2 produced, determined by ^1H NMR spectroscopy.

The DOE benchmark for the rate of H_2 production from any hydrogen fuel is 0.02 g s^{-1} per kW of power output by the engine.[27] We considered an engine running at 150 horsepower (~113 kW) for this calculation, meaning the required rate of H_2 production from the system must be 2.25 g s^{-1}. A system composed of a 3:1 mixture of indoline to amine borane generates half of its H_2 from indoline and half from the amine borane. Therefore, based on the rate of indoline dehydrogenation with respect to the amount of catalyst, in order to generate the requisite 1.13 g s^{-1} of H_2 from indoline dehydrogenation, one would need over 1.9 kg of Pd at 100 ˚C! This amount of precious metal is certainly too large to be practical (at current pricing, 1.9 kg of Pd is almost $50,000), but the amount of heat required to drive the endothermic reaction at that rate may be achievable. This is still a fundamentally important property of the system if other, more practical, ways of increasing the rate of the endothermic system can be discovered.

In order to sustain the energy required for this reaction, 29.6 kJ s^{-1} of heat would need to be supplied (based upon the known indoline dehydrogenation enthalpy of 52 kJ mol^{-1}). All of this heat plus any heat lost to the surroundings must be generated

by the exothermic reaction (i.e. the hydrolysis of **5**). In order to calculate the energy lost to the surroundings as heat, a few assumptions about the final system must be made (Figure 4-5). We assume that a) the insulation around the reaction chamber would be at least equivalent to the insulating ability of standard R-13 PINK FIBERGLAS® insulation (thickness = 8.89 cm), which has a measured heat transfer coefficient (h) of 0.42 J K^{-1} m^{-2} s^{-1}, b) the dehydrogenation chamber is cubic with a side length of 30 cm (surface area, $A = 0.54$ m^2) and c) the temperature difference (ΔT) across the chamber wall is 80 K (T_{rxn} = 100 °C, $T_{outside}$ = 20 °C). With these assumptions, the radiant heat loss can be calculated by Eq. 4-1:

$$heat\ loss = h \times A \times \Delta T \qquad \text{Eq. 4-1}$$

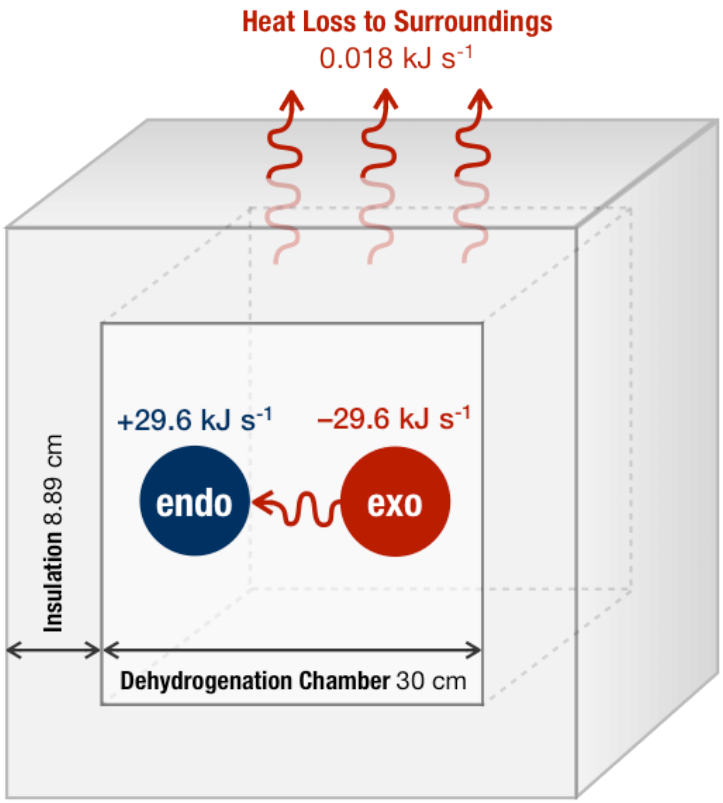

Figure 4-5 • Schematic of theoretical dehydrogenation chamber and heat exchange.

The rate of heat loss is found to be 18.0 J s^{-1}, which is miniscule compared to the heat needed to maintain an adequate rate of hydrogen production from the dehydrogenation of indoline. The exothermic system would then need to supply a total of just over 29.6 kJ s^{-1}. The enthalpy of borane hydrolysis is -156 kJ mol^{-1}, meaning the rate of borane hydrolysis required would be 0.19 mol s^{-1}, producing 1.15 g-H_2 s^{-1}. As mentioned earlier, the rate-limiting factor here is the rate at which water is added, presuming enough dimethylamine borane is available to react with the water; therefore, such reaction rates should be easily achievable. Therefore, the amount of heat radiated to the surroundings at adequate hydrogen production rates is manageable.

Increasing the rate of the endothermic system by simply increasing the amount of catalyst requires an unreasonable amount of precious metal. Therefore other ways of increasing the rate of the endothermic dehydrogenation must be investigated. Previously, Cui *et al*. observed rate enhancements of N-heterocycle dehydrogenation reactions after the introduction of electron donating or conjugating groups outside the ring.[57] It was shown that there is a correlation between the Hammett parameter (σ_p) of the substituent of a piperidine ring and both the calculated enthalpy of dehydrogenation and the $\log_{10}(t_{1/2})$ for these reactions (Figure 4-6). The latter proportionality held true for all substituted piperidines, except for one which had a substituent capable of conjugating with the dehydrogenated ring ($C(O)NH_2$). In this case, the rate was faster than predicted by the Hammett relationship.

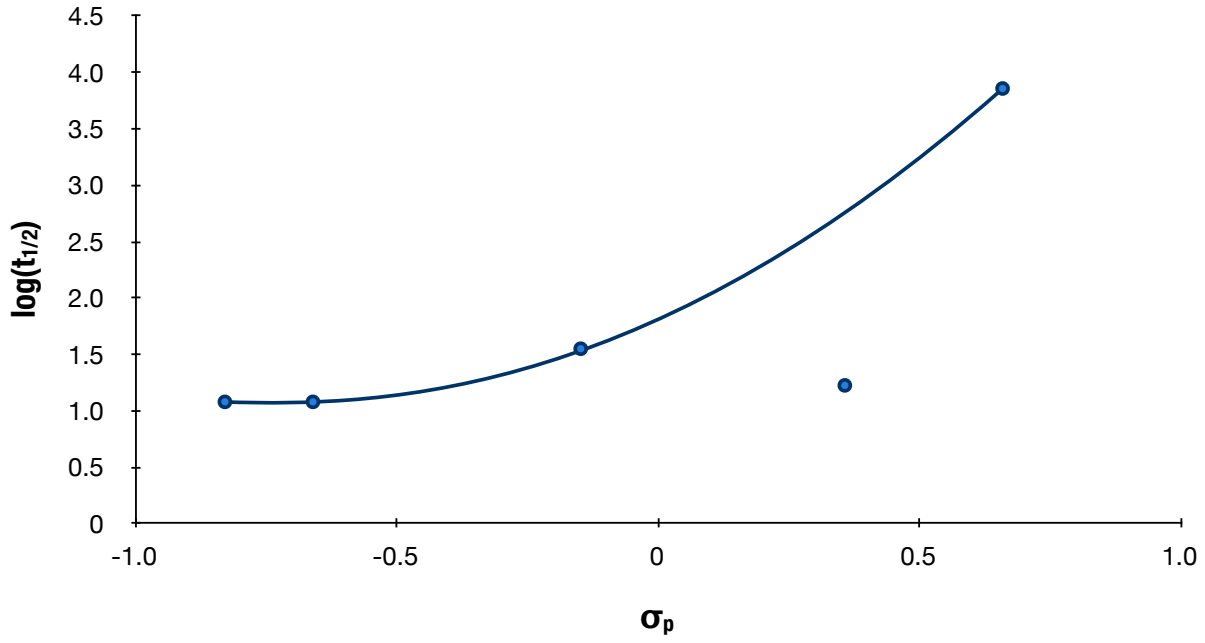

Figure 4-6 • Demonstrated correlation between $\log_{10}(t_{1/2})$ and σ_p for the neat dehydrogenation of para-substituted piperidines at 170 ˚C over 10 mol% loading of 5 wt% Pd/SiO_2, the curve is a quadratic interpolation.[57] - Reproduced by permission of The Royal Society of Chemistry (RSC) for the Centre National de la Recherche Scientifique (CNRS) and the RSC.

With the effect of electronics on the thermodynamics and kinetics of substituted piperidine dehydrogenations having already been described in the literature, other modifications were investigated. Certainly, other strategies can be employed, including changing the catalyst or reaction temperature, or modifying the N-heterocyclic backbone to induce steric interference around the nitrogen atom, in order to increase the rate of dehydrogenation of such endothermic carriers. These strategies were investigated and are presented herein.

4.2.2 • Changing the catalyst

Finding a more efficient catalyst for the dehydrogenation of N-heterocycles could lead to a significant rate increase. Our original studies with mixed dehydrogenation systems used palladium exclusively, with either carbon or silica as the support. To evaluate other catalysts, many different metal-support combinations were prepared by the sol-gel procedure described by Gonzalez and co-workers.[105]

The sol-gel method for preparing heterogeneous catalysts involves mixing an alkoxide precursor of the support (such as tetraethoxysilane for a silica support) in an alcohol solvent with the metal precursor (such as chloride or acetate salts). Water and an acid or base is then added to promote hydrolysis and condensation of the support precursor molecules resulting in the formation of a self-supporting gel. The gel is aged and then dried, either by evaporation (forming a xerogel) or by supercritical drying (forming an aerogel). The resulting dried powder is then calcined at high temperature to produce the final active catalyst.

Table 4-5 • BET measurements for select Pd sol-gel catalysts

Catalyst[a]	BET Surface Area ($m^2 g^{-1}$)	Pore Volume ($cm^3 g^{-1}$)	Pore Diameter (Å)
5 wt% Pd/Al_2O_3	625	1.7	72.5
5 wt% Pd/SiO_2	13.3	0.0084	31.9
5 wt% Pd/SiO_2[b]	274	—	—
5 wt% Pd/TiO_2	609	0.44	23.4
2.5 wt% Pd/ZrO_2	235	0.31	40

a | prepared by sol-gel methodology
b | commercial sample, from Strem Chemicals Inc. for comparison

A myriad of these catalysts, with a number of different metals and supports, was prepared and tested for their activity toward indoline dehydrogenation. After gel formation, the catalysts to be tested were filtered and then dried overnight under static

vacuum in a desiccator. The catalysts were then further dried and purified under static vacuum at 200 °C for 4 h. The BET surface area, pore volume and diameter were measured for four of the Pd catalysts synthesized, as well as a commercial Pd/SiO_2 for comparison (Table 4-5). Overall, the surface areas of the synthesized catalysts were as high or higher than the commercial sample, except for the sol-gel Pd/SiO_2 itself. It shows exceptionally low surface area, with very small pores.

The sol-gel catalysts were exposed to indoline at 1 mol% metal loading at 100 °C for 1 h. Instead of calculating the rate directly, the conversion after 1 h was determined representative of the average rate over the first hour of reaction (Table 4-6). Catalysts based on Co, Cu, Fe, Ir and Ni all showed negligible conversion to product after 1 h. As expected based on previous results, palladium immobilized on a number of supports (Al_2O_3, TiO_2, SiO_2, ZrO_2) showed a range of activities, with conversions after 1 h as low as 25% and up to 81% for the Pd/SiO_2 sol-gel catalyst. For reference, the same loading of commercial 5 wt% Pd/SiO_2 yields indole with a conversion of 74%. This seems illogical based on the measured surface areas; it is expected that activity would increase with surface area. Similarly, the sol-gel Pd/Al_2O_3 catalyst performed better than commercial Pd/Al_2O_3 with conversions of 61 and 45%, respectively. The metal particles in the sol-gel catalyst are expected to be embedded in the support, which may result in a more pronounced positive influence from the support. Alternatively, the size and shape of the particles would certainly be different between the two methods of preparation. It is interesting to note than the catalyst with a mixed support ($Pd/SiO_2 \bullet Al_2O_3$) gave lower activity than those on the individual supports, with a conversion of only 27% compared to 61 and 81% for the Al_2O_3 and SiO_2 catalysts, respectively. It is unknown how Si and Al are distributed throughout the prepared catalyst; it is likely that the interactions between the two metals will have a significant

effect on the morphology and electronic properties of the support and metal atom clusters as they are deposited. The location and size of the metal particles produced on the surface is influenced by the nature of the support; it is likely that the interactions within the support are not ideal for the formation of metal particles with the properties to provide the highest activities for this reaction.

Table 4-6 • Summary of indoline dehydrogenation catalyst screening

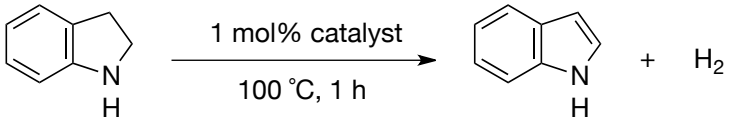

Catalyst[a]	**Conversion (%)**[b]
Co/SiO_2	< 1
Cu/SiO_2	< 1
Fe/SiO_2	< 1
Ir/SiO_2	< 1
Ni/SiO_2	< 1
Pd/Al_2O_3	61 ± 1
Pd/Al_2O_3•3.6 wt% K_2O	23 ± 6
Pd/SiO_2	81 ± 1
Pd/SiO_2•Al_2O_3	27 ± 1
Pd/SiO_2•1.6 wt% K_2O	16 ± 1
Pd/SiO_2•7.6 wt% K_2O	17 ± 1
Pd/TiO_2	25 ± 3
Pd/ZrO_2[c]	32 ± 3
Pd•Rh/SiO_2[d]	< 1
Pt•Pd/SiO_2[d]	< 1
Pt/SiO_2	< 1
Pt/Al_2O_3	10 ± 1
Rh/SiO_2	6 ± 2
Rh/Al_2O_3	11 ± 1
Ru/SiO_2	3 ± 1

a | 5 wt% metal on support based on amount of metal precursor added during preparation
b | determined by ^1H NMR spectroscopy, averaged over two runs with standard deviation shown.
c | 2.5 wt% metal on support based on amount of metal precursor added during preparation
d | metal molar ratio of 1:1

Mixed support catalysts were also prepared with potassium oxides incorporated into either SiO_2 or Al_2O_3 supported Pd catalysts, but at lower amounts. There is a significant amount of literature on the positive effect of potassium on catalytic reactivity, and a recent study with Fe catalysts indicates that the presence of K_2O helps to stabilize particular active metal faces[129] In the present study, however, loadings of 1-8% resulted in lower conversions than the unmodified catalysts. A significant reduction from 61% to 23% was observed when 3.6 wt% K_2O was incorporated in the sol-gel synthesis of Pd/Al_2O_3. With 1.6 wt% and 7.6 wt% incorporation into Pd/SiO_2, a drop in conversion from 81% to 16-17% for both catalysts was observed. The incorporation of K_2O into these catalysts, using this method, does not promote higher conversions for this reaction. Pt/Al_2O_3, Rh/SiO_2 and Rh/Al_2O_3 all also offered non-negligible conversions in 1 h.

Regarding the observed conversions after 1 h with respect to the surface characteristics measured above, some parallels can be drawn. Despite its large surface area, Pd/TiO2 has the smallest measured pore diameter, which could play towards its slower reaction rate as a result of slower mass transfer of the reacting species into the pores, and the products out.[130] As pore size increases from ZrO_2 to Al_2O_3, so does the conversion. The anomaly in this trend is the rate observed over SiO_2. This could have more to do with its electronic properties: a small pore volume could mean that most of the exposed palladium atoms are on the surface, instead of hidden in pores inaccessible to the reacting species. Regardless of its low surface area (compared to both the commercial Pd/SiO_2 and other sol-gel catalysts synthesized), Pd/SiO_2, is the most active of any catalyst tested.

4.2.3 • Increasing the temperature

The effect of temperature on the rate of indoline dehydrogenation was investigated under the same conditions used in the catalyst study outlined above. While the higher temperature will increase the rate of the endothermic reaction, that of the exothermic reaction will be slowed by the same arguments (Le Châtelier's principle). However, since the latter reaction is so much faster, any slowing is expected to be limited and not affect the overall rate of hydrogen production by a prohibitive amount.

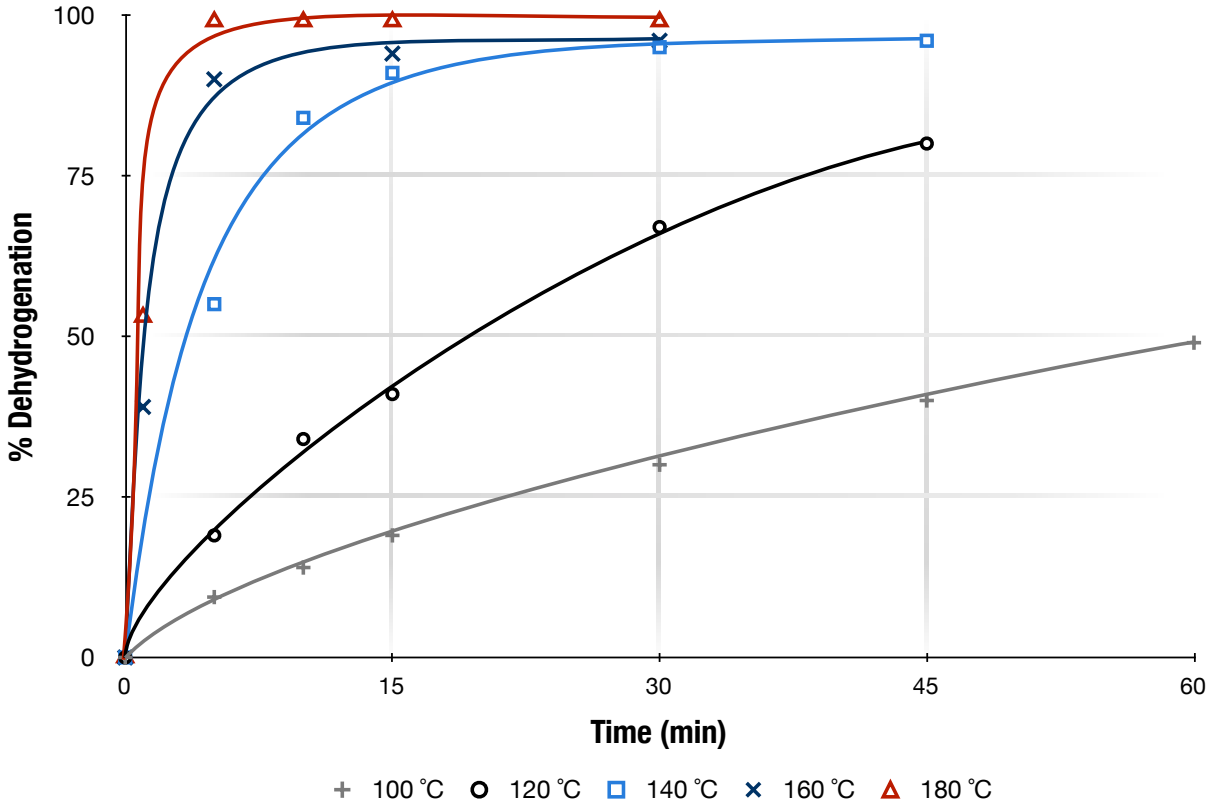

Figure 4-7 • Indoline dehydrogenation conversion (over 1 mol% loading of a 10 wt% Pd/C) curves (measured by ^{1}H NMR spectroscopy) at various temperatures

Indoline and 1 mol% loading of 10 wt% Pd/C were heated to a number of temperatures ranging from 100 °C to 180 °C. In these tests, Pd/C was used rather than

Pd/SiO_2 to enable comparisons with previous experiments in our lab.[107] Small aliquots were removed from the reaction mixture a number of times over the course of an hour, and the yield of H_2 was calculated using ^1H NMR spectroscopy presuming only two products: H_2 and indole (Figure 4-7).

From the dehydrogenation conversion curves above, it is clear that the rate increases with increasing temperature, as expected. While the rate of conversion to indole and H_2 increases, so does the rate of conversion of indoline to other products. Above 140 ˚C, severe degradation of the dehydrogenation product is observed. ^1H NMR spectroscopy of the product mixture showed a mess of peaks representing a number of undesired compounds. With that being said, the above curves do not explicitly represent hydrogen production, but are a rough estimate because the overall amount of byproducts generated is small compared to indole. Two hydrogenolysis products, 2-ethylaniline, **10**, and ethylphenylamine, **11**, were both observed by GC/MS (identified by comparing recorded MS to an EI-MS library). It is known that primary amines such as these tend to undergo Pd-catalyzed disproportionation reactions to give NH_3 and a secondary amine.[131] The three different disproportionation products that are possible from **10** and **11** are bis(2-ethylphenyl)amine, **12**, diphenethylamine, **13**, and 2-ethyl-N-phenylethylaniline, **14**, all of which would have an m/z of 225 (Figure 4-8). A peak of that mass was observed by GC/MS.

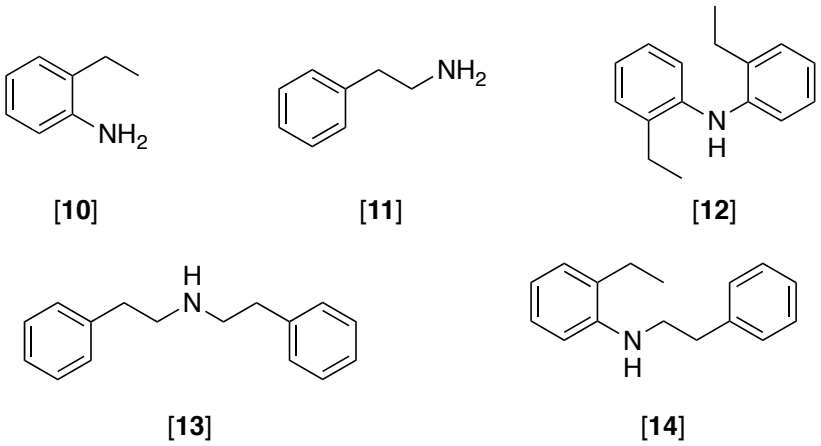

[**10**] [**11**] [**12**]

[**13**] [**14**]

Figure 4-8 • The identified hydrogenolysis products (**10** and **11**) and the subsequent disproportionation products expected from them (**12**, **13** and **14**)

At each temperature, the apparent first-order rate constants were calculated (Table 4-7) from the slope of the line of a plot of $\ln(n/n_0)$, where n is the instantaneous number of moles of indole and n_0 is the original number of moles, versus time (Figure 4-9). It should be noted that calculated rate constants for the reactions at higher temperatures carry more error; the linear regression for these data sets used fewer data points because the reaction was complete before more conversion measurements could be made.

Table 4-7 • Calculated apparent first-order rate constants (k) for indoline dehydrogenation over 1.0 mol% metal loading of Pd/C at various temperatures (T)

Temperature (°C)	**First-order rate constant (x 10^{-4} s^{-1})**[a]
100	1.9 (0.006)
120	6.1 (0.009)
140	28 (0.1)
160	77 (0.08)
180	150 (0.4)

a | first-order rate constants given with standard error of the slope of the line in Figure 4-9 in parentheses

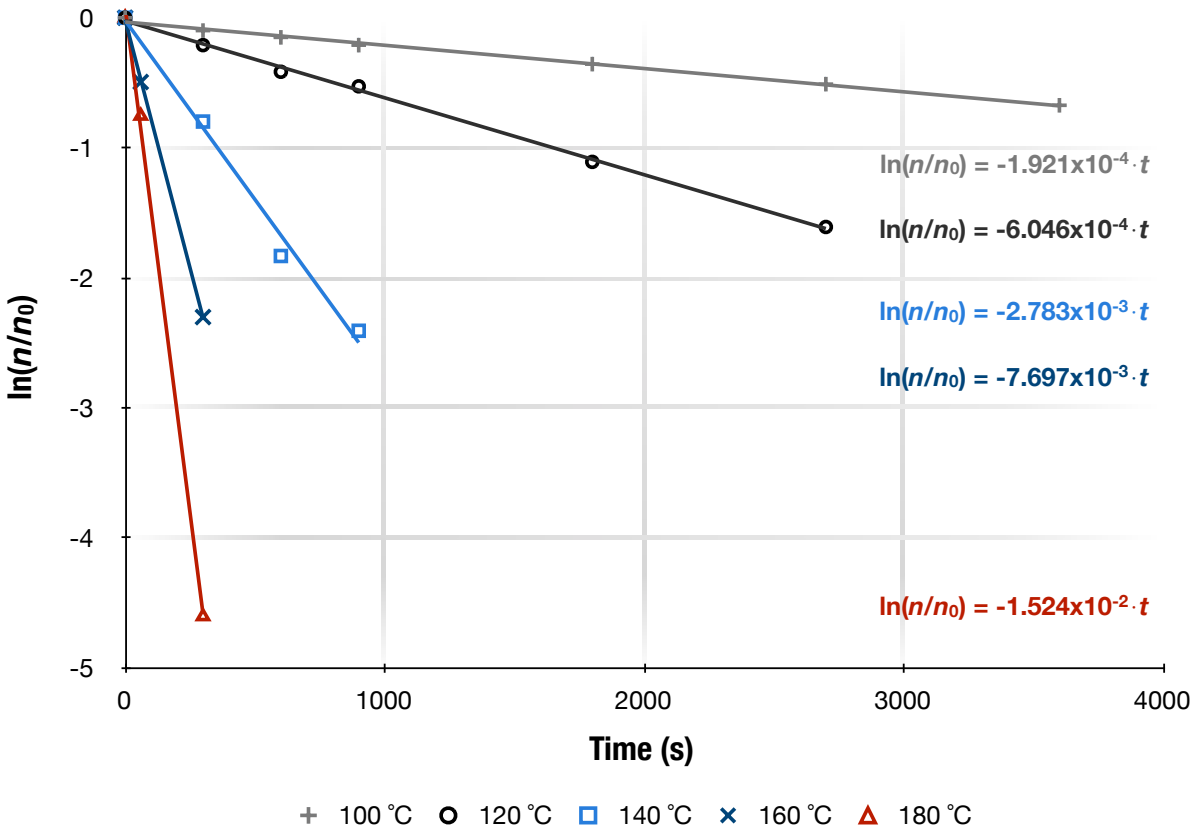

Figure 4-9 • Plots of ln(n/n$_0$) versus time for indoline dehydrogenation over 1.0 mol% metal loading of Pd/C at various temperatures

With the rate constants calculated at a number of temperatures, a number of further calculations are possible. The relationship between the rate constant of a reaction and the reaction temperature is described by the Arrhenius equation:

$$k = A\,e^{\frac{-E_a}{RT}} \qquad \text{Eq. 4-2}$$

where k is the measured rate constant, A is the pre-exponential factor, E_a is the activation energy, R is the ideal gas constant and T is the absolute temperature. The pre-exponential factor describes the empirical relationship between temperature and the rate constant, and its magnitude depends on how often molecules collide, irrespective of their energy, at standard concentrations (1 mol L^{-1}). The activation

energy is classically thought of as being the energy barrier to a reaction; however, it can also be considered as a measure of how sensitive the rate of the reaction is to changes in temperature. The value of $\exp(-E_a/RT)$ describes the fraction of collisions with enough kinetic energy to lead to a reaction as described by the Boltzmann distribution. Therefore, the product of these two factors gives the rate of successful collisions. In order to calculate these two, the natural logarithm of the Arrhenius equation is taken to give:

$$\ln(k) = -\frac{E_a}{R}\left(\frac{1}{T}\right) + \ln(A) \qquad \text{Eq. 4-3}$$

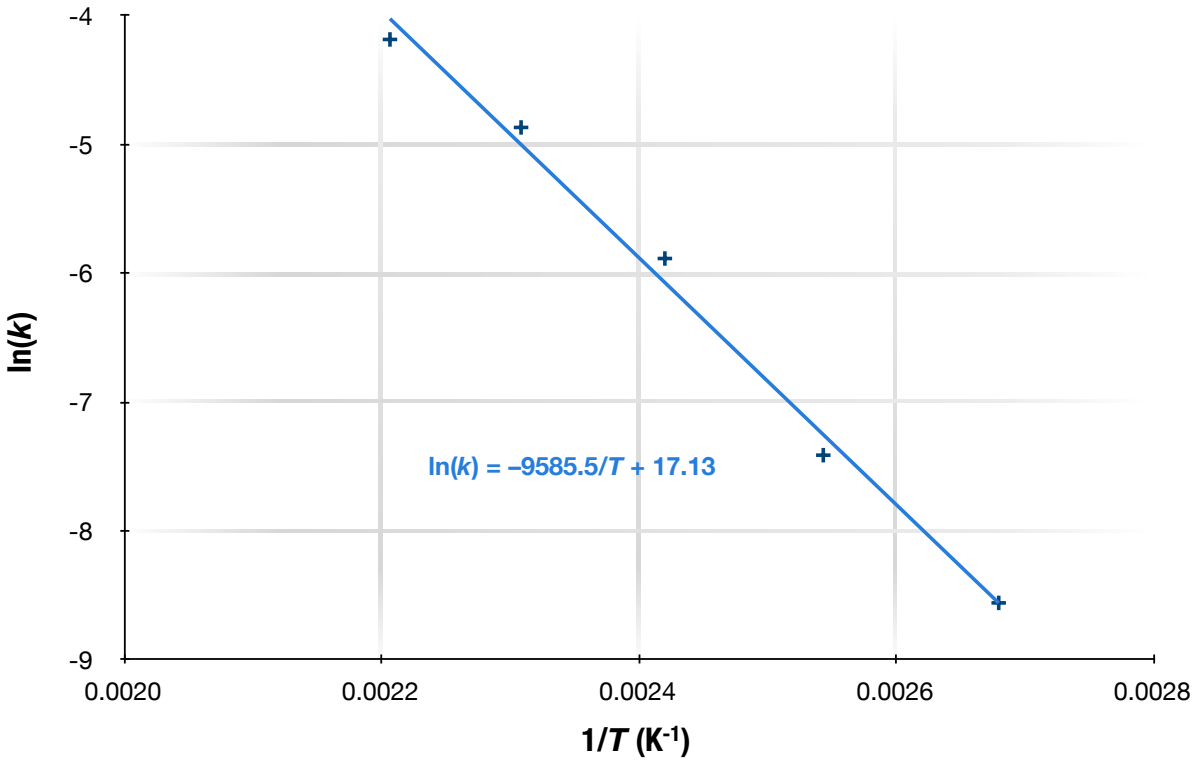

Figure 4-10 • Arrhenius plot for indoline dehydrogenation over 1 mol% metal loading of Pd/C

A plot of ln(k) versus $1/T$ should therefore yield a straight line with a slope equal to $-E_a/R$ and an intercept of ln(A). When these data for the dehydrogenation of indoline are plotted (Figure 4-10) a pre-exponential factor of $A = 2.8 \times 10^7$ s^{-1} and an activation energy of $E_a = 80$ kJ mol^{-1} are obtained.

Further analysis of this kinetic data with respect to temperature can be achieved by considering the Eyring-Polanyi equation:

$$k = \frac{k_B T}{h} e^{-\frac{\Delta G^{\ddagger}}{RT}} \qquad \text{Eq. 4-4}$$

where k_B is Bolztmann's constant (1.381×10^{-23} J K^{-1}), h is Planck's constant (6.626×10^{-34} J s) and $\Delta G^{\ddagger}$ is the Gibbs energy of activation. Based on the definition of $\Delta G^{\ddagger}$ (*i.e.* $\Delta G^{\ddagger} = \Delta H^{\ddagger} - T\Delta S^{\ddagger}$), this expression can be expanded:

$$k = \frac{k_B T}{h} \exp\left(\frac{\Delta S^{\ddagger}}{R}\right) \exp\left(\frac{-\Delta H^{\ddagger}}{RT}\right) \qquad \text{Eq. 4-5}$$

where $\Delta S^{\ddagger}$ and $\Delta H^{\ddagger}$ are the entropy and enthalpy of activation, respectively. As with the Arrhenius equation above, taking the natural logarithm of Eq. 4-5 will yield a linear relationship, this time between ln(k/T) and $1/T$. This can be used to determine the enthalpy and entropy of activation from the slope and intercept, respectively:

$$\ln\left(\frac{k}{T}\right) = -\frac{\Delta H^{\ddagger}}{R}\left(\frac{1}{T}\right) + \left[\ln\left(\frac{k_B}{h}\right) + \frac{\Delta S^{\ddagger}}{R}\right] \qquad \text{Eq. 4-6}$$

A plot of these data (Figure 4-11) yields a straight line indicating a $\Delta H^{\ddagger}$ of 77 kJ mol^{-1} and a $\Delta S^{\ddagger}$ of -110 J mol^{-1} K^{-1}. Based on the expected possible steps of the reaction mechanism including adsorption of indoline and hydrogen, surface reaction, and release of the product, the rate-determining step is likely the adsorption of indoline, as that of hydrogen is already known to be rapid on such metal surfaces and has a $\Delta S^{\ddagger}_{ads}$

on Rh/Al_2O_3 of -159 J mol^{-1} K^{-1}.[132] This is the only other step that would produce such a large, negative entropy of activation.

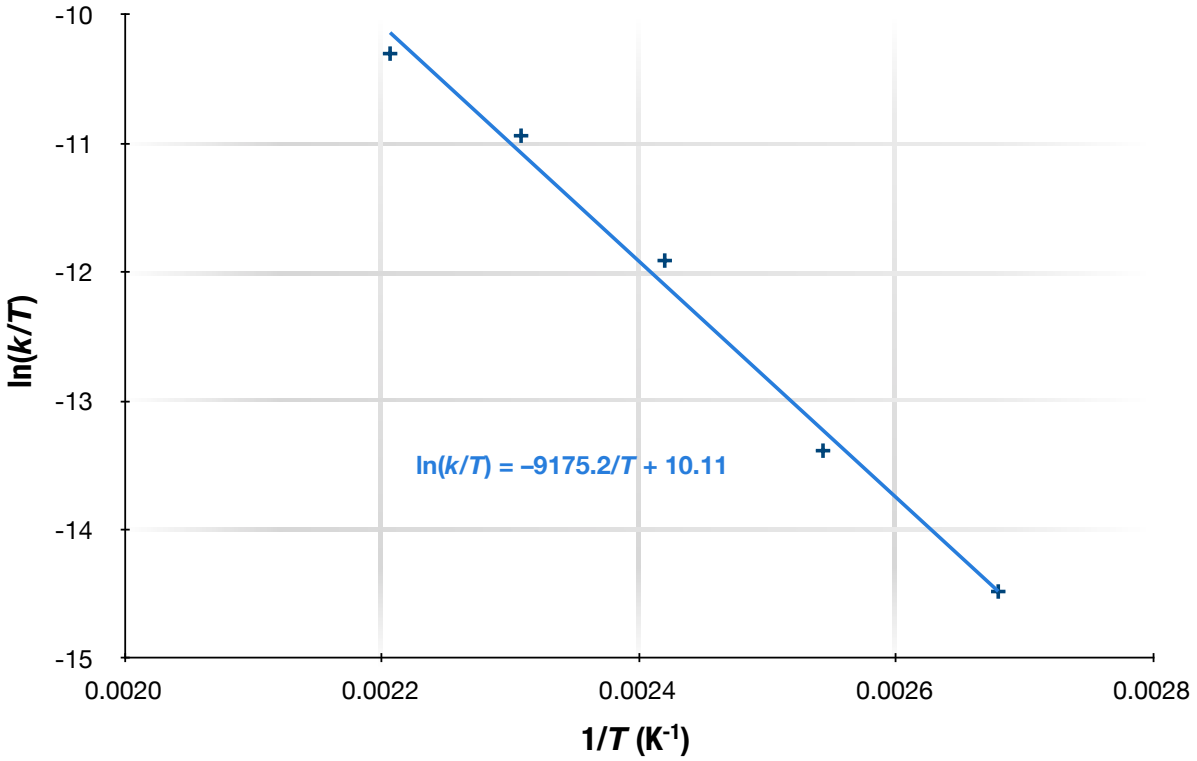

Figure 4-11 • Eyring plot for indoline dehydrogenation over 1 mol% loading of Pd/C

4.2.4 • Sterically protecting the nitrogen lone pair

The third strategy to increasing the rate of N-heterocycle dehydrogenation was discovered somewhat serendipitously. During previous investigations of mixed dehydrogenation systems, we noted that the lone pair of electrons of the heterocyclic nitrogen atom was irreversibly binding to the Lewis-acidic boron, preventing complete hydrogen release.[107] To prevent this interaction, we looked at sterically encumbered piperidines, such as 2,6-dimethylpiperidine, **8**, and 2,6-di-tert-butylpiperidine, **9**. During this investigation, we realized that, under similar conditions, both **8** and **9**

dehydrogenate faster than unsubstituted piperidine. The details of the rate enhancement were then investigated further to determine the usefulness of such a strategy for N-heterocycle dehydrogenation rate enhancement.

It is known that pyridine and piperidine bind to metal surfaces quite strongly through the lone-pair of electrons on the nitrogen atom. This has been suggested as the initial binding mode of pyridine in its hydrogenation mechanism.[133] If this binding of pyridine is strongly favoured at the temperatures investigated, then pyridine binding through the nitrogen atom to the catalyst surface likely leads to poisoning or auto-inhibition. The idea of catalyst poisoning by an N-heterocycle (carbazole) was the topic of discussion in a recent manuscript by Sotoodeh *et al.*[134] It is therefore suggested that sterically blocking the lone pair of electrons of the piperidine nitrogen atom with bulky groups at the 2 and 6 positions should be able to prevent catalyst poisoning, allowing for more rapid dehydrogenation. Okazaki *et al.* have described the effect of a methyl group at the 2- and 8- position of quinoline (Figure 4-12) on the selectivity of the hydrogenation for either the N-ring or the C-ring.[135] It was found that the methyl group in the 2-position (adjacent to the N-atom) allowed for more favourable binding of the π-system of the C-ring than the lone pair of electrons on the N-atom, allowing for selective hydrogenation to the 5,6,7,8-tetrahydroquinoline over the classically favoured 1,2,3,4-tetrahydro derivative. They also argue that release of steric strain upon hydrogenation to a non-planar structure also promotes the hydrogenation reaction. This would theoretically slow the rate of the reverse reaction, dehydrogenation, which is being discussed in this work. The release of steric strain must be less relevant to the reaction than the autopoisoning of the surface by irreversible N-binding because the rate of dehydrogenation of substituted piperidines is observed to be *faster* than the unsubstituted piperidine. It has also been previously reported that the hydrogenation

rate of 2-poly(vinylpyridine) is faster than that of 4-poly(vinylpyridine).[136] It was noted that the strongly favoured binding of the latter's ring nitrogen to the catalyst was likely poisoning the surface toward further reactions. In the case where the polymer prevents such strong binding because of steric interference, as with (2-poly(vinylpyridine)), the hydrogenation is faster.

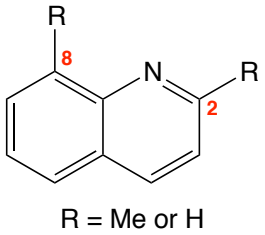

Figure 4-12 • 2- or 8- substituted quinoline

The gravimetric hydrogen capacities of **8** and **9** are greater than that of indoline. They each release 3 eq. of H_2 while indoline releases only one. The latter also contains a fused phenyl ring that does not contain any deliverable hydrogen. In total, indoline can deliver 1.7 wt% H_2, while **8** and **9** can deliver 5.4 and 3.0 wt%, respectively. With a larger storage capacity, the use of the dimethyl analogue is more desirable, although the rate enhancement is not as marked with the less bulky methyl groups. Neither **8** nor **9** has a large enough storage density for standalone use, but depending on the dehydrogenation rates observed, could be viable candidates for hybrid systems such as those discussed previously.

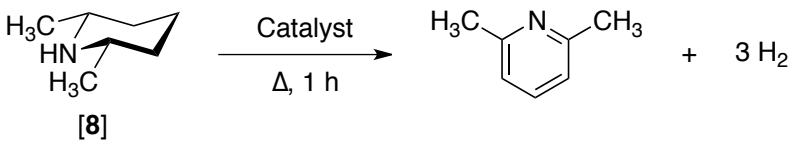

Scheme 4-9 • Dehydrogenation of 2,6-dimethylpiperidine, **[8]**

The dehydrogenation of 2,6-dimethylpiperidine (**8**) only offers a slight rate improvement over the unsubstituted piperidine. At 100 ˚C with 2 mol% metal loading of commercial Pd/C, conversions of between 2-5% were obtained after 2 h, where only trace amounts of pyridine are observed when piperidine itself is exposed to similar conditions. Initially, higher conversions were recorded, likely due to mass loss with flowing Ar (g) flowing over the surface of the reaction mixture at high temperatures. A condenser was added and the gas flow rate was reduced, narrowing the breadth of results obtained.

The possibility of an induction period for the reaction was proposed as another possible reason for the varied conversions observed. Within a single bottle of catalyst, which has homogeneous bulk properties, the local metal atom distribution may be different from sample to sample when working on a small scale. This variation could result in induction periods of different lengths for different experimental runs, therefore producing irreproducible conversions in a short amount of time before equilibrium is reached. To probe this, the reaction conversion profile versus time for the dehydrogenation of 2,6-dimethylpiperidine over 2 mol% metal loading of Pd/C at 100 ˚C was recorded (Figure 4-13). The reaction was performed in toluene-d_8 to facilitate easy NMR sample preparation.

Very little conversion is seen in the first 30 minutes, followed by a rapid release of hydrogen. While the possible error associated with the NMR measurement of conversion may considered to be large, it is unlikely (especially with multiple measurements) that error in the data point at 30 minutes is falsely indicating an induction period. A pretreatment of the catalyst was employed to attempt to homogenize the catalyst surface by reducing all exposed palladium atoms. The dry catalyst was exposed to flowing hydrogen at 200 ˚C for 2 h before the piperidine was

added. The conversion with the pre-treated catalyst was similar to that found with the untreated catalyst, about 4% after 2 h. Regardless, the aforementioned catalyst pre-treatment was used for future runs to ensure that catalyst metal oxidation state inhomogeneity did not alter further observations.

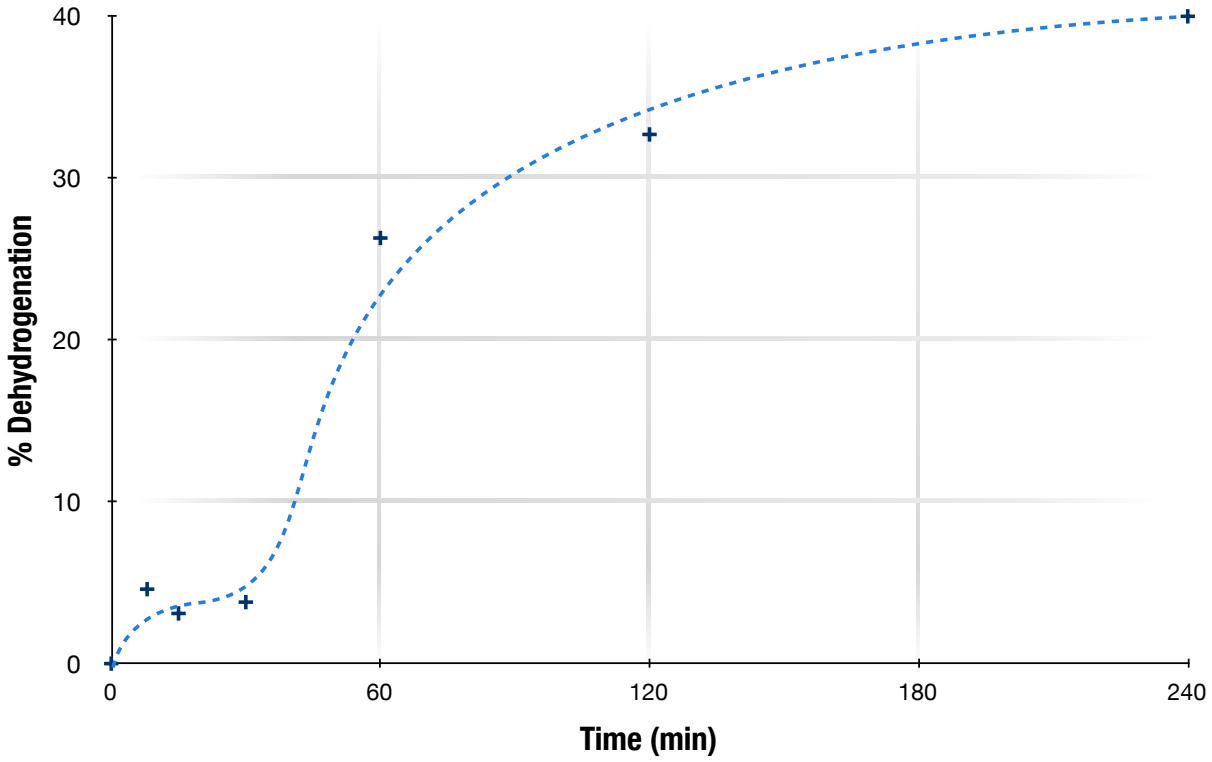

Figure 4-13 • Reaction conversion profile of 2,6-dimethylpiperidine dehydrogenation in toluene-d_8

The use of solvent seems to be the cause of the enhanced rate accompanied by an induction period. It is possible that this induction period is also a symptom of the use of solvent, which would not be possible in any real-world application. The solvent could help to stabilize the nitrogen-containing ring away from the catalyst surface, making it easier to dissociate, preventing auto-inhibition and enhancing the rate. With the above considered, the results with **8** are not as promising as were hoped for.

Limited rate improvement over the parent, piperidine, suggests that the dimethyl groups are not sufficient at blocking the strong N-metal adduct on the surface, especially when the ring is saturated and the lone pair is not in the plane of the substituents. With the two methyl groups of *cis*-2,6-dimethylpiperidine in the equatorial conformation,[137] regardless of whether the lone pair is equatorial or axial, it may be possible to allow for the nitrogen lone pair to possibly get far enough from the methyl groups to still form a strong interaction with the metal surface. With this, the more bulky 2,6-di-*tert*-butylpiperidine (**9**) was investigated.

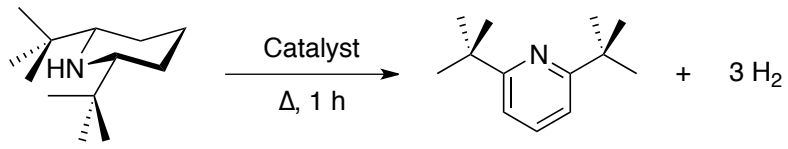

[**9**]

At first, a temperature of 100 ˚C was also used for the dehydrogenation of **9**. After 2 h over 2 mol% metal loading of Pd/C, a conversion of only 12-14% was achieved. At 150 ˚C, 53% conversion is obtained after 2 h, and 63% after 4. With Pd/Al_2O_3 sol-gel catalyst, the conversion after 1 h was 4%. For 2,6-dimethylpiperidine, higher temperatures were not practical because its boiling point is only 127.8-128.1 ˚C. That of **9** is higher, at 223 ˚C (95-97 ˚C at 10 Torr),[138] and the dehydrogenation temperature can therefore be raised to increase the rate of reaction. After 1 h at 170 ˚C, the dehydrogenation of **9**, with 2 mol% loading of Pd/SiO_2 or Pd/Al_2O_3 sol-gel catalysts, yielded 40 ± 4 % and 40 ± 3 % of 2,6-*cis*-di-*tert*-butylpyridine, respectively. The conversion with a commercial Pd/SiO_2 was slightly less reproducible, resulting in an average conversion of 54 ± 10% after 1 h, and as high as 88% (single run) after 2 h. The reason for the range of yields was not probed further; it was likely a result of

inhomogeneity of the catalyst on such a small scale (1-2 mmol piperidine) results in various rates.

Table 4-8 • 2,6-di-*tert*-butylpiperidine dehydrogenation results

Temperature (˚C)	Time (h)	Catalyst[a]	Conversion (%)[b]
100	1	Pd/Al_2O_3 (sol-gel)	4
100	2	Pd/C (comm.)	12
150	2	Pd/C (comm.)	53
150	4	Pd/C (comm.)	63
170	1	Pd/SiO_2 (sol-gel)	40
170	1	Pd/Al_2O_3 (sol-gel)	40
170	1	Pd/SiO_2 (comm.)	54
170	2	Pd/SiO_2 (comm.)	88

a | 2 mol% metal loading, sol-gel catalysts were prepared in house by the method indicated herein, comm. catalysts were purchased from suppliers
b | determined by ^{1}H NMR

Further experimentation with the sterically hindered piperidines was desired to elucidate more information about the rate increase observed. As the inclusion of electron donating groups has been shown to increase the rate of dehydrogenation (Chapter 4.2), it is possible that the addition of two alkyl groups (which are electron donating) could be responsible for the rate enhancement. The extent of dehydrogenation of 1,3-bis(4-piperidinyl)propane, **10**, under the same conditions was also, therefore, determined to compare the dehydrogenation rate of **9** with that of another piperidine with a similar electron donating alkyl substituent that does not provide steric blocking of the N-atom. The dehydrogenation of **10**, with Pd/SiO_2 or Pd/Al_2O_3 sol-gel catalysts resulted in $< 3\%$ conversion after 1 h at 170 ˚C. This demonstrates that the steric effect of the *t*-Bu groups, rather than the electronic effect, is the cause of the enhanced rate.

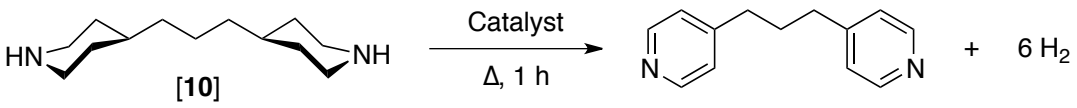

Competition studies have also been performed where both the substituted piperidine and piperidine itself are mixed together and exposed to the aforementioned dehydrogenation conditions. In one experiment, equimolar amounts of both 2,6-di-*tert*-butylpiperidine and piperidine were added together with 2 mol% Pd/C and stirred at 100 °C. After 2 h, the reaction mixture was extracted with deuterated chloroform ($CDCl_3$) and analysed with ^1H NMR spectroscopy. The dehydrogenation of 2,6-di-*tert*-butylpiperidine proceeded to only 1.6 % yield of the corresponding pyridine. Piperidine itself was found to undergo dehydrogenation with 1.2% conversion. Both reactions proceed very slowly; under similar conditions, the substituted piperidine reaches dehydrogenation conversions upwards of 12%. When the dehydrogenation of 2,6-di-*tert*-butylpiperidine was attempted in the presence of pyridine (instead of piperidine) under the same conditions, the dialkyl pyridine was found in less than 1 % yield. Presumably then, pyridine poisons the surface more prevalently than piperidine, it is both a better base, and can bind to the surface through its ring π-system. The hydrogenation of 2,6-di-*tert*-butylpyridine is also affected drastically by the addition of pyridine to the reaction mixture. Equimolar amounts of the two pyridines were hydrogenated over 1 mol% metal loading of Pd/C at 100 ˚C for 6 h resulting in almost exclusive hydrogenation of pyridine (90%) with only trace amounts of the substituted piperidine in the product mixture. These results further demonstrate the facts that pyridine binds much more easily with the catalyst surface resulting in surface poisoning and prevention of ring dehydrogenation, and that the bulky groups surrounding the N-atom can prevent such auto-poisoning.

A hybrid system comprised of 2,6-di-tert-butylpiperidine and dimethylamine borane was then tested to determine the rate of combined dehydrogenation over 2 mol% loading of Pd/C at 170 ˚C. After 2 h, however, ^{1}H NMR spectroscopy indicated only a trace amount of ring dehydrogenation; ^{11}B NMR spectroscopy showed only signals from the starting material. Because it is unexpected that the borane fragment would be able to still form a complex preventing dehydrogenation of the ring, it is more likely that it is the product of dimethylamine borane dehydrogenation is irreversibly binding to the catalyst surface as previously discussed. However, if that problem could be eliminated, the amount of catalyst needed is much more modest than that for the indoline system discussed previously (Chapter 4.2.1). The conversion after 10 min at 170 ˚C over 2 mol% metal loading of a commercial Pd/SiO_2 was measured to be 15.4%, translating to an initial rate of 0.036 mol-H_2 s^{-1} g-Pd^{-1} or 0.073 g-H_2 s^{-1} g-Pd^{-1} (assuming that the rate increased linearly with increasing catalyst as seen with indoline). Remembering that 1.13 g-H_2 s^{-1} is required from the endothermic system, that means that only ~16 g of Pd would be needed to achieve the necessary rate of hydrogen production.

Finally, this steric-induced rate enhancement was compared to that from electron donating and conjugating groups previously demonstrated by Cui *et al.*[57] First, 2,6-di-*tert*-butylpiperidine was dehydrogenated using the same conditions used therein: the piperidine was heated to 170 °C with 10 mol% loading of Pd/SiO_2 with constant, but slow inert gas flow. After only 10 minutes under these conditions, the dehydrogenation product was found in 46% yield by ^{1}H NMR spectroscopy compared to 32% reported by Cui for 4-aminopiperidine. It should be noted, however, that in the absence of a solvent, the liquid substrate was not enough to even wet all of the catalyst, and magnetic stirring was impossible. This led to a reduction in the amount of catalyst to 2 mol%. After

10 min, the conversion to the dehydrogenated product of the 2,6-di-*tert*-butylpiperidine was 15%. The piperidine with the greatest observed rate increase in the Cui study, 4-aminopiperidine, was subjected to these same conditions. After 10 minutes, the dehydrogenated product was found in 16 % yield. This suggests that the effect of two *ortho*-*tert*-butyl groups on piperidine offers as much enhancement of the initial rate as the *para*-amino group.

Looking forward, although the *tert*-butyl groups accelerate the reaction, they do not have any hydrogen that can be released. Also, they add much more weight than the amino group of 4-aminopiperidine, which is shown to similarly enhance the dehydrogenation rate. Any groups that are incorporated into the molecule that do not have any deliverable hydrogen diminish the maximum gravimetric H_2 density, and should be kept to a minimum. For this reason, it is also of interest to look at other substituents, including substituents that could dehydrogenate to produce useable hydrogen as well as provide steric protection of the nitrogen atom. Two additional heterocyclic compounds were analysed: 6,6′-dimethyl-2,2′-bipiperidine, **15a** and 2,2′:6′2″-terpiperidine, **16a**. These compounds were not available directly from any supplier, but the unsaturated versions of both were purchased and used without purification (from Aldrich).

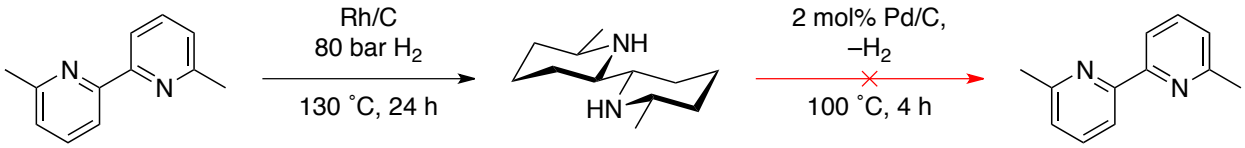

[15b] **[15a]**

The hydrogenation of 6,6′-dimethyl-2,2′-bipyridine, **15b** and 2,2′:6′,2″-terpyridine, **16b** were both attempted in a 31 ml steel pressure vessel, pressurized with 80 bar of

hydrogen and 2 mol% Rh/C, stirring at 130 °C for 24-27 h. Compound **15a** was isolated by this method in quantitative yield, as confirmed by 1D and 2D ^{1}H NMR spectroscopy and mass spectrometry. The dehydrogenation of **15a** over 2 mol% metal loading Pd/C at 100 °C was unsuccessful with no conversion back to **15b** after 4 h as determined by ^{1}H NMR spectroscopy.

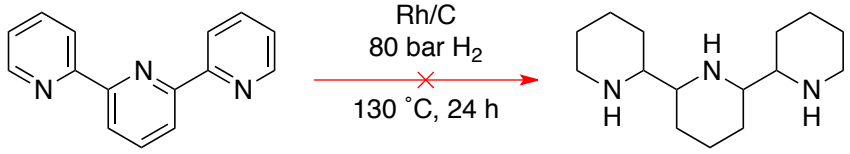

[16b] **[16a]**

The ^{1}H NMR analysis of the product mixture after the attempted hydrogenation of **16b** indicated that complete hydrogenation had taken place; all of the aromatic proton peaks had shifted upfield to the aliphatic region. Proton peak integrations did not indicate formation of the desired product cleanly. Also, the ^{13}C NMR spectrum of the product mixture showed far too many unique carbon signals to be only representative of **16a**. To the best of our knowledge, **16a** has not been reported in the literature, and therefore no comparison of the ^{1}H NMR spectra was possible. With this being said, it was unknown whether product degradation, such as ring opening, had occurred, but this was likely the case. Regardless, the dehydrogenation was attempted under similar conditions as those attempted for the dehydrogenation of **15a**. After 4 h, ^{1}H NMR spectroscopy showed no change in the reaction mixture. This means one of two possibilities: either the hydrogenation of **16b** was unsuccessful due to ring opening, or, less likely, that **16a** was indeed successfully formed, its ^{1}H NMR spectrum is more complicated than predicted, and the molecule simply does not dehydrogenate under

the conditions used. Both possibilities are undesirable and only further indicate that these multiple heterocyclic rings are not appropriate for hydrogen storage applications.

Two of the three strategies employed to increase the rate of the endothermic system dehydrogenation, including increasing the temperature and altering the N-heterocycle backbone, were successful in increasing the rate of dehydrogenation. However, other problems were introduced, specifically selectivity and hydrogen storage capacity. Overall, none of the strategies look promising toward a working hybrid system, despite their possible application elsewhere. At this point, the Jessop group abandoned the development of new hybrid hydrogen storage systems. The information garnered from these studies, however, should aid future endeavors toward different hydrogen storage technologies. The discovery of new endothermic and exothermic systems with improved properties for this application may yet come to fruition, possibly opening up avenues for further hybrid, net-energy-neutral, hydrogen release systems.

Chapter 5 • Thermally Regenerative Fuel Cells

As discussed previously, a thermally regenerative fuel cell is one that converts waste heat into electrical energy. The successful search for a hydrogen-carrying liquid and catalysts that will provide high rates and selectivities, for both the dehydrogenation and hydrogenation reactions, is necessary before the invention can come to fruition. The results discussed below are with regard to the effect of the identity of the catalyst and that of the aryl alkyl ketone on its hydrogenation activity and selectivity. The effects of changing the catalyst metal and support are both investigated, along with the effect of different surface modifiers. The electronic and steric effects of substituents on the parent ketone are also mapped.

We chose to use a batch system employing a neat slurry of powdered catalyst and the desired ketone under 1 atm H_2 (g) as a model for the reduction reaction that would take place at the cathode. While this is not quite representative of the proposed system, these studies produced valuable information about the trends in reactivity and selectivity. These trends are expected to be comparable because both the electrochemical reduction and chemical hydrogenation are reactions that take place on a metal surface.

5.1 • Initial Catalyst Screening

The major challenge in developing the hydrogenation catalyst and liquid system is finding a match that provides, not only rapid, but also highly selective dehydrogenation and hydrogenation. The catalyst investigation began with the screening of commercially available, heterogeneous catalysts based on the most popular metals for fuel cell catalysis (Pd, Pt, Rh, Ru). While no clear answers can be drawn from our initial results (Table 5-1), some useful information can be garnered. There are very few catalysts that offer selectivities even close to the desired 99.9% benchmark at any appreciable conversion. The two best selectivities, for Pd/PEI/SiO_2 and Pd/SiO_2, are impressive, at 98.0 and 99.99% by GC, respectively (entries 8–9, where PEI is polyethyleneimine). However, the conversions after the first hour, crude measures of the average rate of the reaction in the time, are very low, both under 6%. In general, carbon supported catalysts (entries 4-5, 12, 17 and 18) all give higher conversions after 1 h, whether the metal is Pd or Pt. Both metals, supported on carbon, give conversions and selectivities that are moderate to good with respect to the rest after 1 h. Longer reaction times of 2 and 5 h (entries 13-14) give increased conversion with decreased prevalence of the desired alcohol in the product mixture. In an actual embodiment of the invention a flow system would likely be implemented, so long residency times of the liquid over the catalyst at high temperature would be minimized. The results over the commercial Vulcan XC-72 Carbon catalysts (entries 17-18) are quite promising. Vulcan XC-72 is an industry standard conductive and static dissipating carbon black with high surface area that has shown promise for fuel cell catalyst applications. While the selectivity observed is still far from the level required, they are still modest, and are

found at relatively high conversions. The use of Pd supported on Vulcan XC-72 was also investigated, and will be discussed later as the catalysts were not purchased commercially, but instead prepared by the author.

Table 5-1 • Hydrogenation of propiophenone over various heterogeneous catalysts

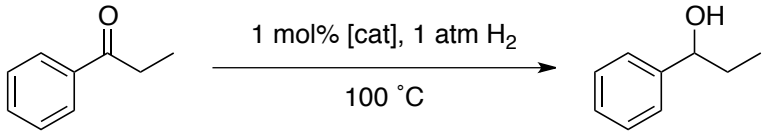

Entry	Catalyst	Time (h)	Conversion (%)[a]	Selectivity (%)[a]
1	5 wt% Pd/Al_2O_3	1	2 ± 1	56 ± 3
2	5 wt% $Pd/BaCO_3$	1	7 ± 1	88 ± 2
3	5 wt% $Pd/BaSO_4$	1	5 ± 1	77 ± 10
4	5 wt% Pd/C	1	26 ± 7	95 ± 1
5	10 wt% Pd/C	1	17 ± 1	88 ± 1
6	5 wt% $Pd/CaCO_3$	1	24 ± 6	71 ± 14
7	5 wt% $Pd/CaCO_3$•1.6wt% Pb	1	6 ± 5	92 ± 10
8	3 wt% $Pd/PEI/SiO_2$[c]	1	4.0 ± 0.3[b]	98.0 ± 0.9[b]
9	5 wt% Pd/SiO_2	1	6 ± 2	≥ 99.99[b]
10	5 wt% Pd/SiO_2	2	17 ± 4	96 ± 5
11	5 wt% Pt/Al_2O_3 pellets	1	7± 5	44 ± 2
12	10 wt% Pt/C	1	22 ± 5	89 ± 1
13	10 wt% Pt/C	2	34 ± 3	87 ± 2
14	10 wt% Pt/C	5	58 ± 7	77 ± 1
15	5 wt% $Pt/CaCO_3$	1	15 ± 3	78 ± 8
16	5 wt% Pt/SiO_2	1	4 ± 2	55 ± 23
17	10 wt% Pt/Vulcan XC-72	1	22 ± 1	89 ± 1
18	20 wt% Pt/Vulcan XC-72	1	27 ± 1	83 ± 1
19	5 wt% Rh/Al_2O_3	1	9 ± 2	90 ± 1
20	5 wt% Ru/Al_2O_3	1	5 ± 1	86 ± 1

a | determined by ^{1}H NMR spectroscopy, averaged over two runs with standard deviation shown.
b | determined by GC, averaged over two experimental runs
c | PEI = polyethyleneimine

The metal oxide supported catalysts gave significantly lower activity toward the hydrogenation of the phenyl ketone than the carbon supported catalysts. This may be

due to the ability for reactant molecules, after being chemisorbed to the metal surface, to "spillover" on the carbon surface, in that they then exist, for example, as C–H instead of M–H (where M = metal). This occurs with hydrogen to such an extent that carbon itself has been suggested as a hydrogen storing material. It's also possible that additional hydrogen can adsorb to the support surface and undergo reverse-spillover onto the metal clusters promoting reaction. It has been suggested that the chemical reaction can then proceed on the metal surface and the support, meaning the total rate of hydrogenation is the rate of hydrogenation on the metal plus that on the support.[139] While it is possible that the reaction on the support may not lead to the desired product resulting in a lower selectivity, it would still contribute to a higher conversion in the same amount of time. It has been suggested in the literature, however, that such spillover does not take place onto defect-free non-reducible supports such as silica and alumina.[140] It is unlikely that the supports of the catalysts employed herein are defect-free, and likely contain surface OH groups that will allow for hydrogen spillover. The hydrogen pre-treatment should, however, mitigate these sites by reducing them. Whether the surface is completely defect-free or not, the spillover would still be expected to occur to a lesser extent than with the carbon based catalysts. Having hydrogen atoms able to exist on the support itself increases the number of active sites available on the metal where the reaction can take place, increasing its rate. Also, with these oxide supports being acidic in nature, they would make the metal atom clusters more electron poor, possibly slowing the interactions with adsorbates and leading to lower conversions

Regarding selectivity, one might initially suggest that the oxide-supported catalysts be better. While this may be true based on the absolute data, the cause may not be the nature of the support and its interactions with the metal, but instead be the

low conversions observed with these catalysts. With Pd/SiO_2, the catalyst that offers the highest selectivity after 1 h, propiophenone dehydrogenation continues and after 5 h, a conversion of 17% is achieved but the selectivity decreases to 96% (entry 10). So, while the production of unwanted side products is evidently slower on these catalysts, they are still being produced to an appreciable amount, especially on a more relevant time scale of hours, towards weeks in an actual embodiment of the invention. With that being said, some of the carbon-based catalysts are able to offer relatively high conversions with comparable selectivities.

Regarding the metals tested, on similar supports, Pt either gives similar or worse selectivity at the same conversion than other metals, specifically Pd. It is likely that platinum is more active toward all of the hydrogenation pathways leading from propiophenone. Contrarily, palladium seems to offer a more focused catalysis of the formation of the desired alcohol product. This could be for a number of reasons, likely including both the nature of the metals themselves and how the properties manifest in the size, shape and distribution of the metal particles during the catalyst synthesis. Future optimization may be obtained by measuring these values directly, including metal particle sizes, shape and location within the support using electron microscopy and metal surface area using chemisorption experiments, and correlating these results to the observed catalyst activity. Neither alumina supported Rh or Ru offered conversions or selectivities of note compared to the other catalysts tested.

It must be realized that any system modification that results in a higher rate toward the desired product may lead to a similar increase in rate to unwanted byproducts. The ideal situation, of course, would be to find a modification where this not the case, in that the rate toward the desired product would be increased, both absolutely, and with respect to the competing reaction pathways, leading to both a

higher conversion and selectivity. Also required is a support that offers electrical conductivity. Because these catalysts will be employed in an electrochemical fuel cell, the incoming electrons from the external circuit must be able to be conducted from the electrode, through the support, to the catalyst metal. Carbon supports are highly capable in such respects, and are also easily able to conduct protons in the same manner, as discussed above with regards to spillover. From this, moving toward catalyst customization and modification, it is noted that a carbon support is necessary and that it may be beneficial to choose Pd over Pt, as the former seems to be less active toward the undesired pathways.

5.2 • Other catalysts and modifications

A number of other catalysts were also prepared in house, and tested in a similar fashion to the commercial ones above. This allowed for further customization of the metal and support combinations, as well as the introduction of different catalyst modifications either during or post production.

The first modification investigated was the inclusion of promoters such as K_2O and Se, incorporated into sol-gel catalysts as they were being made. A similar procedure was used to produce K_2O promoted sol-gel catalysts previously and the same motivations in using those promoters apply here as well. Four different Pd/SiO_2 catalysts were made by this method, incorporating different proportions of the additive, metal and support (Table 5-2). The incorporation of K_2O into the support led to a

significant increase in conversion, accompanied by a similarly marked decrease in selectivity (entry 1). The catalyst with the highest loading of Se was actually tested first and after performing poorly, prompted the synthesis of catalysts with lower loadings. The effect is definitely significant, with just 0.1 wt% Se giving huge increases in rate. Disappointingly, however, it is obvious that Se also significantly increases the rates of the competing pathways toward undesired byproducts. These types of additives were therefore ruled out toward further optimization.

Table 5-2 • Effect of additives to sol-gel Pd/SiO_2 catalyst

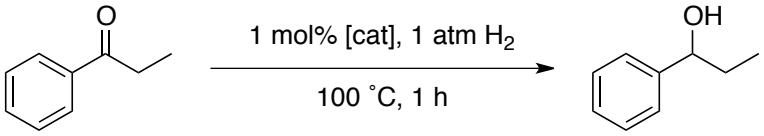

Entry	Catalyst[a]	Conversion (%)[b]	Selectivity (%)[b]
0	5 wt% Pd/SiO_2	6	> 99
1	4.8 wt% $Pd/1.6$ wt% K_2O/SiO_2	37	56
2	4.8 wt% $Pd/0.1$ wt% Se/SiO_2	23	31
3	4.8 wt% $Pd/0.2$ wt% Se/SiO_2	20	60
4	4.8 wt% $Pd/1.6$ wt% Se/SiO_2	4	96

a | sol-gel catalysts, loading based on stoichiometry of precursors added
b | determined by ^1H NMR spectroscopy, averaged over two experimental runs
c | for commercial 5 wt% Pd/SiO_2 catalyst, for reference only

As discussed previously, Zaccheria *et al.* have reported high selectivities (97-100%) with high conversions (>99%) for the hydrogenation of a selection of phenyl ketones with an 8 wt% Cu/Al_2O_3 catalyst.[102] The catalyst was prepared by a simple impregnation of copper from a $(CuNH_3)_4^{2+}$ solution onto a commercial Al_2O_3 support. In the paper, they also briefly mention a similar SiO_2 catalyst that had been prepared previously that was not as selective for the alcohol due to its acidity. This observation is consistent with those made above during the initial commercial catalyst screening for this project. In their experiment, propiophenone (100 mg) was exposed to 100 mg of the

Cu/Al_2O_3 catalyst in 8 ml of *n*-heptane at 90 ˚C under 1 atm H_2. That works out to be about 17 mol% metal loading with respect to the amount of ketone. They report 94% selectivity at 86% conversion after 0.5 h. After 1 h, conversion has reached completion (100%) with an overall selectivity of 90%. While these selectivities are still relatively poor, the rates are significantly greater than those discussed herein. This is likely due to the high catalyst loading (9 times what is used in our experiment) and the use of solvent. The solvent helps to stabilize molecules away from the surface, enhancing their partitioning into solution, preventing catalyst auto-inhibition. The other benefit of employing a copper catalyst would be cost, as palladium and platinum are much more expensive.

Similar catalysts were, therefore, prepared in house for testing under our prescribed hydrogenation conditions. A commercial source of the specific alumina powder they used could not be found, and therefore two different copper catalysts were made from two different alumina sources. The two involved similar impregnation procedures on either an Al_2O_3 xerogel prepared in-house (BET surface area = 367 $m^2\ g^{-1}$) or onto crushed 1/8″ Al_2O_3 pellets. The catalysts were both exposed to the usual hydrogenation conditions (1 mol% Cu loading, 100 ˚C, 1 h) and no conversion was seen in either case. The xerogel-impregnated catalyst was then exposed to acetophenone under the same conditions published originally, an experiment for which they report 96% conversion and 98% selectivity after 1.5 h. In *n*-heptane, after 1.5 h at 90 ˚C, ^1H NMR spectroscopy shows no conversion to products. With this, these copper catalysts were abandoned.

5.2.1 • Carbon-based Catalysts

Carbon-based catalysts were then investigated further. The benefit of these carbon-supported catalysts, beyond the electron conductivity of the support, is the greater rate of hydrogenation relative to SiO_2-supported catalysts. Only Pt/Vulcan XC-72 catalysts were available commercially, and because the reaction selectivity with Pd-based catalysts has been shown superior to that of Pt-based catalysts, two different 5 wt% Pd/Vulcan XC-72 catalysts were prepared by wet-impregnation on a commercially available Vulcan XC-72 support. These were generated from two different Pd sources, $PdCl_2$ and $Pd(OAc)_2$ and tested for the hydrogenation of propiophenone.

Table 5-3 • Pd/Vulcan XC-72 Catalysts

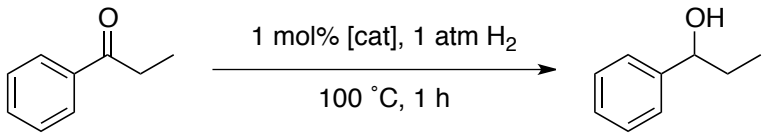

Entry	Metal Loading	Pd precuror	Conversion (%)[a]	Selectivity (%)[a]
1	5 wt% Pd	$PdCl_2$	8 ± 2	54 ± 2
2	5 wt% Pd	$Pd(OAc)_2$	14 ± 1	98 ± 1
3	10 wt% Pd	$Pd(OAc)_2$	7 ± 1	> 99

a | determined by ^1H NMR spectroscopy, averaged over two runs with standard deviation shown.

The results for the two different Pd/Vulcan XC-72 catalysts are markedly different: 54% selectivity at 8.2% conversion for that from the chloride salt, and 98% selectivity at 14% conversion for that from the acetate salt (1 h and 1 mol% catalyst loading). This disparity is likely due to residual chlorine on the $PdCl_2$ based catalyst's surface; it has been shown to hinder the selectivity of such reactions.[141,142] Chlorine is usually volatilized from the surface by high temperature calcination after impregnation

(≥ 530 °C), but calcination is not possible with Vulcan XC-72 based catalysts because they undergo loss of carbon powder above 350 °C.[143,144] A 10 wt% Pd/Vulcan XC-72 was also prepared from $Pd(OAc)_2$ precursor, and gave a lower conversion, with similar selectivity, compared to the 5 wt% sample (the same trend is observed for commercial Pd/C catalysts, see Table 5-1, entries 4–5). This would indicate that, while the amount of Pd is increasing, the number of sites active toward hydrogenation is actually *lessened*. Larger metal clusters are likely forming on the support surface, which will have different electronic properties than the smaller clusters, leading to different reactivity. Again, this should be probed directly in the future embodiments of this work. It is also evident that the proportion of sites active toward the desired hydrogenation, compared to those leading to unwanted activity, is not changing, since selectivity remains relatively constant. Compared to commercial Pd/C catalysts, those prepared from $Pd(OAc)_2$ both give higher selectivities to the desired alcohol, approaching those required for the invention to come to fruition. This is somewhat balanced out by the fact that the reactions are slower, achieving lower conversion after 1 h.

5.2.2 • *n*-Butyl Tin Modification

Santori *et al.* have reported that the modification of a heterogeneous catalyst's surface with organometallic *n*-butyl tin moieties increases the hydrogenation selectivity and conversion for a number of related compounds (Figure 5-1).[106] They report evidence for ionic tin on the surface, which increases the favourability of end-on and side-on adsorbing of the C=O moiety to the surface, the binding modes that lead to the ketone hydrogenation. Once bound, the positively charged tin-modified environment helps to

weaken the C=O bond by withdrawing electron density. The presence of butyl groups sterically hinders planar phenyl ring binding to the catalyst surface to prevent ring hydrogenation.

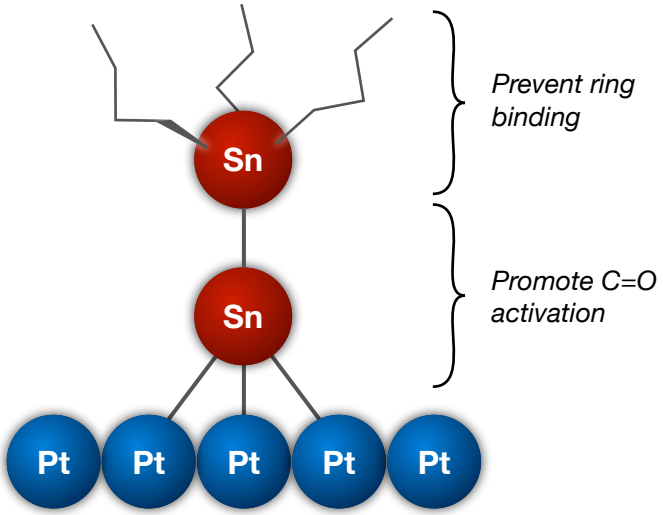

Figure 5-1 • Proposed *n*-butyltin moiety binding mode

Thus, commercial 5 wt% Pd/C and Pd/SiO_2 catalysts were modified by butyl tin moieties to give Sn:Pd atom ratios of 1:5.6 and 1:5.2, respectively (about 1 wt% for both catalysts). These catalysts were then exposed to propiophenone under the usual hydrogenation conditions and the results compared to unmodified catalysts (Table 5-4). For Pd/C, at 100 ˚C, this modification yielded only a decrease in rate, with no increase in selectivity toward the desired alcohol for the propiophenone hydrogenation reaction (entries 1–2). At 140 ˚C, where only 58% selectivity (at 43% conversion) was observed with the commercial catalyst, as received, > 99% selectivity was achieved with the modified catalyst (entries 3–4). This, however, is accompanied by a significant decrease in conversion, only 14% compared to 43% for the unmodified catalyst over the same

reaction time. The decrease in rate is not surprising considering the use of a selective poison, where it is added specifically to cover some of the active catalytic sites. In contrast, the tin-modification of 5 wt% Pd/SiO_2 at 140 ˚C results in the propiophenone hydrogenation conversion actually slighly *increasing* relative to the unmodified catalyst, 12% compared to 9.6%. The reaction selectivity was > 99% for both the modified and unmodified catalysts. At 100 ˚C, the difference is less marked, and likely the same within experimental error. The effect of the Sn modification is likely different for the two catalysts due to a difference in the interaction between the *n*-butyl tin moieties and the oxide support surface compared to those with the carbon support. This is still promising as the modification is more beneficial with those catalysts supported on carbon, which has already been identified as the more likely catalyst support.

Table 5-4 • *n*-Butyl tin catalyst modifications

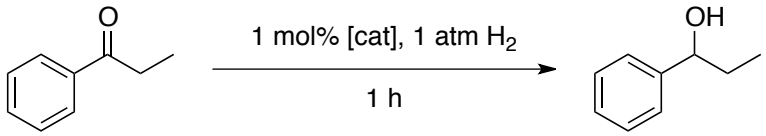

Entry	Catalyst	Temp (˚C)	Sn added (wt%)[a]	Conversion (%)[b]	Selectivity (%)[b]
1	5 wt% Pd/C	100	0	26	95
2	5 wt% Pd/C	100	1	6	94
3	5 wt% Pd/C	140	0	43	58
4	5 wt% Pd/C	140	1	14	> 99
5	5 wt% Pd/SiO_2	100	0	5	> 99
6	5 wt% Pd/SiO_2	100	1	3	> 99
7	5 wt% Pd/SiO_2	140	0	10	> 99
8	5 wt% Pd/SiO_2	140	1	12	> 99
9	20 wt% Pt/Vulcan XC-72	100	0	27	83
10	20 wt% Pt/Vulcan XC-72	100	1	26	75
11	20 wt% Pt/Vulcan XC-72	100	5	6	> 99

a | to commercial catalyst, loading based on stoichiometry of precursor added
b | determined by ^1H NMR spectroscopy

These tin-modifications have indeed proven beneficial to the selectivity of the reaction after 1 h at low to moderate conversions. The difference is more marked at 140 ˚C, which is likely due to the higher overall rate of all reactions, with the relative rates being affected *more* by the tin additive. To see if such enhancements may be possible with the Vulcan XC-72 based catalysts, two different Sn-modified commercial 20 wt% Pt/Vulcan XC-72 with different modifier loadings was made and tested (Table 5-4, entries 8-11). Under the standard hydrogenation conditions, a conversion of 26%, with a selectivity of 75%, was achieved, which is a similar conversion than achieved with the unmodified catalyst (27%) with a lower selectivity (compared to 83%). A higher loading of Sn (5 wt%) almost completely arrested the catalytic activity: the conversion was only 6%, but the reaction was completely selective for the desired alcohol. Overall, the decision to use Sn modified catalysts or not will have to be based on more information, such as the temperature of the fuel cell employed, the ketone used and the behavior of these catalysts toward the electrochemical reduction of the ketone. Also, the toxicity of the tin would have to be taken into consideration.

While some of these modifications indeed resulted in improved catalyst characteristics, none provided the required rate and selectivity for the hydrogenation of propiophenone under the prescribed conditions. Strides, however, have been made toward the benchmarks, and the effect of substituents on the phenyl ring and the identity of the alkyl chain will now be considered.

5.3 • Ketone Screening

In order to see what kind of effect steric and electronic factors have on the reactivity of the phenyl ketone, a number of substituted phenyl ketones were screened for their ability to undergo chemoselective hydrogenation over 1 mol% loading of 5 wt% Pd/SiO_2. Both the alkyl group and the *para*-substituent of the phenyl group were varied.

Table 5-5 • Hydrogenation of aryl alkyl ketones over 5 wt% Pd/SiO_2

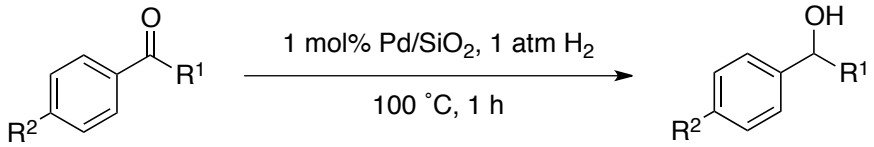

Entry	R^1	R^2	Conversion (%)[a]	Selectivity (%)[a]
1	Me	H	2 ± 1	> 99
2	Me	Me	3 ± 1	> 99
3	Me	OMe	4 ± 1	> 99
4	Et	*t*-Bu	11 ± 1	97 ± 1
5	Et	Me	3 ± 1	> 99
6	Et	H	6 ± 2	> 99
7	Et	OMe	5 ± 2	> 99
8	Et	F	6 ± 3	91 ± 2
9	Et	CF_3	21 ± 1	> 99
10	*i*-Pr	H	7 ± 1	> 99
11	*t*-Bu	H	12[b]	> 99

a | determined by ^1H NMR spectroscopy, averaged over two runs with standard deviation shown.
b | only one experimental run due to limited availability of ketone

While many analogues still undergo poor conversions to products, there is a marked dependence on both R groups. First, we consider the effect of varying the alkyl group R^1 (where R^2 = H, entries 1, 6, 10, 11) on conversion and selectivity (Table 5-5). A

selectivity of $>99\%$ is maintained for all of these unsubstituted phenyl ketones. Regarding rate, it is difficult to differentiate between steric and electronic effects as both the steric bulk and the electron donating nature of the substituents increase in parallel. Nonetheless, the rate of hydrogenation increases with increasing electron donating ability and steric bulk (*i.e. t*-Bu > *i*-Pr > Et > Me). Deconvoluting the influence of these substituents may be possible after examining the effect of varying the phenyl substituent, R^2, on conversion and selectivity. The trends, at least with respect to electronic factors, are expected to be the same or similar.

Several propiophenone analogues substituted at the *para*-position were then examined under our hydrogenation conditions (Table 5-5, entries 4-9). These results also indicate a correlation between the identity of the *para*-substituent and the rate of the reaction. To quantify the nature of the relationship with the reaction rate, estimates of the first order rate constants were calculated by using two data points, 0% conversion at time = 0 and the measured conversion after 1 h. The conversions after 1 h are low in all cases and it is therefore expected that these rate constants will be representative of the initial rate. The natural logarithms of the normalized values were then plotted versus the *para*-Hammett parameter for the substituent (Figure 5-2).

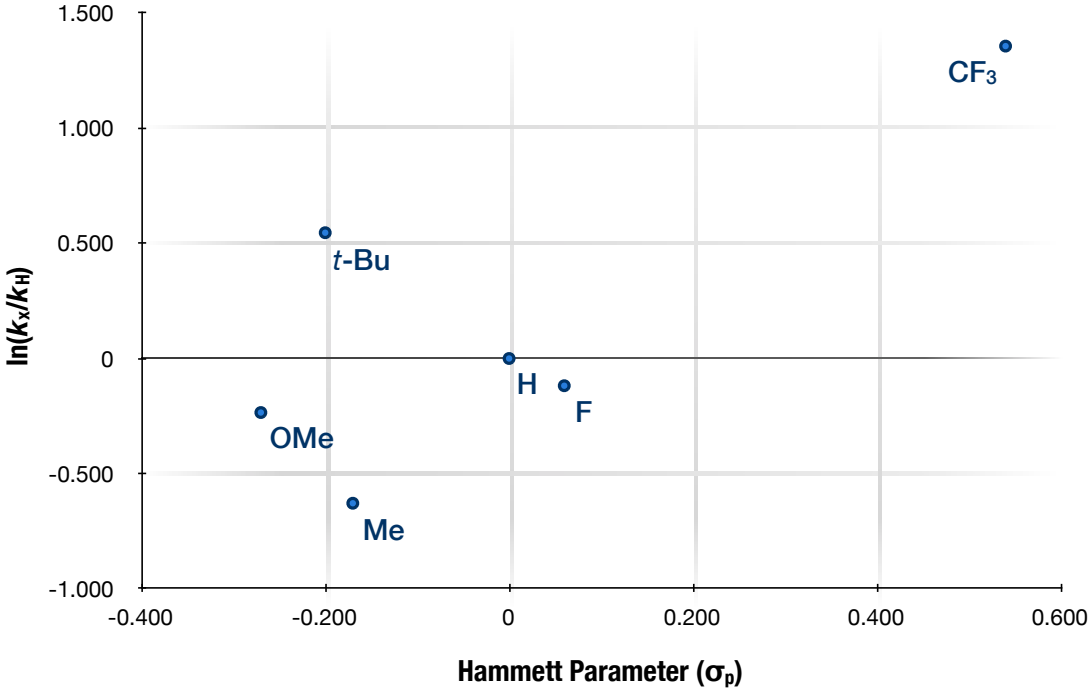

Figure 5-2 • Plot of $\ln(k_X/k_H)$ versus the *para*-sigma Hammett parameter (σ_p) for the hydrogenation of *p*-substituted propiophenones over 1.0 mol% loading of 5 wt% Pd/SiO_2 at 100 ˚C under 1 atm H_2.

It is clear to see that there is an increase in the rate of hydrogenation with increasing electron withdrawing ability. This observation may be an effect of the ability of the ketone to bind via unreactive binding modes, as will be discussed below. Electron withdrawing groups would also weaken the C=O π-bond facilitating attack by hydrogen atoms on the surface, leading to an increased rate of reaction. The spatially demanding substituents, *t*-butyl and CF_3, offer even more marked enhancements in the hydrogenation rate over unsubstituted propiophenone and those ketones with small *p*-substituents. It has been suggested in the literature[106,145] that the η^1-(O) adsorption mode on the metal surface is more reactive toward hydrogenation than the η^2-(C,O) adsorption mode (Figure 5-3). Bulky groups on the phenyl ring and next to the ketone functionality prevent coplanar binding, limiting the number of catalytic sites being

occupied by molecules binding through unreactive binding modes. The electron withdrawing groups could also be partially responsible for directing the binding of the ketone in through the oxygen to promote formation of the desired product, and while the availability of the lone pair will also be affected, likely not to as great of an extent. The η^2-(C,O) binding mode would also place the phenyl ring in the appropriate configuration for its π-system to overlap with metal orbitals of the surface atoms, leading to ring hydrogenation. Also, any molecules adsorbed to the surface via these undesirable binding modes would decrease the number of active sites available for adsorption of hydrogen and the ketone via the η^1-(O) mode. This would explain why those with bulky groups show higher rates of conversion. Among the ketones with small *p*-substituents, the rate of reaction increases with increasing electron-withdrawing ability of the substituent. Regarding selectivity, only two of the substituted propiophenones led to the formation of unwanted side products under the prescribed conditions: where R^2 = *t*-Bu and F. No conclusions, however, can be drawn here as to the effect of the substituent toward selectivity.

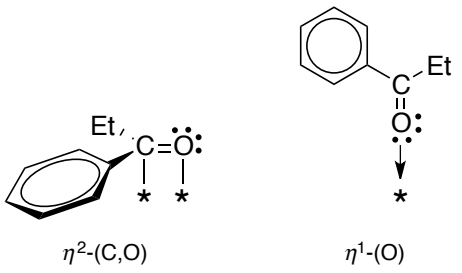

Figure 5-3 • Possible C=O–metal (*) binding modes for propiophenone hydrogenation

It should be mentioned here that the proposed mechanism for the electrochemical reduction of phenyl ketones involves initial approach of the electropositive carbon atom of the carbonyl functionality toward the electrode surface (Figure 5-4).[146,147] This,

however, is inferred from electrochemical data where molecular details could be not distinguished, no surface characterization was performed. Also, in this case, protons would are supplied from the (acidic) reaction media, and not as surface reactants supplied from the membrane. This leads to an ever further complicated picture of what may be happening on the electrode surface, including the possibility (as might be expected) that the reactive binding modes are similar in both catalytic and electrochemical reduction. Regardless, preventing side-on binding of the ketone to the electrocatalyst surface should still be beneficial in order to prevent blocking of active sites. The use of bulky groups at the *para* position though would be ill advised because it may prevent the necessary binding with the electrode. Moving the substituents to the *ortho*-position instead would allow for the same magnitude of electron donating or withdrawing ability and the blocking of side-on ring binding, without preventing the required binding mode. A more positive carbonyl carbon atom from electron withdrawing groups is also still beneficial, favouring its initial approach toward the electronegative cathode surface. Further experimentation to find the mechanism of the proposed reaction may need to be undertaken in order to make any clear conclusions.

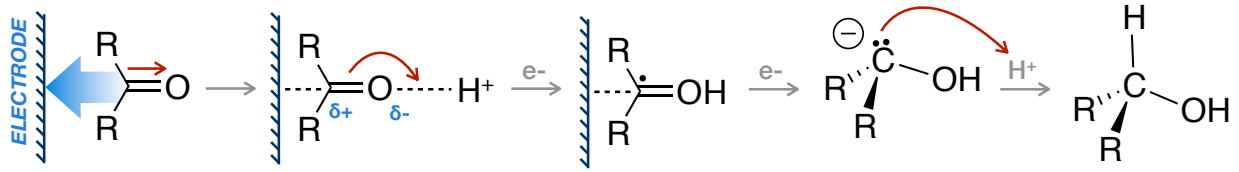

Figure 5-4 • Proposed mechanism for the electrochemical reduction of phenyl ketones[146,147]

Varying R^2 led to the observation that increasing substituent bulk has a significant positive effect on the hydrogenation rate, while increasing electronic withdrawing nature of the substituent had a less pronounced positive effect. The opposite trend in

rate was observed with the increasing electron-donating ability of R^1, where the rate was instead slowed. This suggests that the differences in electronics of the R^1 substituents have little effect on the rate, while the sterics of these substituents has a relatively more marked and observable effect. Overall, the rate observed with 4'-trifluoromethylpropiophenone is promising (27% after 1 h) considering the selectivity over Pd/SiO_2 is > 99% (Table 5-5, Entry 11). Disappointingly, the presence of the *p*-CF_3 group on the analogous alcohol has been shown, qualitatively, to be detrimental to dehydrogenation reactivity.[96]

A number of experiments with the ketone that gave the best results (4'-trifluoromethylpropiophenone) were also carried out with the Sn-modified catalysts previously discussed (Chapter 5.2). A higher temperature (140 °C) and loading of the catalyst (2 mol%) were used to elaborate the differences observed between the modified and unmodified catalyst. The conversions after 1 h using the standard hydrogenation procedure were recorded (Table 5-6). Indeed, the differences in observations between the modified and unmodified catalysts are quite marked. For Pd/C, the starting material is almost completely converted to product after 1 h with a conversion of 74%, albeit mostly to unwanted side products as the selectivity was only 12%. The addition of 1 wt% *n*-butyl tin to the commercial catalysts results in a significant change; the conversion drops drastically to only 9% with an increase in selectivity to 68%, an improvement, but not sufficient enough. With the modified Pd/SiO_2, the conversion drops from 59% to 28% with the addition of tin to the catalyst. The selectivity of the unmodified catalyst is already relatively high at 63%, but with the addition of tin, it increases to 99% (with a small amount of the ring-hydrogenated product being formed). This is one of the highest reported rates with a selectivity ≥ 99%. As mentioned before,

however, the presence of the 4′-CF_3 group has disastrous consequences on the reactivity of the analogous alcohol's dehydrogenation.

Table 5-6 • *n*-Butyl tin catalyst modifications for 4'-trifluoromethylpropiophenone hydrogenation

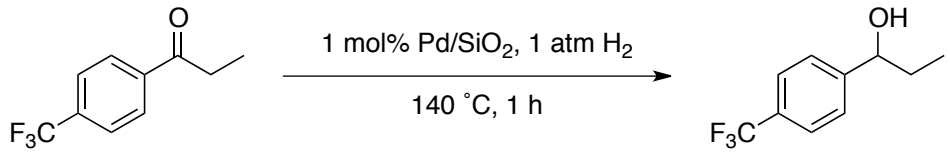

Entry	Catalyst	Sn added (wt%)[a]	Conversion (%)[b]	Selectivity (%)[b]
1	5 wt% Pd/C	0	74	12
2	5 wt% Pd/C	1	9	68
3	5 wt% Pd/SiO_2	0	59	63
4	5 wt% Pd/SiO_2	1	28	99

a | to commercial catalyst, loading based on stoichiometry of precursor added
b | determined by ^1H NMR spectroscopy

It is clear that significant changes in the hydrogenation reactivity of these phenyl ketones can be procured by subtle changes in the molecule structure. Sterically encumbering the molecule around the phenyl ring and the ketone functionality both lead to an increased rate. The withdrawing of electron density from the ketone also yields higher rates of reaction.

5.3.1 • Modified catalysts for dehydrogenation

During the early days of this project, I performed a small screening of modified sol-gel catalysts toward the dehydrogenation at 1-phenyl-1-propanol under the TRFC conditions (Table 5-7). In the proposed TRFC, the dehydrogenation of the alcohol takes place in a separate reaction chamber juxtaposed to the engine to facilitate a reaction temperature of ~200 ˚C. The H_2 produced is then delivered to the fuel cell anode. Two different modifiers, selenium and potassium, were individually incorporated into

Pd/SiO_2 and Pd/Al_2O_3 sol-gel catalysts by the addition of selenium tetrachloride and potassium methoxide during gel formation in order see if higher selectivity could be achieved than that found for the best commercial catalyst, Pd/SiO_2, which facilitated the hydrogenation of 1-phenyl-1-ketone in 35% conversion and 99.65% selectivity (by GC) after 1 h at 200 ˚C.[96] These catalysts were therefore mixed with the alcohol at 200 ˚C for 1 h, after which time the conversion and selectivity toward propiophenone were measured by ^1H NMR spectroscopy (Table 5-7).

Table 5-7 • Modified sol-gel catalysts for 1-phenyl-1-propanol dehydrogenation

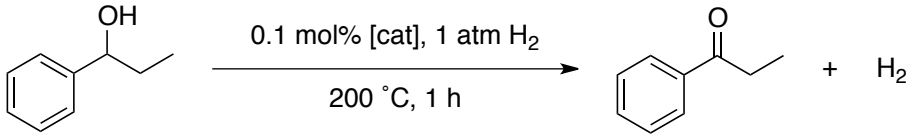

Entry	Catalyst[a]	Conversion (%)[b]	Selectivity (%)[b]
1	5 wt% Pd/SiO_2	65 ± 2	99 ± 1
2	4.8 wt% Pd/0.2 wt% Se/SiO_2	68 ± 3	98 ± 1
3	4.8 wt% Pd/1.6 wt% Se/SiO_2	66 ± 2	90 ± 3
4	5.1 wt% Pd/7.6 wt% Se/SiO_2	3 ± 1	84 ± 8
5	4.8 wt% Pd/1.6 wt% K_2O/SiO_2	53 ± 8	97 ± 2
6	5.1 wt% Pd/7.6 wt% K_2O/SiO_2	56 ± 2	98 + 1
7	4.8 wt% Pd/0.8 wt% K_2O/Al_2O_3	99 ± 1	70 ± 2
8	4.9 wt% Pd/3.6 wt% K_2O/Al_2O_3	98 ± 1	67 ± 1

a | produced in house from sol-gel methodology, wt% based on amount of precursor added during synthesis.
b | determined by ^1H NMR spectroscopy, averaged over two runs with standard deviation shown.

Starting with the modified SiO_2 catalysts, small amounts of Se incorporation do not effect the conversion in one hour but the distribution of products does change. With increasing incorporation of Se, less of the desired ketone was being produced in favour of the hydrogenolysis product, propylbenzene. At 7.6 wt% Se, the activity of the catalyst is almost completely arrested, with only 3% conversion after 1 h; the product mixture contains a further increased fraction of propylbenzene. The addition of K_2O

results in a slight decrease in conversion, while maintaining a similar selectivity within experimental error, making its inclusion unbeneficial. Moving on to the modified Al_2O_3 based catalysts, a surprisingly high conversion is observed after 1 h. Almost quantitative conversion after only 1 h is observed. While the activity of an unmodified Pd/Al_2O_3 sol-gel catalyst was not assessed, a screening of commercial Pd/SiO_2 and Al_2O_3 catalysts suggests that the activity is similar with the latter yielding a slightly lower selectivity toward propiophenone. The modification is then surely responsible for the incredible catalyst activity, thus far unseen in the investigations into this system within the Jessop Research Group. Disappointingly, however, the selectivity is monstrously affected, resulting in a significantly higher fraction of propylbenzene being produced.

5.4 • Effect of temperature

We now shift our focus back to the hydrogenation of propiophenone, and the investigation of ways to increase the rate of the hydrogenation reaction while maintaining high selectivity. If raising the temperature of the reaction results in a large increase in the rate of the desired reaction, while not affecting that of the side reactions to as great of an extent, the yield of the desired alcohol could be increased while maintaining high selectivity. The effect of raising the temperature was therefore investigated. While simple kinetic theory would suggest that the rate of reaction increases with temperature in that $k \propto \exp(-E_a/RT)$ if it demonstrates Arrhenius

behaviour. It is possible, however, that the temperature dependence on the rate of some reactions is not Arrhenius in nature, due to the complex nature of the rate law or competing reactions. This will be discussed in more detail for this reaction below.

With that being said, the temperature dependence of the hydrogenation rate in these systems is not what would be classically expected (Table 5-8). The standard hydrogenation reaction conditions with commercial 5 wt% Pd/SiO_2 were employed at three higher temperatures: 130, 140 and 150 ˚C. At 100 ˚C, the conversion is ~6% in 1 h, and this rises only modestly at 130 and 140 ˚C to 8 and 11% respectively. At a higher temperature still, 150 ˚C, the conversion after 1 h actually decreases. The fact that the conversion decreases at higher temperatures is surprising. The boiling points of the two individual components are, indeed, below 150 ˚C and therefore it may be suggested that this unexpected result is due to evaporative loses. However, it is unlikely that the products would evaporate to a greater extent than the starting material because they have similar boiling points, meaning that, while mass may be lost, it is unlikely that this mass loss would result in an enrichment of the product in the mixture contributing to a smaller observed conversion. While fewer data points have been collected, comparisons of this complicated temperature dependence can be made with a few other catalysts as well. With each of the catalysts studied (5 wt% Pd/C, 10 wt% Pt/C and 20 wt% Pt/Vulcan XC-72), only mild increases in rate were observed at the higher temperatures. For Pt/C, the conversion is actually the same within experimental error at 100 ˚C and 150 ˚C. It should also be noted that with the carbon-supported catalysts at increased temperatures, the selectivity decreases to a greater extent than conversion increases. This indicates that the reaction pathways leading to unwanted side products are relatively *more* favoured at these higher temperatures, as opposed to less as would be desired.

Table 5-8 • Effect of temperature on propiophenone hydrogenation

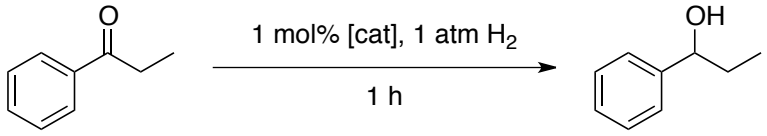

Entry	Catalyst	Temp (˚C)	Conversion (%)[a]	Selectivity (%)[a]
1	5 wt% Pd/SiO_2	100	6 ± 1	> 99
2	5 wt% Pd/SiO_2	130	8 ± 3	> 99
3	5 wt% Pd/SiO_2	140	11 ± 5	> 99
4	5 wt% Pd/SiO_2	150	8 ± 1	> 99
5	5 wt% Pd/C	100	26 ± 7	95 ± 1
6	5 wt% Pd/C	140	43 ± 1	58 ± 1
7	10 wt% Pt/C	100	22 ± 5	89 ± 1
8	10 wt% Pt/C	150	25 ± 7	75 ± 5
9	20 wt% Pt/Vulcan XC-72	100	27 ± 1	83 ± 1
10	20 wt% Pt/Vulcan XC-72	130	32[b]	48[b]

a | determined by ^{1}H NMR spectroscopy, averaged over two runs with standard deviation shown.
b | only one experimental run

Due to the low boiling points of propiophenone and its analogous alcohol, if increasing the temperature were to be employed as a strategy to increase the hydrogenation rate, a higher boiling ketone/alcohol pair would have to be employed. An adequate temperature difference (~100 ˚C) between the two reactions must be maintained to uphold the driving force behind the system. Valerophenone is the simplest ketone whose boiling point, along with that of its analogous alcohol, is high enough to allow the temperature of the dehydrogenation reaction to be raised significantly higher; it is already at 200 ˚C. The boiling point of the ketone is 244-245 ˚C while the alcohol boils at 254 ˚C. Mixtures usually boil at higher temperatures than the individual components, and the system will be under mild pressure, so the temperature of the two reactions can be raised as high as 150 and 250 ˚C for hydrogenation and dehydrogenation, respectively. With that, the best commercial catalysts for the

hydrogenation of propiophenone were exposed to valerophenone at 150 ˚C under otherwise standard hydrogenation conditions (Table 5-9).

Table 5-9 • High temperature catalyst screening for valerophenone hydrogenation

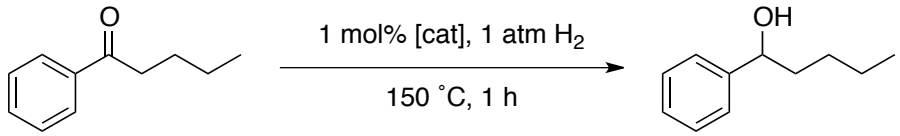

Entry	Catalyst	Conversion (%)[a]	Selectivity (%)[a]
1	5 wt% Pd/$CaCO_2$•1.6wt% Pb	12 ± 3	91 ± 1
2	5 wt% Pd/PEI/SiO_2[b]	11 ± 1	87 ± 4
3	5 wt% Pd/SiO_2	20 ± 2	> 99
4	5 wt% Pd/Vulcan XC-72[c]	6 ± 2	13 ± 2

a | determined by ^{1}H NMR spectroscopy, averaged over two runs with standard deviation shown.
b | PEI = polyethyleneimine
c | made by impregnation on commercial support from $PdCl_2$

The best catalyst is Pd/SiO_2 (entry 3), just as it was at lower temperatures with propiophenone. However, with what has been learned about the effect of the side chain size, one would expect that a longer chain along with an increased reaction temperature of 50 ˚C would contribute to a more marked increase in the rate. The other oxide supported catalyst faired mildly worse, with neither reaching the required selectivity. The result with the Pd/Vulcan XC-72 catalyst is particularly interesting. The conversion is similar to that obtained with this catalyst at 100 ˚C for propiophenone hydrogenation, while the selectivity is far worse at an unprecedented low of 13%; the only other product was pentylbenzene. Overall, however, it appears again that the reaction rate's dependence on temperature is complicated. With the poor results obtained here, it was clear that other means of increasing the rate of the reaction had to be considered besides simply increasing the temperature.

In order to further probe this temperature dependence, isobutyrophenone (*i.e.* isopropyl phenyl ketone, $R^1 = i\text{-Pr}$, $R^2 = H$) was employed. With a boiling point of > 200 ˚C, it is unlikely that significant evaporative losses could contribute significantly to the observed result. Three experiments were performed with 5 wt% Pd/SiO_2, two at 100 ˚C and one at 130 ˚C on larger volumes of the reagent (2.0 ml) in order to allow for samples to be taken regularly to follow the reaction, while avoiding the use of solvent. Following the reaction progress allows one to see if an induction period is present, which may affect how the reaction proceeds. Avoiding solvent was motivated by observations earlier where solvent greatly affected the results. Neat catalyst was pretreated for 2 h under flowing H_2 at 200 ˚C immediately preceding the reaction to ensure that the catalyst was uniform before proceeding. A second run at 100 ˚C without catalyst pretreatment was performed to see the effect, and whether the results could be more generally compared to other experiments. The results are not surprising considering what was observed with propiophenone itself previously (Table 5-10, Figure 5-5). First, it is important to point out that the pre-treatment of the catalyst had little (if any) effect on the overall rate of the reaction over the first 3 h at 100 ˚C (same conversion after this time) or on the shape of the line relating conversion with time; no induction period is noted in either case. At 130 ˚C, a similarly straight line is observed in the conversion-time plot, with a slightly greater slope indicating a slightly higher reaction rate, but not as high as would be expected with a 30 ˚C increase in reaction temperature.

Table 5-10 • Effect of temperature and pre-treatment on isobutyrophenone hydrogenation

	Conversion (%)[a]		
Time (min)	**100 ˚C, no pre-treatment**	**100 ˚C**	**130 ˚C**
5	0.5	0.5	0.9
10	0.7	1.0	1.4
15	1.2	1.3	1.8
30	2.1	1.9	3.7
60	4.1	4.6	7.4
120	9.2	8.9	14.6
180	15	13	22.3

a | determined by ^{1}H NMR spectroscopy where a series of ~10 μL aliquots were removed from reaction mixture, *via* needle and syringe, at intervals throughout the reaction after being added to ~0.5 ml $CDCl_3$ and filtered to remove catalyst.

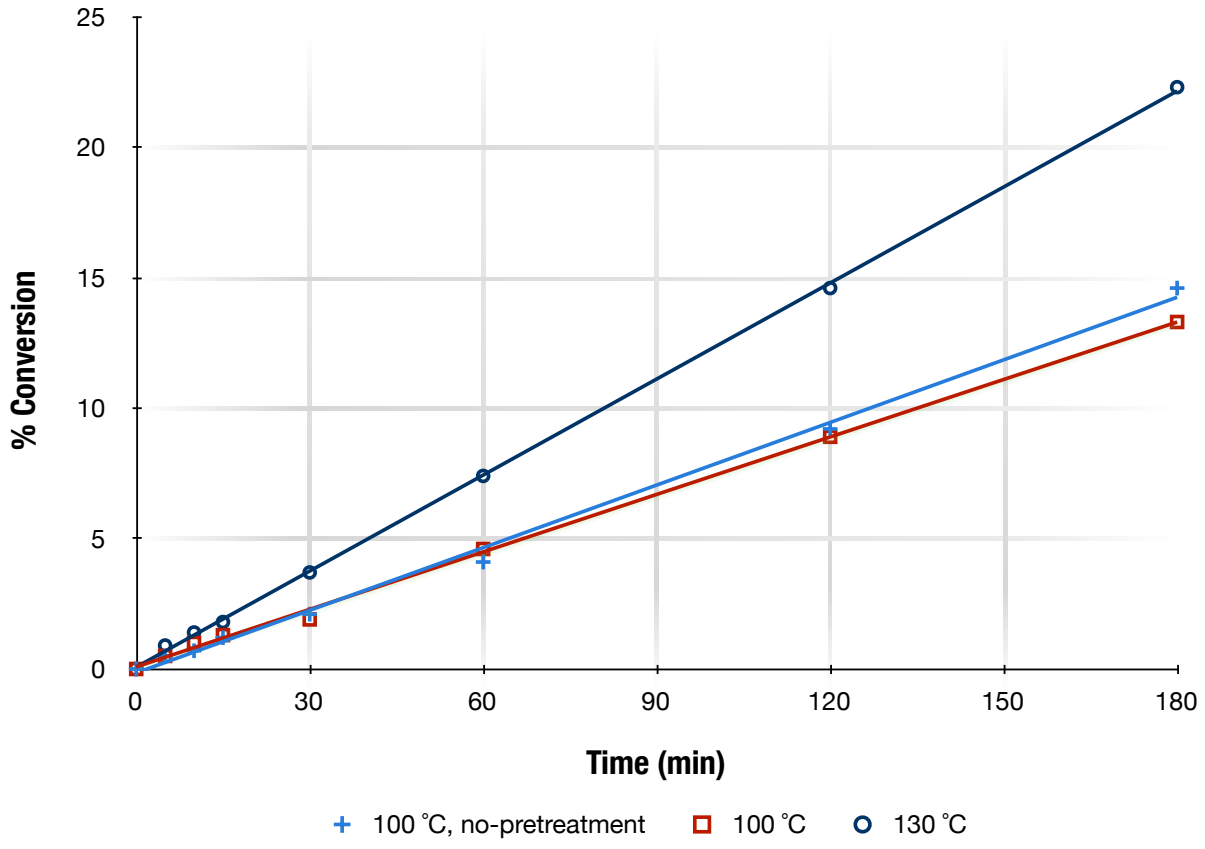

Figure 5-5 • Effect of temperature and pre-treatment on isobutyrophenone hydrogenation

Multiple examples of the surprisingly weak correlation between temperature and hydrogenation rate have been observed, with various catalyst metals and supports and a myriad of phenyl ketones. The reason for this is not known for certain; it has been suggested in the literature that non-Arrhenius behaviour in the initial rate of catalytic surface reactions can be explained by the influence of interactions between adsorbates.[148] The authors suggested that the rate of individual elementary steps, such as thermal desorption, surface diffusion and chemical reaction, can all be influenced by interactions between adsorbates. Adsorbate-adsorbate interactions on the catalyst surface will change the adsorbate-metal potential energy surface, and therefore alter the rate constant of the reaction through changes in the activation energy and pre-exponential factor. It is expected that these effects would be local, and that the influence would only extend throughout the local environment. A number of different "local environments" can then be envisioned, leading to a number of different individual rate constants. Therefore, the *net* rate coefficient (k_{net}) is actually a summation of all of these rates, as in:

$$k_{\text{net}} = \sum_i \chi_i k_i \qquad \text{Eq. 5-1}$$

where χ_i is the mole fraction of adsorbates of local environment i, and k_i is the rate coefficient in that environment, each of which is independently influenced by the temperature. As the temperature is varied, the effect on the rate in each individual local environment will be different, leading to a non-Arrhenius temperature dependence.

The complex rate law of surface reactions can also lead to complex temperature dependences. The mechanism involves many elementary steps, each of which is affected differently by temperature. While the rate of the surface reaction and desorption of the product may increase with temperature, the adsorption of reactants

leading to reaction may be negatively affected. Regardless of the reason, however, within the limited temperature range available based on the restrictions of the system increasing the temperature is not a viable strategy for increasing the rate of hydrogenation.

5.5 • Electrochemical behaviour

A preliminary look into the electrochemical behaviour of propiophenone was also undertaken. While further catalyst and hydrogen carrier optimization will take place on board a thermally regenerative fuel cell prototype currently being developed, some preliminary details regarding its behaviour in an electrochemical system were desired.

As this will be a very basic analysis of the cyclic voltammetry results, a brief explanation of the technique will be included here. Cyclic voltammetry is an electroanalytical technique that traces the path of a redox reaction occurring within a cell as a change in current with the cyclic variation of the voltage across the system between two *switching potentials*. The cell is charged with an electrolyte solution that also contains an electrochemically active analyte and three electrodes are submerged in the solution. The reactivity being probed happens on the surface of the working electrode, which is used as the cathode in the forward scan and the anode in the reverse scan. The voltages measured are with respect to the standard reference electrode, which acts as the opposite electrode to the working electrode. Finally, the counter electrode is used to prevent a buildup of electric current through, and therefore the

warming of, the system. In the experiments herein, a Pt-disc electrode was used as the working electrode, while a platinum wire functioned at the counter electrode. An Ag/AgCl reference electrode was used with a standard half-cell potential of 0.222 V.

The shape of a cyclic voltammogram gives a significant amount of information about the electrochemical reversibility of the system. A redox system that is electrochemically reversible will result in a symmetrical plot with a number of mathematical truths resulting from the Nernst equation (Figure 5-6). The cathodic peak and anodic peak both have two values associated with them, the current (I_{pc} and I_{pa}) and voltage (E_{pc} and E_{pa}). For a reversible system, $\Delta E_p = 0.059/n$ and $I_{pa}/I_{pc} = 1$ and are independent of the scan rate. Also, from a reversible system, the standard half-cell potential can be calculated as $E^0 = (E_{pc} + E_{pa})/2$.

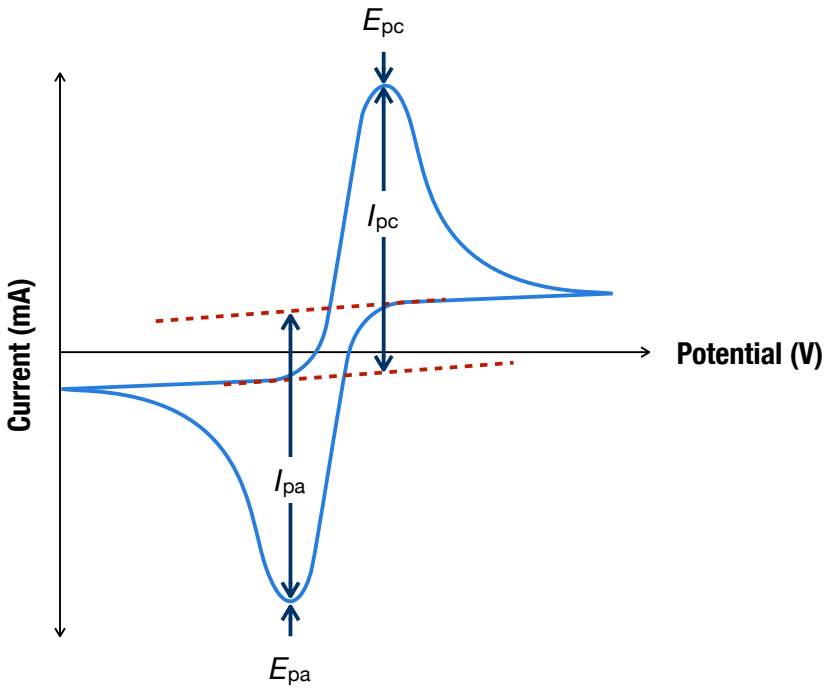

Figure 5-6 • Schematic of a cyclic voltammogram from an electrochemical reversible system

The shape of a system that is electrochemically irreversible is not symmetric. This can either be caused by slow electron exchange reactions at the working electrode or a secondary chemical reaction taking place which removes the reduced species from the vicinity of the electrode surface, meaning that it does not get reoxidized on the reverse scan. In such a case, the equations above no longer hold true, the separation of the peak potentials is $> 0.059/n$ V and becomes dependent on the scan rate. Therefore, there is little information that can be gleaned easily from such voltammograms. One thing that is possible to note is if the shape changes from scan to scan. New peaks may indicate the generation of a second electrochemically active species at the surface that can then undergo a second oxidation or reduction.

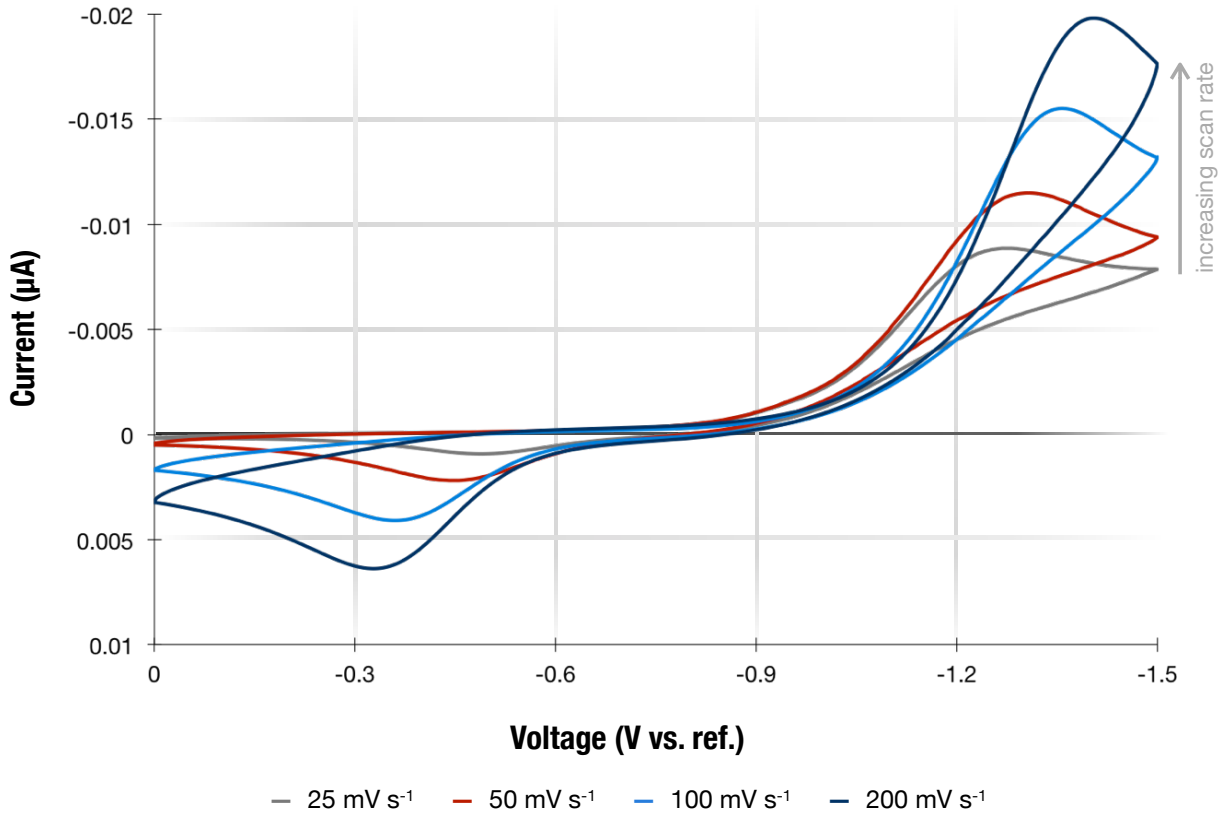

Figure 5-7 • Cyclic voltammograms of a 0.1 M solution of propiophenone in 0.1 M sulfuric acid in acetonitrile at room temperature with various scan rates.

Cyclic voltammograms of a 0.1 M solution of propiophenone in 0.1 M sulfuric acid in acetonitrile were performed from 0 to -1.5 V at room temperature with various scan rates (Figure 5-7). Again, an $Ag^{+}/AgCl$ standard electrode ($E^{0} = 0.222$ V) was used with a Pt wire counter electrode and a Pt-disc electrode as the working electrode. Sulfuric acid was used as the electrolyte so that protons would be available in the system, as would be needed in the second step of the suggested mechanism after the ketone accepts the first electron (Figure 5-4, Chapter 5.3).[146,147] In an actual embodiment of the TRFC system, protons would be supplied through the fuel cell's proton exchange membrane, and the catalyst would certainly behave differently under a potential. The analyte is not soluble in water, and therefore acetonitrile was used as the reaction solvent. The presence of the solvent may affect the reaction, and will not be present in the final system, again indicating that any real further optimization requires live testing in a fuel cell prototype.

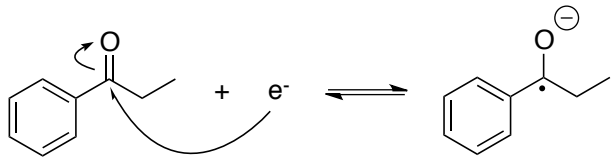

Scheme 5-1 • One electron redox equilibrium of propiophenone

The cyclic voltammograms show that there is, what appears to be, a one-electron transfer happening on the forward and reverse voltage scans (Scheme 5-1). It seems that, even if protons are being transferred to the product of the first electron transfer, the voltages scanned are not sufficient to result in transfer of the second electron. Performing the experiment at elevated temperatures may lower the energy required and allow for complete reduction of the ketone. It is also evident from the shape of the trace that the reaction is not electrochemically reversible under these conditions. The

larger peak, however, corresponds to the first electron being added to the ketone. This does not cause an issue since the oxidation of the alcohol will be done thermally over a precious metal catalyst in another part of the system, and not electrochemically at the anode. It is also possible that this apparent electrochemical reversibility is because of the *chemical irreversibility* of the addition of a proton from the electrolyte after the addition of the first electron. Regeneration of the radical is unlikely, which would explain why the anodic peak is much smaller.

Despite repeated scans over the described voltage region, the system did not seem to generate any other electrochemical products as would have been evident by new peaks appearing in the voltammogram. Because the reduction is not electrochemically reversible, it is not possible to calculate the E^0 of the redox pair. The cathodic and anodic peak potentials were measured, however, for each of the four scan rates (Table 5-11). The fact that these values are changing with the scan rates indicates that the reaction is not completely electrochemically reversible. You can also see this visually in the voltammogram as its shape changes depending on the scan rate. Also, the difference between the anodic and cathodic peaks should equal $0.059/n$, where n is the number of electrons per mole of reaction (in this case, 1); this is not the case at any scan rate.

Table 5-11 • Cathodic and anodic peak potentials with respect to $Ag^+/AgCl$ reference electrode from propiophenone cyclic voltammograms (Figure 5-7)

Scan Rate (mV s^{-1})	E_{pc} (V vs. V_{ref})	E_{pa} (V vs. V_{ref})
25	-1.28	-0.50
50	-1.31	-0.45
100	-1.36	-0.36
200	-1.40	-0.32

This preliminary investigation gives few useful results. It is clear that the two-electron reduction is not taking place; higher temperatures and the use of an electrode doped with one of the catalysts studied, however, may lead to more information. This is an equally poor representation of the final system, and further optimization of the end system using voltammetry may not be possible, and should be done when a prototype is complete.

5.6 • Implications on TRFC viability

While the research of the hydrogenation reaction was presented completely herein, the small amount of work discussed regarding the dehydrogenation of the alcohol couples with more exhaustive studies of another researcher in the Jessop group. This research is described elsewhere,[96] but briefly the best catalyst found for the thermal dehydrogenation of 1-phenyl-1-propanol at 200 °C was a commercial 5 wt% Pd/SiO_2. Regarding the reaction selectivities, the best achieved for the dehydrogenation was 99.65% after 1 h. For the hydrogenation, the best achieved was 98% (for Pd/Vulcan XC-72 made from $Pd(OAc)_2$ impregnation, Table 5-3). It is likely that this is a low estimate of the achievable selectivity for the reduction of propiophenone at the cathode and further testing in a TRFC prototype is needed. Regardless, if one complete chemical cycle, including the dehydrogenation XH_2 and the rehydrogenation of X, achieved these selectivities (97.66% overall per cycle), the number of chemical cycles possible would be about 30 before 50% of that fluid has been converted to side products, and would need

to be replaced. Even a slight enhancement of the overall cycle efficiency to 99% would result in this number of cycles increasing to 67.

While these numbers may seem low, it should be noted that the length of time the system may be in operation before this benchmark is reached is dependant on both the number of cycles *and* the volume of liquid used (the more molecules in the system originally, the longer it will take to exhaust all of their available chemical cycles). The flow rates required to achieve the necessary power will also have a large effect on how the number of cycles translates into running time. The flow rates could also be dynamic in the final system, in that they could be adjusted to compensate for the changing reaction rates and power demands of the vehicle.

Regarding the implications of the reaction rates, the initial rate of dehydrogenation of 1-phenyl-1-propanol over Pd/SiO_2 at 200 °C is 22 mol H_2 per mol Pd per min over the first 10 min, or 0.21 mol H_2 per g Pd per min. The rate of the electrochemical reduction at the cathode is not known; however, the overall rate can be adjusted by simply adjusting the number of fuel cells (i.e. the amount of catalyst) relative to the amount of catalyst employed in the reaction chamber for the dehydrogenation. Assuming a rate similar to the chemical hydrogenation (0.70 mol H_2 per mol Pd per min), a hydrogenation catalyst loading of approximately 31 times the loading of the dehydrogenation catalyst would be required. Presuming the fuel cell stack could indeed convert all of the hydrogen evolved to electricity at this rate with perfect efficiency, this would be equivalent to 665 A per g Pd in the dehydrogenation reactor.

A modest fuel cell voltage estimate of ~0.3 V means that this system would be able to provide 200 W at maximum rate with 1 g Pd in the dehydrogenation chamber. Commercial trucking alternators, the technology that this aims to supplant, operate at 12 V with a current of 100-300 A, meaning a power output of 1200-3600 W, significantly

higher than that estimated above for the TRFC. In order to increase the rates of the two reactions in order to produce this much power, about 195 g of palladium would be required. Currently, Pd prices are approximately 700 USD oz^{-1}. (or 25 USD g^{-1}), meaning the cost of the palladium alone would be upwards of $5000. This may be prohibitive both financially and with respect to natural resource depletion, but if one considers possible monetary savings, the former may seem like less of an issue. As discussed previously, savings of 4919-9279 L fuel and $6000-11000 per truck per year could be expected. Therefore, the cost of the unit, even will a large amount of catalyst, could be paid with one year of fuel cost savings. Also, the projected CO_2 emissions reduction for the entire Canadian trucking industry would be about 1.7 billion kg.[149] While the cost may not necessarily be that excessive, cost is not the only barrier to using such a large amount of a precious metal; its depletion must also be considered. With this in mind, a system that only partially replaces the power generated by the alternator may be considered. The authors also anticipate that further improvements for both reactions will be achievable with further testing and optimization with a TRFC prototype; without such improvements, the system would not be viable. These studies are currently underway by other members of the Jessop Group; their results will follow.

Chapter 6 • Conclusions & Recommendations

6.1 • Hybrid Hydrogen Storage

While several physically bound N-heterocycle borane complexes were made and tested for their ability to undergo hydrogen release under relatively mild conditions, few were unsuccessful in the latter transformation. It is suggested that the binding of the borane moiety through the lone pair of electrons on the nitrogen results in the ring being too electron deficient for facile dehydrogenation. This leads to the successful hydrolysis of the BH_3 fragment, or dehydrogenation across the B-N bond, while the ring remains fully hydrogenated. One bound example, however, was produced that was able to undergo some ring hydrogenation. Indoline-borane was able to undergo full hydrolysis of the borane and 71% dehydrogenation of the indoline rings after 2 h at 100 °C over Pd/C. This is the best bound-hybrid system found, with a gravimetric storage of ~6 wt% H_2 and an enthalpy of H_2 release of -26 kJ per mol H_2.

Separating the two moieties in two different molecules to prevent the above mentioned issue was met with mixed results. Mixtures of indoline and different amine boranes were exposed to catalyst at elevated temperatures to attempt their mutual dehydrogenation. When attempting this in the absence of water (thermolysis of N-B bond), borane transfer to the heterocycle, or the catalyst surface, resulted in no other reactivity being observed by NMR spectroscopy. However, with the addition of water,

resulting in the hydrolysis of the borane instead, four different combinations proved successfully dehydrogenated. The combination of indoline with sodium borohydride, ammonia borane, dimethylamine borane and triethylamine borane all lead to complete dehydrogenation of the organic ring and hydrolysis of the borane moiety. The stoichiometry of these mixtures was such as to produce hydrogen at a net zero enthalpy.

Despite these findings, however, greater rates of endothermic dehydrogenation are still required before the hybrid exothermic/endothermic mixed fuel systems can be practical. These results should then be taken and applied to the development of new systems. As mentioned in the text, more work was indeed done on these systems by other researchers in the group. Moving forward, the discovery of new endothermically and exothermically hydrogen-releasing systems prompts the assessment of their practicality in such a mixed system.

6.2 • Overcoming the Rate Disparity

To eliminate the disparity in the hydrogen release rates of the endothermic and exothermic reactions of a mixed system, several strategies were analyzed. Finding ways to increase the rate of N-heterocycle dehydrogenation is of utmost importance as it became apparent that the amount of Pd that is required to facilitate the necessary H_2 release rate from our first generation mixed system is prohibitive. Increasing the temperature, although successful in increasing the rate of indoline dehydrogenation significantly, also decreased the selectivity for indole, the desired product. At 180 ˚C,

complete indoline dehydrogenation was observed in 5 minutes, but it was accompanied by severe degradation to the hydrogenolysis and disproportionation products. From these experiments, however, a number of thermodynamic factors were calculated for the heterogeneously catalyzed dehydrogenation of indoline including the Arrhenius pre-exponential factor ($A = 2.75 \times 10^7\ s^{-1}$), the activation energy ($E_a = 79.7\ kJ\ mol^{-1}$) and the enthalpy and entropy of activation ($\Delta H^{\ddagger} = 76.3\ kJ\ mol^{-1}$ and $\Delta S^{\ddagger} = 113\ J\ mol^{-1}\ K^{-1}$). Catalyst choice makes a significant difference in the dehydrogenation rate of indoline, and similar trends would be expected for other N-heterocycles. After screening a myriad of sol-gel catalysts prepared from many metals and supports, it was found that Pd/SiO_2 and Pd/Al_2O_3 both gave the highest activities toward the dehydrogenation of indoline, yielding conversions of 81 and 61%, respectively. Future work in this vein should be focused on further characterization of the catalyst surface composition and topography in order to be able to make more concrete conclusions about the results obtained. Further to this point, verification the heterogeneity of the catalyzed reaction should also be considered whereas the reaction mechanism may involve leaching of the metal, whether it be lost to the reaction mixture or deposited back on the support surface. If such leaching is occurring, it may hinder the applicability of the catalyst by the fact that it cannot be effectively isolated spatially within a flowing fuel cell system. Leaching of the metal into the reaction mixture can be probed by mass spectroscopy techniques and by filtering the solid catalyst part way through a reaction and determining whether the reaction is able to continue. Also, electron microscopy of the surface before and after the reaction may indicate severe metal cluster reconstruction, which would be an indication of metal leaching and deposition during the reaction.

Steric hindrance about the nitrogen atom causes a marked increase in the dehydrogenation rate of piperidine derivatives. The extent of dehydrogenation of 2,6-

di-*tert*-butylpiperidine after 1 h at 100 ˚C was significantly greater than that for other piperidine derivatives without as significant steric hindrance around the nitrogen atom. As it is known in the literature that electron donating groups increase the rate as well, the dehydrogenation of 1,4-di-(4-piperidinyl)propane was attempted. It would be expected to have a similar electronic advantage to 2,6-di-*tert*-butylpiperidine without the steric advantage. Its conversion to product after a 1 h was only trace amounts, significantly lower than that observed for the sterically hindered piperidine under the same conditions.

While the improvements to the rate were not as substantial as hoped, a significant amount of information was garnered about the thermodynamics and kinetics of indoline dehydrogenation. Also, the rate enhancement effect of steric bulkiness about the basic nitrogen atom was characterized. This general effect may be able to applied to other similar systems, either for future envisioned hybrid hydrogen releasing mixtures or more classically.

6.3 • Thermally Regenerative Fuel Cells

So far, the stringent selectivity requirements originally described for the thermally regenerative fuel cell system described herein have not been achieved simultaneously with adequate rate. However, significant strides have been made toward identifying methods to increase both the rate and selectivity of the heterogeneously catalyzed hydrogenation of propiophenone analogues by modifying the ketone, by varying the

catalyst metal, support and employing surface modifications. Catalyst choice is also of importance for achieving the high rates and selectivities required. From the initial commercial screening, Pd/SiO_2 proved the best catalyst for this application with >99.99% selectivity at only 6% conversion after 1 h under 1 atm H_2 at 100 ˚C. There are two issues here, the slow rate of reaction and the fact that silica is not an electron-conducting support. Other catalysts were therefore investigated, with commercial 10 wt% Pt/C (or Vulcan XC-72) giving 89% selectivity at 22% conversion and a prepared 5 wt% Pd/Vulcan XC-72 giving 98% selectivity at 14% conversion. The addition of an *n*-butyl tin modification to carbon based catalysts resulted in an increase in selectivity with a decrease in rate. One example with a modification to a SiO_2 catalyst yielded both a higher selectivity and a slightly higher conversion under the same conditions. Further characterization of the catalyst surface before, during, and after the reaction using electron and photo spectroscopies will allow for further customization of the size, distribution and placement of the metal particles, hopefully leading to more active and selective catalysts. The ultimate decision about the usefulness of these modifications must, however, be based on further investigations in an electrochemical system and the toxicity of the resulting catalysts. As previously, the heterogeneity of the (eventual) electrochemical reaction should be confirmed; it is a very important characteristic of the system, preventing unwanted reactivity elsewhere in the TRFC.

A wide array of benzylic ketones close to the structure of propiophenone were also dehydrogenated to see the effect of these substitutions on the rate of the hydrogenation reaction. Both steric and electronic factors are important in the choice of ketone. This has been attributed to either a more facile binding of the reactant to the surface of the catalyst in the binding mode that leads to hydrogenation, or the more facile nucleophilic attack from the hydrogen atoms on the surface. Steric bulk around

the ketone and the phenyl ring both also increase the rate of the hydrogenation reaction. It is thought that this relates to the prevention of auto-inhibition of the catalyst surface that such steric protection provides. It may also prevent the ring from being able to find in such a way as to lead to its hydrogenation.

The dependence of the reaction rate on temperature is complicated. It has been shown that it is certainly not Arrhenius in nature, and this is attributed to the complex rate law that exists for such a system on a surface, as discussed in the text.

Also, a limited investigation into the electrochemical behaviour of propiophenone on a Pt-disc electrode was carried out. While it was demonstrated that the first electron reduction of the ketone is not electrochemically reversible in the system, this should certainly not be taken as a deterrent to the possible functioning of the final system. Further investigation is required, most beneficially *in situ* with a prototype thermally regenerative fuel cell system. I believe that it is unwise to continue optimization of the system in any situation other than this.

We have been able to show trends in rate and selectivity for heterogeneous hydrogenation reactions of neat phenyl ketones under mild conditions based on catalyst choice and ketone functionalization. Regardless of the implications for a possible thermally regenerative fuel cell system, these results may also be of interest to the community with respect to the heterogeneously catalyzed chemoselective hydrogenations of such benzylic ketones in other applications. With respect to the TRFC, however, now that these factors have been identified, future work will involve continued development with testing at the cathode of a fuel cell.

References

1) Spiegel, C. S. In *Designing and Building Fuel Cells*; McGraw-Hill: Toronto, 2007; pp. 15-34.

2) *Annual Energy Outlook 2011*; United States Energy Information Administration, 2011.

3) White, C.M.; Strazisar, B.R.; Granite, E.J.; Hoffman, J.S.; Pennline, H.W. *J. Air Waste Manage. Assoc.* **2003**, *53*, 645-715.

4) Şen, Z. In *Solar Energy Fundamentals and Modeling Techniques*; Springer-Verlag: London, England, 2008; pp. 21-45.

5) Sperling, D.; Cannon, J. S. In The Hydrogen Energy Transition: Moving Toward the Post Petroleum Age in Transportation; Elselvia Inc.: Burlington, MA, 2004; pp. 1-19.

6) *2009 Canadian Vehicle Survey: Annual*; Ministry of Industry: Statistics Canada, 2010.

7) Statistics Canada; *Sales of fuel used for road motor vehicles, by province and territory*, http://www40.statcan.ca/l01/cst01/TRADE37A-eng.htm (accessed Aug 29, 2011).

8) US Environmental Protection Agency; *Emission Facts: Average Carbon Dioxide Emissions Resulting from Gasoline and Diesel Fuel*, http://www.etieco.com/content-files/EPA%20emissions%20calc%20420f05001.pdf (accessed Feb 2, 2012).

9) Swedish Energy Agency; *Energy in Sweden, 2010, Facts and Figures*, http://webbshop.cm.se/System/TemplateView.aspx?p=Energimyndigheten&view=default&cat=/Broschyrer&id=e0a2619a83294099a16519a0b5edd26f (accessed Jan 5, 2012).

10) Government of Canada National Energy Board; *Statistics - Energy Conversion Tables*, http://www.neb.gc.ca/clf-nsi/rnrgynfmtn/sttstc/nrgycnvrsntbl/nrgycnvrsntbl-eng.html (accessed Aug 31, 2011).

11) CRC Handbook of Chemistry and Physics, 91st Edition (Internet Version 2011); Haynes, W. M., Ed.; CRC Press/Taylor and Francis: Boca Raton, FL.

12) Broom, D. P. In *Hydrogen Storage Materials*; Green Energy and Technology; Springer Verlag: London, England, 2011; pp. 1-17.

13) G. Collodi; F. Wheeler *Chem. Eng. Trans.*, **2010**, *19*, 37–42.

14) Keith, J.M. *The short-term hydrogen economy: fueling fuel cells from natural gas*, **2011**, http://www.knovel.com.proxy.queensu.ca/web/portal/browse/display?_EXT_KNOVEL_DISPLAY_bookid=3717&VerticalID=0 (accessed Aug 28, 2011).

15) *The Hydrogen Economy: A non-technical review*; United Nations Environment Programme, 2006.

16) Bossel, U.; Eliasson, B. *Energy and the Hydrogen Economy*; energyvision.org, 2003.

17) Nocera, D.G.; Kanan, M.W.; Moore, T.A.; Surendranath, Y.; Reece, S.Y.; Esswein, A.J., (Massachusetts Institute of Technology, USA). Catalytic materials, photoanodes, and photoelectrochemical cells for water electrolysis and other electrochemical techniques. US Patent 20100133110, Jun 3, 2010.

18) Stubbert, B.D.; Peters, J.C.; Gray, H.B. *J. Am. Chem. Soc.* **2011**, *133*, 18070-18073.

19) Kohl, S.W.; Weiner, L.; Schwartsburd, L.; Konstantinovski, L.; Shimon, L.J.W.; Ben-David, Y.; Iron, M.A.; Milstein, D. *Science* **2009**, *324*, 74-77.

20) Grove, W. *Philos. Mag. J. Sci.* **1939**, *XIV*, 127-130.

21) Grove, W. *Philos. Mag. J. Sci.* **1842**, *XXI*, 417-420.

22) *Fuel Cell Technology Handbook*; Hoogers, G., Ed.; CRC Press: New York, 2003.

23) US Department of Energy; *Comparison of Fuel Cell Technologies* **2011**, http://www1.eere.energy.gov/hydrogenandfuelcells/fuelcells/pdfs/fc_comparison_chart.pdf (accessed Sep 28, 2011).

24) Mauritz, K. A.; Moore, R. B. *Chemical Reviews* **2004**, *104*, 4535-4586.

25) van Grotthuss, C.J.D. *Ann. Chim* **1806**, *58*, 54-74.

26) Riis, T.; Hagen, E.F.; Sandrock, G.; Vie, P.J.S.; Ulleberg, O. *Hydrogen Production and Storage, International Energy Agency*: Paris, **2006**, http://www.iea.org/Textbase/publications/free_new_Desc.asp?PUBS_ID=1591 (accessed Sep 14, 2011).

27) US Department of Energy; *Hydrogen Storage 2011 Interim Update* **2011**, http://www1.eere.energy.gov/hydrogenandfuelcells/mypp/pdfs/storage.pdf (accessed Sep 27, 2011).

28) Felderhoff, M.; Weidenthaler, C.; von Helmolt, R.; Eberle, U. *Phys. Chem. Chem. Phys.* **2007**, *9*, 2643– 2653.

29) Lemmon, E. W.; McLinden, M. O.; Friend, D. G. "Thermophysical Properties of Fluid Systems" in *Nist Chemistry WebBook, NIST Standard Reference Database Number 69*; Lindstrom, P. J.; Mallard, W. G., Eds.; National Institute of Standards and Technology: Gaithersburg, USA, http://webbook.nist.gov (accessed Sep 27, 2011).

30) Vogel, G. *Science* **2004**, *305*, 966-967.

31) Honda FXC Clarity - Refueling http://automobiles.honda.com/fcx-clarity/refueling.aspx (accessed Sep 15, 2011).

32) Stephens, F.H.; Pons, V.; Baker, R.T. *Dalton Trans*. **2007**, 2613-2626.

33) Eberle, U.; Felderhoff, M.; Schüth, F. *Angew. Chem. Int. Ed.* **2009**, *48*, 6608-6630.

34) Panella, B.; Hirscher, M.; Roth, S. *Carbon* **2005**, *43*, 2209-2214.

35) Corma, A.; Diaz-Cabanas, M.J.; Jorda, J.L.; Martinez, C.; Moliner, M. *Nature* **2006**, *443*, 842-845.

36) Thomas, K.M. *Catal. Today* **2007**, *120*, 389-398.

37) Wong-Foy, A.G.; Matzger, A.J.; Yaghi, O.M. *J. Am. Chem. Soc.*, **2006**, 128, 3494-3495.

38) Rowsell, J.L.C.; Millward, A.R.; Park, K.S.; Yaghi, O.M. *H. Am. Chem. Soc.*, **2004**, *126*, 5666-5667.

39) van der berg, A.W.C.; Areán, C.O. *Chem. Comm.* **2008**, 668-681.

40) Mackay, K.M. In *Comprehensive Organic Chemistry*; Bailar, J.C.; Emeleus, H.J.; Nyholm, R.; Trotman-Dickenson, A.F., Eds.; Pergamon Press: Oxford, **1975**.

41) Mauron, P.; Buchter, F.; Friedrichs, O.; Remhof, A.; Bielmann, M.; Zwicky, C.; Züttel, A. *J. Phys. Chem. B* **2008**, *112*, 906-910.

42) Vajo, J.J.; Skeith, S.L.; Mertens, F. *J. Phys. Chem. B* **2005**, *109*, 3719-3722.

43) Lu, J.; Fang, Z.Z.; Sohn, H.Y. *J. Phys. Chem. B*, **2006**, *110*, 14236; Nakamori, Y.; Ninomiya, A.; Kitahara, G.; Aoki, M.; Noritake, T.; Miwa, K.; Kojima, Y.; Orimo, S. *J. Power Sources* **2006**, *155*, 447-455.

44) Pinkerton, F.E.; Meisner, G.P.; Meyer, M.S.; Balogh, M.B.; Kundrat, M.D.; *J. Phys. Chem. B* **2005**, *109*, 6-8.

45) Zhu, M.; Wang, H.; Ouyang, L.Z.; Zeng, M.Q. *Int. J. Hydrogen. Energy* **2006**, *31*, 251-257.

46) Alapati, S.V.; Johnson, J.K.; Sholl, D.S. *J. Phys. Chem. B* **2006**, *110*, 8769; S.V. Alapati, S.V.; Johnson, J.K.; Sholl, D.S. *Phys. Chem. Chem. Phys.* **2007**, *9*, 1438-1452.

47) Fakioğula, E.; Yürum, Y.; Veziroğlu, T.N. *Int. J. Hydrogen Energy* **2004**, *29*, 1371-1376.

48) Moores, A.; Poyatos, M.; Luo, Y.; Crabtree, R.H. *New J. Chem.* **2006**, *30*, 1675-1678.

49) Fugii, T.; Saito, Y. *J. Chem. Soc., Chem. Commun.* **1990**, 757-758.

50) Aoki, T.; Crabtree, R.H. *Organometallics* **1993**, *12*, 294-298.

51) Burk, M.J.; Crabtree, R.H.; McGrath, D.V. *J. Chem. Soc., Chem. Commun.* **1985**, 1829-1930.

52) Crabtree, R.H.; Parnell, C.P.; Uriarte, R.J. *Organometallics* **1987**, *6*, 696-699.

53) Burk, M.J.; Crabtree, R.H. *J. Am. Chem. Soc.* **1987**, *109*, 8025-8032.

54) Yukawa, K.; Fujii, T.; Saito, Y.; Fujii, T. *J. Chem. Soc., Chem. Commun.* **1991**, 1548-1549.

55) Yukuwa, K.; Saito, Y. *Bull. Chem. Soc. Jpn.* **1991**, *64*, 938-941.

56) Kariya, N.; Fukuoka, A.; Ichikawa, M. *Appl. Catal. A* **2002**, *233*, 91-102.

57) Cui, Y.; Kwok, S.; Bucholtz, A.; Davis, B.; Whitney, R.A.; Jessop, P.G. *New J. Chem.* **2008**, *32*, 1027-1037.

58) Mohring, R.M.; Wu, Y. *AIP Conf. Proc.* **2003**, *671*, 90.

59) Niedenzu, L.; Dawson, J.W. *Boron-Nitrogen Compounds* Academic Press Inc.: New York, **1965**.

60) Sutton, A.D.; Burrell, A.K.; Dixon, D.A.; Garner III, E.B.; Gordon, J.C.; Nakagawa, T.; Ott, K.C.; Robinson, P.; Vasiliu, M. *Science*, **2011**, *331*, 1426-1429.

61) Jaska, C.A.; Temple, K.; Lough, A.J.; Manners, I. *J. Am. Chem. Soc.* **2003**, *125*, 9424-9434.

62) Wechsler, D.; Cui, Y.; Dean, D.; Davis, B.; Jessop, P.G. *J. Am. Chem. Soc.* **2008**, *130*, 17195-17203.

63) Gelsey, J; U.S. Patent 7108933, Intel Corporation, **2006**.

64) Thorn, D.L.; Tumas, W.; Ott, K.C.; Burrell, A.K. U.S. Pat. Appl. US 2007183967, **2007**.

65) Berzelius, J.J. *Annales chimie physiques* **1836**, *61*, 146; Translated in: Leicester, H.M.; Klickstein, H.S. In *A Source Book in Chemistry 1400-1900*; Harvard University Press: Cambridge, MA, **1959**.

66) IUPAC; In *Compendium of Chemical Terminology, 2nd ed. (the "Gold Book")*. McNaught A.D.; Wilkinson, A., Eds.; Blackwell Scientific Publications, Oxford, **1997**. XML on-line corrected version: http://goldbook.iupac.org (2006-) created by M. Nic, J. Jirat, B. Kosata; updates compiled by A. Jenkins.

67) Thomas, J.M.; Thomas, W.J. *Principles and Practice of Heterogeneous Catalysis*, VCH: New York, **1997**.

68) Datye, A.K. *Top. Catal.* **2000**, *13*, 131-138.

69) Libuda, J.; Freund, H.-J. *J. Phys. Chem. B.* **2002**, *19*, 4901-4915.

70) Lauritsen, J.V.; Besenbacher, F. *Adv. Catal.* **2006**, *50*, 97-145.

71) Bond, G. C. In *Metal-Catalysed Reactions of Hydrocarbons*; Springer Science+Business Media: New York, NY, **2005**; pp. 40-47.

72) Wegener, S.L.; Marks, T.J.; Stair, P.C. *Acc. Chem. Res.* **2012**, *45*, 206-214.

73) Anderson, E.B.; Buchmeiser, M.R. *Chem. Cat. Chem.* **2012**, *4*, 30-44.

74) Dave, P.N.; Malpani, P.R.; Pande, S.K. In *Recent Progress in Chemistry and Chemical Engineering Research (2010)*; Haghi, A.K., Ed.; Nova Science Pub Inc., **2010**; Chapter 10.

75) Mondloch, J.E; Bayram, E.; Finke, R.G. *J Mol. Catal. A* **2012**, *355*, 1-38.

76) Brunauer, S.; Emmett, P.H.; Teller, E. *J. Am. Chem. Soc.* **1938**, *60*, 309-319.

77) Bond, G.C. *Stud. Surf. Sci. Catal.* **1982**, *11*, 1-10.

78) Schwab, G.M. *Adv. Catal.* **1978**, *27*, 1-22.

79) Solymosi, F. *Catal. Rev.* **1967**, *1*, 233-255.

80) Verykios, X.E.; Stein, F.P.; Coughlin, R.W. *J. Catal.* **1980**, *66*, 147-154.

81) Dowden, D.A. *Specialist Periodical Reports, Catalysis* **1980**, *3*, 136-168.

82) Bond, G.C.; Sermon, P.A. *J. Chem. Soc. Farad. Trans. I* **1980**, *76*, 889-900.

83) a) Wang, S.-Y.; Moon, S.H.; Vannice, M.A. *J. Catal.* **1981**, *71*, 167-174; b) Burch, R. *J. Catal.* **1979**, *58*, 220-229.

84) Tauster, S.J.; Fung, S.C.; Baker, R.T.K.; Horsley, J.A. *Science* **1981**, *211*, 1121-1125.

85) Bond, G.C. *Metal-catalysed reactions of hydrocarbons*, Springer: New York, **2005**.

86) Sterba, M.J.; Haensel, V. *Ind. Eng. Chem. Prod. Res. Dev.* **1976**, *15*, 2-17.

87) Chang, J.-R.; Chang, S.-L.; Lin, T.-B. *J. Catal.* **1997**, *169*, 338-346.

88) Maurel, R.; Leclercq, G.; Barbier, J. *J. Catal.* **1975**, *37*, 324-331.

89) Norcross, J.A.; Slichter, C.P.; Sinfelt, J.H . *Catal. Today* **1999**, *53*, 343-356.

90) *Regenerative EMF Cells*; Crouthamel, C.E.; Recht, H.L., Eds.; American Chemical Society: Washington D.C., **1967**; and ref. therein.

91) Plambeck, J.A.; Elder, J.P.; Laitnen, H.A. *J. Electrochem. Soc.* **1966**, *113*, 931-937.

92) Ando, Y.; Tanaka, T.; Doi, T.; Takashima, T. *Energy Convers. Manage.* **2001**, *42*, 1807-1816.

93) Ando, Y.; Aoyama, Y.; Sasaki, T.; Saito, Y.; Hatori, H.; Tanaka, T.; *Bull. Chem. Soc. Jpn.*, **2004**, *77*, 1855-1859.

94) Akimoto, K. Heat-regenerative fuel cell system, involving dehydrogenation and hydrogenation of an organic compound, and circulation of fuel for the fuel cell. Japan Patent 2007287357. November 1, 2007.

95) Carrier, A.J.; Davis, B.R.; Jessop, P.G; Huynh, K.H. (Queen's University at Kingston, CA). Catalyst and liquid combinations for the thermally regenerative fuel cell. US Patent Application 2011274994, Nov 10, 2011.

96) Carrier, A.J.; Dean, D; Little, V.R.; Vandersleen, J.; Davis, B.; Jessop, P.G. *Energy Environ. Sci.* **2012**, *5*, 7111-7123.

97) Demirdoven, N.; Deutch, J. *Science* **2004**, *305*, 974-976.

98) J. P. Hermans, in *Basic Research Needs to Assure a Secure Energy Future – DOE Report from the Basic Energy Sciences Advisory Committee*, 2003.

99) Fuel savings are estimated by taking maximum likely fuel savings listed herein (10%) over 124537-234914 km travelled per truck and average fuel mileage [Natural Resources Canada; *Fuel Efficiency Benchmarking in Canada's Trucking Industry*, http://oee.nrcan.gc.ca/transportation/business/reports/884 (accessed Feb 9, 2010], and a current average Canadian fuel cost of \$1.22 L^{-1} [http://www.gasbuddy.com (accessed Feb 9, 2012)].

100) Santori, G.F.; Moglioni, A.G.; Vetere, V.; Iglesias, G.Y.M.; Casella, M.L.; Ferretti, O.A. *Appl. Catal. A: Gen.* **2004**, 215-223.

101) Matthew, S.P.; Rajasekharam, M.V.; Chaudhari, R.V. *Catal. Today* **1999**, 49-56.

102) Zaccheria, F.; Ravasio, N.; Psaro, R.; Fusi, A. *Tet. Lett.*, **2005**, *46*, 3695-3697.

103) Ribeiro da Silva, M.A.V.; Cabral, J.I.T.A.; Gomes, P.; Gomes, J.R.B *J. Org. Chem.* **2006**, *71*, 3677-3685.

104) Francis, R.F.; Colling Jr., E.L. *J. Org. Chem.* **1986**, *51*, 1889-1891.

105) Lopez, T.; Herrera, L.; Gomez, R.; Zou, W.; Robinson, K.; Gonzalez, R.D. *J. Catal.* **1992**, *133*, 247-259.

106) Santori, G.F.; Casella, M.L.; Ferretti, O.A. *J. Mol. Catal. A* **2002**, *186*, 223-239.

107) Wechsler, D.; Davis, B.; Jessop, P.G. *Can. J. Chem.* **2010**, *88*, 548-555.

108) Phillips, W. D; Miller, H. C.; Mutterties, E. L. *J. Am. Chem. Soc.* **1959** , *81* , 4496-4500.

109) Amezcua, C. A.; Bell, K. E.; Kelly, H. C. *Inorg. Chim. Acta* **1999**, *290*, 80–85.

110) Chitsaz, S.; Breyhan, T.; Pauls, S.; Neumuller, B. *Z. Anorg. Allg. Chem.* **2002,** *628,* 956–964.

111) Khasnis, D. V.; Lattman, M.; Siriwardane, U. *J. Chem. Soc., Chem. Commun.* **1989,** 1538–1540.

112) Chadara, M.; Xu, Q. *J. Power Sources* **2006**, *159*, 855-860.

113) Xu, Q.; Chandra, M. *J. Alloys Compd.* **2007**, *446-447*, 729-732.

114) ΔH_{rxn} for the dehydrogenation of indoline was calculated with Gaussian03[114a,b] using the B3LYP/6-311++G** basis set. a) Frisch, M. J. *et al.*; *Gaussian 03,* revision B.04; Gaussian Inc.: Wallingford, CT, 2004. b) Dennington, R., II; Keith, T.; Millam, J.; Eppinnett, K.; Hovell, W. L.; Gilliland, R. *GaussView,* version 3.08; Semichem, Inc.: Shawnee Mission, KS, 2003.

115) Kulkarni, A.; Zhou, W.; Török, B. *Org. Lett.* **2011**, *13*, 5124-5127.

116) Gribble, G.W.; Hoffman, J.H. *J. Am. Chem. Soc.* **1974**, *96*, 7812-7813.

117) Amendola S.C.; Sharp-Goldman, S.L.; Janjua, M.S.; Spencer, N.C.; Kelly, M.T.; Petillo, P.J.; Binder, M. *Int. J. Hydrogen Energy* **2000**, *25*, 969-975.

118) Calculated from standard formation enthalpies at 25 ˚C, see: Andrieux, J.; Swierczynski, D.; Laversenne, L.; Garron, A.; Bennici, S.; Gouraudier, C.; Miele, P.; Auroux, A.; Bonnetot, B. *Int. J. Hydrogen Energy* **2009**, *34*, 938-951.

119) Davis, W.D.; Mason, L.S.; Stegeman, G. *J. Am. Chem. Soc.* **1949**, *71*, 2775-2781.

120) Kojima, Y.; Suzuki, K.; Fukumoto, K.; Saski, M.; Yamamoto, T.; Kawai, Y.; Hayashi, H. *Int. J. Hydrogen Energy* **2002**, *27*, 1029-1034.

121) Oliveri, I.P.; Maccarrone, G.; Di Bella, S. *J. Org. Chem.* **2011**, *76*, 8879-8884.

122) Aylett, B.J.; Hakim, M.J. *J. Chem. Soc. A* **1969**, *4*, 639-642.

123) Booth, H.; Little, J.H. *Tetrahedron* **1968**, *24*, 279-287.

124) Brown, H.C.; Kanner, B. *J. Am. Chem. Soc.* **1966**, *88*, 986-992.

125) Duetsch, E.; Cheung, N.K.V. *J. Org. Chem.* **1973**, *38*, 1123-1126.

126) Noeth, H.; Beyer, H. *Chem. Ber.* **1960**, *93*, 928-938.

127) Cory, A.; Jaska, C.A.; Clark, T.J.; Clendenning, S.B.; Grozea, D.; Turak, A.; Lu, Z.; Manners, I. *J. Am. Chem. Soc.* **2005**, *127*, 5116-5124.

128) Lanum, M. *J. Chem. Eng. Data* **1969**, *14*, 93-97.

129) Huo, C.-F.; Wu, B.-S.; Gao, P.; Yang, Y.; Li, Y.-W.; Jiao, H. *Angew. Chem. Int. Ed.*, **2011**, *50*, 7403-7406.

130) Rigby, S.P.; Watt-Smith, M.J.; Fletcher, R.S. *J. Catal.* **2004**, *227*, 68-76.

131) Vedage, G.A.; Armor, J.N. Ger. Pat., DE 19602679 A1, **1996**.

132) Efstathiou, A.M.; Bennett, C.O. *J. Catal.* **1990**, *124*, 116-126.

133) Sonnemans, K.; Janus, J.M.; Mars, P. *J. Chem. Phys.* **1976**, *80*, 2107-2110.

134) Sotoodeh, K.; Smith, J. *Ind. Eng. Chem. Res.* **2010**, *49*, 1018-1026.

135) Okazaki, H.; Onishi, K.; Soeda, M.; Ikefuji, Y. *Bull. Chem. Soc. Jpn.* **1990**, *63*, 3167-3174.

136) Aoyama, Y.; Novak, B.M. *Macromolecules* **2001**, *34*, 6842-6844.

137) Booth, H.; Little, J.H.; Feeney, J. *Tetrahedron*, **1968**, *24*, 279-287.

138) Day, J.C. *J. Org. Chem.*, **1978**, *43*, 3646-3649.

139) Filikov, A.V.; Myasoedov, N.F. *J. Phys. Chem.* **1986**, *90*, 4915-4916.

140) Prins, R. *Chem. Rev.* **2012**, *112*, 2714-2738.

141) Liberková, K.; Touroude, R. *J. Mol. Catal.* A **2002**, *180*, 221-230.

142) Consonni, M.; Jokic, D.; Murzin, D.Y.; Touroude, R. *J. Catal.*, **1999**, *188*, 165-175.

143) Purgato, F.L.S.; Montoro, L.A.; Ribeiro, J.; Kokoh, K.B.; Olivi, P. *Electrocatal.* **2010**, *1*, 122-128.

144) Hájek, J.; Kumar, N.; Mäki-Arvela, P.; Saimi, T.; Murzin, D.Y.; Paseka, I.; Heikkilä, T.; Laine, E.; Laukkanen, P.; Väyrynen, J. *Appl. Catal. A* **2003**, *251*, 385-396.

145) van Druten, G.M.R.; Ponec, V. *React. Kinet. Catal. Lett.* **1999**, *68*, 15-23.

146) Elving, P.J.; Leone, J.T. *J. Am. Chem. Soc.* **1958**, *80*, 1021-1029.

147) Davies, W. C.; Evans, D.P. *J. Chem. Soc.* **1939**, 546-554.

148) Fichthorn, K.A.; Balan, P.G. *J. Chem. Phys.* **1994**, *101*, 10028-10037.

149) a) *2009 Canadian Vehicle Survey: Annual*; Ministry of Industry: Statistics Canada, **2010**, b) US Environmental Protection Agency; *Emission Facts: Average Carbon Dioxide Emissions Resulting from Gasoline and Diesel Fuel*, http://www.etieco.com/content-files/EPA%20emissions%20calc%20420f05001.pdf (accessed Feb 9, 2012).

Appendix A • Surface Rate Law Calculations

As described in the text, the elementary steps for a bimolecular reaction on the surface are as follows:

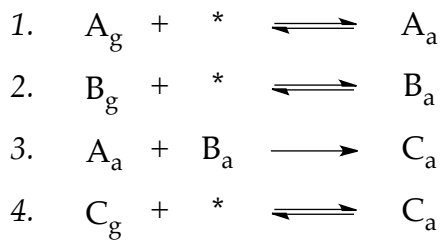

where step 3 is rate determining and irreversible. The rate for the reaction on the surface is then equal to $k_3\theta_A\theta_B$.

The first thing that must be done is to determine the expression for the coverage of each of the species that appear in the rate law, A and B. Assuming that the adsorption equilibrium will be established rapidly, it can be assumed that the rate of association and dissociation with the surface will be similar, and therefore the rate of these two processes will be equal. For A from 1 above, therefore:

$$k_1 P_A \underbrace{\left(1-\theta_A-\theta_B-\theta_C\right)}_{\text{fraction of the surface available for binding}} = k_{-1}\theta_A$$

Rearranging this allows one to solve for θ_A:

$$\theta_A = K_1 P_A \left(1-\theta_A-\theta_B-\theta_C\right)$$

A similar analysis can be done to solve for θ_B. The end goal will be to have a rate law that does not contain these instantaneous coverages. Therefore, because it appears

in the expression above for θ_A, that for θ_C will also required, and can be found in a similar way:

$$\theta_B = K_2 P_B \left(1 - \theta_A - \theta_B - \theta_C\right) \quad \text{and} \quad \theta_C = K_4 P_C \left(1 - \theta_A - \theta_B - \theta_C\right)$$

Next, taking the ratio of two of these at a time, in turn, gives six expressions:

$$\frac{\theta_A}{\theta_B} = \frac{K_1 P_A \left(1 - \theta_A - \theta_B - \theta_C\right)}{K_2 P_B \left(1 - \theta_A - \theta_B - \theta_C\right)} \qquad \frac{\theta_A}{\theta_C} = \frac{K_1 P_A \left(1 - \theta_A - \theta_B - \theta_C\right)}{K_4 P_C \left(1 - \theta_A - \theta_B - \theta_C\right)} \qquad \frac{\theta_B}{\theta_C} = \frac{K_2 P_B \left(1 - \theta_A - \theta_B - \theta_C\right)}{K_4 P_C \left(1 - \theta_A - \theta_B - \theta_C\right)}$$

$$\theta_A = \frac{K_1 P_A}{K_2 P_B}\theta_B \qquad \theta_B = \frac{K_2 P_B}{K_1 P_A}\theta_A \qquad \theta_A = \frac{K_1 P_A}{K_4 P_C}\theta_C \qquad \theta_C = \frac{K_2 P_C}{K_1 P_A}\theta_A \qquad \theta_B = \frac{K_2 P_B}{K_4 P_C}\theta_C \qquad \theta_C = \frac{K_4 P_C}{K_2 P_B}\theta_B$$

which can then be substituted back into the original expressions to give the coverage function for each adsorbate with respect only to pressures of the reagent and product gases and the equilibrium constants. For A:

$$\begin{aligned}
\theta_A &= K_1 P_A \left(1 - \theta_A - \theta_B - \theta_C\right) \\
\theta_A &= K_1 P_A \left(1 - \theta_A - \left\{\frac{K_2 P_B}{K_1 P_A}\theta_A\right\} - \left\{\frac{K_4 P_C}{K_1 P_A}\theta_A\right\}\right) \\
\theta_A &= K_1 P_A - K_1 P_A \theta_A - K_2 P_B \theta_A - K_4 P_C \theta_A \\
\theta_A &+ K_1 P_A \theta_A + K_2 P_B \theta_A + K_4 P_C \theta_A = K_1 P_A \\
\theta_A &\left(1 + K_1 P_A + K_2 P_B + K_4 P_C\right) = K_1 P_A \\
\theta_A &= \frac{K_1 P_A}{1 + K_1 P_A + K_2 P_B + K_4 P_C}
\end{aligned}$$

and similarly for B. Plugging these two coverages back into the original rate expression then gives:

$$rate = \frac{k_3 K_1 P_A K_2 P_B}{\left(1 + K_1 P_A + K_2 P_B + K_4 P_C\right)^2}$$

Appendix B • GC Quantification

In order to determine selectivities for propiophenone hydrogenation more accurately, and allow for a precise assessment of those > 99%, a gas chromatography method was developed using a hexadecane internal standard. For this method, the injector and FID (flame ionization detector) were both held at 250 ˚C for the duration of the experiment. The column (Agilent Technologies DB-5ms Ultra Inert column, length ~30 m, inner diameter 0.25 mm, film thickness 0.25 μm) temperature was ramped using the temperature profile delineated (Table B-1).

Table B-1 • Oven/column temperature profile for quantification experiments.

Rate (˚C/min)	Temp (˚C)	Hold (min)
Initial	70	0.0
15.0	90	1.0
10.0	120	2.0
10.0	230	1.0
40.0	70	0.0

Three calibration curves were made using a Shimadzu GC-17A for propiophenone, 1-phenyl-1-propanol and propylbenzene. The ratios of the integrated peak area of the analyte peaks and internal standard peak (response ratio) were then plotted versus a similar ratio of the masses (mass ratio). A linear regression was performed in each case with a forced intercept of (0,0) to determine the response factor, which were then used to determine unknown quantities of the analytes in product mixtures as indicated in the text. The response factor for all byproducts was assumed to be the same as that measured for propylbenzene.

In each case, five stock solutions were prepared for analysis, each containing 100.0 μL (77.3 mg) of the internal standard measured by an adjustable micropipette. The analyte amount was varied from 0 to 1000 μL. The samples were dissolved in approximately 15 ml of HPLC-grade methanol. Exact concentrations are not required based on the internal standard methodology used. 150 μL of each solution were then removed into a new 4-dram vial and diluted with a further 15 ml methanol. The vials were capped and inverted 40 times before three 1 ml aliquots were removed to a GC sample vials for analysis. The response ratios for each sample were averaged before plotting and regression analysis. The raw data, calibration curves, and linear regression fits are delineated below.

1-Phenyl-1-propanol

Sample	Analyte added (μL)	Mass (mg)	Mass Ratio	Mean Response Ratio
A	0.0	0.0	0.000	0.000
B	250.0	248.5	3.215	3.022
C	500.0	497.0	6.429	5.977
D	750.0	745.5	9.644	8.604
E	1000.0	994.0	12.86	11.26

Linear regression gives: *response ratio* = 0.890 (*mass ratio*) + 0.010 with an $R^2 = 0.999$.

Propiophenone

Sample	Analyte added (μL)	Mass (mg)	Mass Ratio	Mean Response Ratio
A	0.0	0.0	0.000	0.000
B	250.0	252.3	3.263	2.942
C	500.0	504.5	6.527	5.648
D	750.0	756.8	9.790	9.526
E	1000.0	1009.0	13.05	12.14

Linear regression gives: *response ratio* = 0.933 (*mass ratio*) + 0.017 with an $R^2 = 0.999$.

Propylbenzene

Sample	Analyte added (µL)	Mass (mg)	Mass Ratio	Mean Response Ratio
A	0.0	0.0	0.000	0.000
B	250.0	215.5	2.788	3.860
C	500.0	431.0	5.576	7.336
D	750.0	646.5	8.364	11.50
E	1000.0	862.0	11.15	15.67

Linear regression gives: *response ratio* = 1.38 (*mass ratio*) + 0.01 with an $R^2 = 0.999$.

Plot

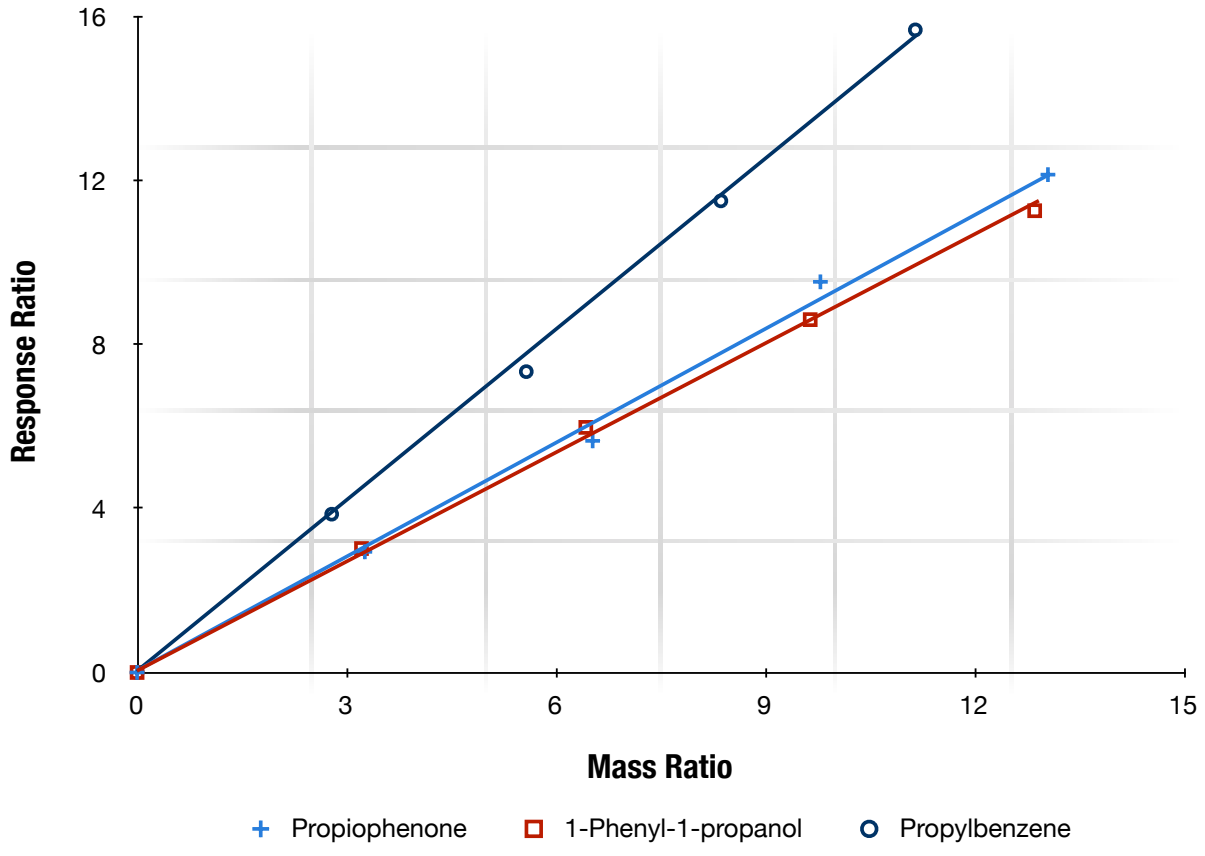

Appendix C • Sol-gel Calculator

In order to easily calculate the amounts of reagents needed for the myriad of sol-gel catalysts that were synthesized, a calculator was developed using a data analysis program (Microsoft Excel) and the details of that calculator are included herein.

The relative amounts of reagents (as well as the procedure used) were based on those from the literature.[105] The number of moles water and base added were in the same proportions with respect to the molar ratios found in the reference. The number of moles of the metal and modifier precursor (when used) was determined by the desired loading(s). The amount of solvent was chosen first to set the scale of the reaction, and the amount of precursor was determined based on the molar/volume ratio used in the reference. An example calculation sheet for a desired 5 wt% Pd/5 wt% Se/SiO_2 catalyst is shown below where red values are those calculated by the program. The relevant reagent ratios from the reference and example calculations are also included below.

Reagent Ratio Calculations

$$\frac{4.8\ ml\ TEOS}{2\ ml\ solvent}\times\frac{0.933\ g}{ml}\times\frac{mol}{208.33\ g}\times\frac{1000\ mmol}{mol}=\frac{10.748\ mmol\ precursor}{ml\ solvent}$$

$$\frac{0.3\ ml\ solution}{0.0215\ mol\ precursor}\times\frac{0.9\ g}{ml}\times\frac{30\ g\ NH_4OH}{100\ g\ solution}\times\frac{mol}{35.05\ g}=\frac{0.108\ mol\ NH_4OH}{mol\ precursor}$$

$$\frac{2\ ml\ H_2O}{0.0215\ mol\ precursor}\times\frac{1\ g}{ml}\times\frac{mol}{18.02\ g}=\frac{5.163\ mol\ H_2O}{mol\ precursor}$$

Example Worksheet

A	B	
Volume Solvent (ml)	**2**	1
		2
Precursor MM (g/mol)	208.33	3
Precursor d (g/ml)	0.933	4
Mol Support/Mol Support Precursor	1	5
Support MM (g/mol)	60.0838	6
Amount of precursor (ml)	**4.8**	7
Amount of NH_4OH (30%, ml)	**0.3**	8
Amount of H_2O (ml)	**2**	9
		10
Metal precursor MM (g/mol)	177.326	11
Metal stoichiometric ratio	1	12
Metal MM (g/mol)	106.42	13
Desired loading (wt%)	5	14
Amount of metal precursor (mg)	**126.3**	15
		16
wt% Additive	5	17
Additive precuror MM (g/mol)	220.77	18
Additive MM (g/mol)	78.96	19
Mol in additive/Mol in Precursor	2	20
Amount of additive precursor (mg)	**313.0**	21
		22
mass M (mg)	**75.8**	23
mass modifier (mg)	**111.9**	24
mass support (mg)	**1291.6**	25
		26
Actual wt% M	**5.1%**	27
Actual wt% modifier	**7.6%**	28
Actual wt% support	**87.3%**	29

Cell Calculations

The amount of metal precursor (B15) is equal to the total mass of support and modifier used, multiplied by the desired loading and converted from mass of metal needed to mass of metal support needed.

B15 = ((B7*B4/B3*B5*B6)+(B21/B18*B20*B19/1000))*B14/100/B13*B11*B12*1000

The amount of additive precursor is calculated in a similar way, except it does not include the weight of the metal. This is why, as can be seen in cells B27-B29, the actual wt% of the modifier ends up being slightly higher than the desired loading (cell B17).

B21 = B7*B4*B17/100/B19/B20*B18*1000

Finally, to determine the actual wt% of all components in the catalyst, a simple calculation of the theoretical masses of each of the components in the final system, with the percentages calculated from that. For the metal, for example:

B23 = B15/B11*B12*B13

B27 = B23/SUM(B23:B25)